SKB

TECHNICAL REPORT 93-06

Mineralogy, geochemistry and petrophysics of red coloured granite adjacent to fractures

Thomas Eliasson

Chalmers University of Technology and University of Göteborg, Department of Geology, Göteborg, Sweden

March 1993

SVENSK KÄRNBRÄNSLEHANTERING AB
SWEDISH NUCLEAR FUEL AND WASTE MANAGEMENT CO
BOX 5864 S-102 48 STOCKHOLM
TEL. 08-665 28 00 TELEX 13108 SKB S
TELEFAX 08-661 57 19

MINERALOGY, GEOCHEMISTRY AND PETROPHYSICS OF RED COLOURED GRANITE ADJACENT TO FRACTURES

Thomas Eliasson

Chalmers University of Technology and University of Göteborg, Department of Geology, Göteborg, Sweden

March 1993

MINERALOGY, GEOCHEMISTRY AND PETROPHYSICS OF RED COLOURED GRANITE ADJACENT TO FRACTURES

Thomas Eliasson

March 1993

Chalmers University of Technology
and University of Göteborg
Department of Geology
S-412 96 GÖTEBORG, SWEDEN

Keywords: Äspö, Stripa, Bohus granite, granite, fracture, red colouration, hydrothermal alteration, weathering, mineralogy, geochemistry, petrophysics

ABSTRACT

Mineralogical, geochemical and petrophysical investigations were conducted of red-coloured alteration rims and of the neighbouring unaltered equivalents along fractures within granite from Äspö. An investigation was made also of a weak to rather strong, red-coloured granite from the Stripa mine, as well as a weak brownish-red colouration, definitely not hydrothermal in origin, of weathered rinds at a glacial polished rock surface in the Bohus granite.

When approaching the fracture planes in the Äspö granite, the most diagnostic alteration features are *1)* the saussuritisation and Fe-oxyhydroxide staining of plagioclase, *2)* the crystallisation chlorite pseudomorphs after biotite and *3)* the hematisation of magnetite. The porosity within the alteration zones increases generally 2 to 3 times compared with the protolith rock, whereas the densities decrease by some 5 to 10 %. The oxidation of magnetite gives as much as a tenfold lowering of the magnetic susceptibility.

The red colouration of the Stripa granite is caused by hematite ± Fe-oxyhydroxide formation along microfractures, grain boundaries and, subordinately, the main minerals. Oxidisation and re-precipitated of iron liberated during a retrograde muscovitisation of principally chlorite is interpreted to be the cause of the formation of the ferric oxides. The rather homogeneous density and porosity values of the grey and of the red-coloured granites reflect the minor change in the mineralogy when going from fresh into altered granite.

Weathering and whitening of plagioclase in the bleached, outer zone and precipitation of small quantities of Fe-oxyhydroxides/hydroxides in the brownish-red zone cause the macroscopic colouration of the weathering rind below the glacial polished rock surface of Bohus granite. There is a marked increase in porosity from the interior fresh (c. 0.4-0.5%) towards the exterior bleached zone (c. 1.5-2%) of the subaerialy, weathered Bohus granite surface. The incipient decomposition of magnetite is shown as a slight lowering of the magnetic susceptibility of the outermost bleached zone.

ABSTRACT (SWEDISH)

Mineralogiska, geokemiska och petrofysiska undersökningar har genomförts av rödfärgade omvandlingszoner, samt av det angränsande oomvandlade sidoberget längs sprickplan i granit från Äspö. Undersökningar genomfördes även av svagt till relativt kraftigt rödfärgad granit från Stripa gruva, samt av en svag brun-rödfärgning av vittringshud på hällar av Bohusgranit.

De mest signifikanta hydrotermala mineralogiska omvandlingar längs sprickplanen i graniten från Äspö är 1) saussuritiseringen och Fe-oxihydroxid färgningen av plagioklas, 2) kristallisationen av klorit pseudomorfer efter biotit och 3) hämatitisering av magnetit. Porosititeten i de hydrotermalt omvandlade zonerna ökar vanligtsvis 2 till 3 gånger i jämförelser med det oomvandlade sidoberget emedan densiteten minskar med 5 till 10 %. Oxideringen av magnetit orsakar en minskning av den magnetiska susceptibiliteten upp till tio gånger.

Rödfärgningen av Stripagraniten orsakas av bildning av hämatit ± Fe oxihydroxid längs mikrosprickor, korngränser och underordnat i huvudmineralen. Oxidering och utfällning av järn, frigjort under en retrograd muskovitisering av främst klorit, tolkas som orsaken till bildningen av ferrooxiderna. Den relativt likartade (homogena) densiteten och porositeten i oomvandlad grå granit och rödfärgad granit är en avspegling av den ringa förändring i mineralogin mellan frisk och omvandlad granit.

Vittring och vitfärgning av plagioklas i den yttre, bleka zonen samt utfällning av Fe-oxihydroxider in den brun-rödfärgade zonen, orsakar den makroskopiskt identifierbara färgningen av vittringshuden på de glacialslipade hällarna av Bohus granit. Porositeten uppvisar en markant ökning från den inre (0.4-0.5%) ovittrade graniten till den yttre bleka zonen (1.5-2%) i den subaerielt vittrade hällytan. En begynnande nedbrytning av magnetit visar sig som en svag sänkning av den magnetiska susceptibiliteten i den yttre, bleka zonen.

CONTENTS

1. INTRODUCTION

Narrow zones of red-coloured rock adjacent to both hydraulically open and presently sealed fractures are commonly observed in granitic crystalline rocks. The aim of the present study was to investigate the cause of the redness of the colouration. The petrophysical properties effective porosity, density and magnetic susceptibility of the red coloured rock, as well as of the "uncoloured" wall rock (protolith), were also investigated.

The paper starts with a brief description, additional to the methodological section, of the unaltered/fresh granites, after which the alteration features are examined. For the purposes of this paper, the uncoloured, protolith granite neighbouring (interior to) the altered zones will be termed "fresh" granite. These rocks are apparently unaffected by the hydrothermal and/or the low temperature weathering alteration processes responsible for the colouration in the fracture vicinity. Alteration features pre-dating the red colouration, e.g. weak gneissosity textures and late-magmatic mineralogical modifications, may thus occur in the fresh granites.

The fresh granites investigated are quite homogeneous. This implies that it is possible to make mineralogical and petrophysical comparisons between the fresh granites and their altered equivalents on the meter scale traverses.

The *mineralogical composition* of the red-coloured selvages along the fracture planes are, beside the mineralogy of the fracture filling, an important parameter for the sorptive properties of the rock. It is therefore essential to have knowledge of the mineralogy of the red-coloured alteration selvages.

The petrophysical investigation was performed to study the correlations between degree of alteration (red colouration) and porosity, and density and magnetic susceptibility.

The *porosity* data give information on the permeability/sorptive area of the altered rock underlying the fracture surfaces and, thus, its ability to participate in the retention of radionuclides transported in the fracture groundwater. The *density* of the rock depends on the porosity and mineral composition of the rock. This implies that hydrothermal alteration and the formation of secondary, hydrated, low-temperature minerals cause a decrease in the rock density. In rocks with high primary (pre-alteration) susceptibility, the *magnetic susceptibility* measurements give a good indication of the degree of hydrothermal alteration owing to the highly redox dependent stability of magnetite.

2. INVESTIGATION LOCALITIES

The study of the alteration features was focused mainly on rock material from a biotite granite from the Äspö-Laxemar area just north of the Simpevarp Nuclear Power Plant on the southeast coast of Sweden. Additionally, an investigation was made of a weak to rather strong red colouration of a muscovite±biotite granite from the Stripa mine, as well as a weak brownish-red colouration, definitely not hydrothermal in origin, of weathered rinds at and near a glacial polished rock surface in the post-kinematic Bohus monzogranite.

This chapter gives a short summary of the geology of the rocks investigated. The sampling sites and a brief macroscopic description of the sampled rocks are also presented.

2.1 Äspö granite

Samples were collected from the presently constructed access ramp to the planned underground Äspö Hard Rock Laboratory (SKB Annual Report, 1991). Eleven samples from altered zones between 516 and 547 metres of tunnel length and one sample from a highly altered and red-coloured granite at 781 m were collected. Samples at about 516 m are thus from the fracture zone presently investigated in the Large Scale Redox experiment (Barnwart et al., 1992). The sample locations and rock descriptions are presented in Table 1.

In this study, rock specimens were collected of the up to 10 cm wide, faintly red to deeply red-coloured granite selvages along fracture planes, as well as of the macroscopically unaltered, protolith, biotite granite adjacent to the red-coloured rock.

The fact that red-coloured alteration zones occur adjacent to hydraulically open as well as presently sealed fractures implies that no simple correlation exists between red the colouration and hydraulic conductivity (present day) of fractures. Further, as seen below, this type of red colouration is caused by high-temperature, water-rock interaction processes (hydrothermal) rather than low-temperature weathering processes.

The granitoids in the Äspö-Laxemar area belong to the huge, roughly S-N trending, mid-Proterozoic Transcandinavian igneous belt (TIB) made up principally of monzo-diorite, monzonite and granite (Gorbatschev, 1980). Granodiorite, diorite and gabbro are subordinate within the batholithic part of the belt. Associated with the plutonics are supracrustal rocks, chiefly

basic and intermediary volcanites. A detailed description of the lithology on the Äspö island was presented by Kornfält, & Wikman (1988). The fracture-filling mineralogy and geochemistry, as well as some aspects of the post-magmatic deformation history of the TIB granitoids in the Äspö area, are given in e.g. Talbot & Riad (1987), Tullborg (1989), Landström & Tullborg (1991) and Barnwart et al. (1992).

Table 2.1 Sample locations and rock descriptions for samples from the Äspö tunnel.

Sample, (m)	tunnel lenght	Rock description	Section[1]
Ä1,	546	Red coloured granite zone, 4 cm wide, adjacent to epidote+prehnite+chlorite±vermiculite±calcite filled (c. 2 mm thick) fracture. Striations and small steps on fracture plane.	546.4 m, sp 0.1 H_2O 192/73
Ä2,	546	Grey to reddish-grey, medium grained, fresh granite. 20 cm east of Ä1.	
Ä3,	538	Red coloured granite zone, 4-6 cm wide, adjacent to epidote+chlorite±calcite (tot c. 1 mm thick) covered fracture. Smooth, somewhat undulating fracture plane. Rich in microfractures parallel to main fracture plane.	538 m, sp 0.1 050/45, Chl+cc+oxi
Ä4,	538	Fresh wall-rock (same as Ä2) 40 cm east of Ä3.	
Ä5,	525	Reddish, medium-grained, altered granite. Adjacent to 2-3 mm wide calcite coated fracture. Microfractures perpendicular to main fracture plane	
Ä6,	525	Red to pinkish-red, medium-grained, altered granite. The granite is cut by a sealed, 5 to 15 mm wide microbreccia with a matrix rich in rather large prehnite and chlorite grains.	529.1 m, sp 0.1, H_2O 83/85, Chl+Ep+cc
Ä7,	516.6	20-30 cm wide zone of pervasively fractured proto-mylonitic, intensely altered granite. Parallel arrange-ment of chlorite±epidote±Ti-oxide altered biotite grains. Quartz-epidote micro-breccia.	516.6 m, Zon;Z0, 066/78
Ä8,	516	Intensely altered and cataclasitic granite. Fractured with late calcite and clay precipitation/formation.	
Ä9a,	516	Red, altered granite	
Ä9b,	516	Grey, somewhat bleached variety of the granite Ä9a.	
Ä10,	516	Light red granite with micro-fractures of quartz.	
Ä11,	526	3-4 cm wide alteration zone along an epidote+ chlorite covered fracture. Fracture plane relatively smooth and partly healed by fracture fillings.	526 m, sp 0.2 002/84, chl+ep + cc
Ä12,	526	Fresh, grey granite 20 cm W of fracture plane.	
Ä13,	781.1	Red, pervasively altered granite adjacent to 5 mm wide epidote-filled fracture with striations and ±harnesk	781.1 m, sp 10 95/50, Ep

1) fracture documentation (position, character, orientation, filling etc.) according to SKB tunnel mapping program.

2.2 Stripa granite

It was decided to investigate the red colouration of the grey, medium-grained granite from the abounded iron ore Stripa mine in Bergslagen in south central Sweden. Altered granite, penetrated by six boreholes (D1 to D6) from the Site Characterisation and Validation (SCV) block located along the northeastern edge of the mine at a level of 382 to 390 m, were to be used in the study. These 99 m long, sub-horizontal, parallel boreholes were drilled in the trajectory (287° from mine north) of the validation drift with a spacing of less than three metres. For more details regarding drill hole locations and geometry and fracture pattern and tectonics, see Gale et al. (1990). When the validation drift was later constructed, the geology predicted from the core logs was compared with the geology observed in the validation tunnel.

Sixteen samples of fresh to gradually more red-coloured (altered) granite were collected from drill core D3 (see Table 2.3 and Fig. 8.2). The majority of the samples were collected from a zone with rather strong hydrothermal alteration and a red colouration at 20 to 30 m of borehole length. This alteration zone is associated with the north-south trending "fracture zone H" (Gale et al., 1990). According to the core log, the altered granite between 21.10 m and 31.60 m has a central portion of tectonised granite bordered by a epidotised and chloritised halo and/or oxidised granite (Fig. 8.2).

Samples S16 to S19 (Table 2) are from borehole D5. According to the rock log (Gale et al., 1990), S16 and S17 are from a weakly oxidised granite, whereas S18 and S19 are from the miarolitic and sericitisised granite in the section 81.45 to 86.80 m. This zone belongs to the vertical N-S to northeast-southwest trending "fracture zone B" (Gale et al. 1990). It is notable is that the miarolitically altered granite is not found in the other D-boreholes (at a distance of less than three metres from D5).

The Stripa granite is, as reported in the comprehensive compilation by Carlsten (1984), a small, steep-sided pluton of a serorogenic, U- and Th-rich (high heat production, HHP) granite. It is intrusive into a lithology dominated by acid metavolcanics. The exposed part of the pluton is about 1.5 x 0.5 km. The vertical depth is estimated to be limited to about 1.5 km. The granite is massive to weakly foliated and petrographically homogeneous with a monzogranitic composition. Monomineralic as well as mixed fracture fillings with chlorite, carbonate minerals, quartz, sericite, epidote, flourite and opaques are reported (Carlsten, 1984).

Table 2.3 Core sample locations (drill core length in metres) and rock descriptions of samples from boreholes D3 and D5 from the SCV-block in the Stripa mine.

Sample: core length		Rock description
DRILL CORE D3		
S1:	3.03-3.13	Grey to greenish-grey, medium to coarse-grained, weakly foliated (gneissic), muscovite±chlorite±biotite granite. **"Fresh."**
S2:	19.73-19.83	Grey, weakly foliated granite, same as S1. **"Fresh."**
S3:	21.13-21.22	Faintly reddish-grey (weak incipient colouration), medium to coarse-grained, weakly foliated granite.
S4:	21.46-21.52	Reddish-grey, medium to coarse-grained, weakly foliated, biotite granite.
S5:	22.12-22.31	Reddish-gray granite same as S4, with a zone of green colouration.
S6:	22.64-27.74	Red coloured (altered), medium to coarse-grained granite.
S7:	23.81-23.91	Dark red coloured (altered), medium to coarse-grained granite (protolith; granite as above). Micro-fractures sealed with chlorite.
S8:	24.82-24.96	Dark greenish-red coloured (altered) medium to coarse-grained granite (protolith; granite as above). Rather rich in micro-fractures sealed with chlorite.
S9:	25.72-25.87	Light reddish (altered), medium to coarse-grained, salic granite. Micro-fractures sealed by chlorite±calcite. Somewhat silicified. The red colouration is later/traverse the greyish silicification).
S10:	27.05-27.14	Reddish-grey (somewhat altered), medium to coarse-grained granite.
S11:	28.72-28.84	Reddish medium to coarse-grained, weakly foliated, granite.
S12:	30.44-30.61	Slightly red-coloured, medium-grained, biotite granite. Increased red colouration close to fracture plane.
S13:	33.23-33.42	Grey, medium-grained, biotite granite. **Fresh.**
S14:	60.81-60.92	Grey, with a weak incipient red colouration, medium-grained, biotite granite.
S15:	92.26-92.48	Grey, with a weak incipient red colouration, medium-grained, biotite granite.
DRILL CORE D5		
S16:	66.13-66.38	Grey, faintly red, medium to coarse-grained, slightly foliated granite.
S17:	81.22-81.36	Slightly reddish and bleached, medium to coarse-grained granite. Low content of mafic phases (salic granite)
S18:	82.62-82.83	Altered, light greyish red, medium-grained, slightly bleached, porous, salic granite.
S19:	85.17-85.38	Altered, greenish-grey, medium-grained, slightly bleached and porous granite.

2.3 Bohus granite

Three rock samples (see appendix A:3) were collected from a site in the north-eastern part of the 920 Ma old Bohus monzogranite (Eliasson & Schöberg, 1991) situated on the west coast of Sweden. The granite massif consists of a number of monzogranitic intrusions of slightly different petrography and chemistry. Its post-tectonic and post-regional metamorphic setting is shown by the undeformed primary magmatic textures and structures and generally preserved magmatic mineralogy.

These samples were investigated in order to compare the mineralogical and petrophysical features in assumed low-temperature, brownish-red coloured weathering/alteration zones of the Bohus granite with the hydrothermally red-coloured Äspö and Stripa granites.

Sample B1 is from a vertical road cut with a sub-vertical, hydraulically open fracture bordered by a bleached, greyish-white, leached zone, c. 5 mm thick and an approximately 5 cm wide weathering/ alteration zone further into the granite. The samples were collected at the fracture plane about two metres below the glacial polished rock surface.

The brownish-red coloured granite neighbouring the fracture plane shows no evidence of high-temperature, hydrothermal alteration. Further, the absence of remnants of hydrothermal fracture fillings along the fracture plane evince the "recent," low-temperature origin of the fracture. At the intersection between the fracture plane and the glacial polished rock surface, it can be seen that the alteration zone is a "continuation" of the post-glacial (< 12.000 years, Johansson, 1982) weathering rind. It should be noted that this type of 1 to 10 cm wide weathering profile is generally observed along hydraulically open fractures in the Bohus granite (as well as in other granitic crystalline rocks in Sweden).

Samples B2 and B3 are surface specimens with an ocularly identified, approximately 3 cm-deep brownish-red weathering rind. These samples were collected from the same outcrop, with a spacing of about 1 m. The weathering rind is composed of an upper 1 to 3-mm thin, bleached, greyish-white zone. It is followed by reddish-brown zone with a slight yellowish tint. The interior unweathered and uncoloured protolith granite is reddish-grey and medium-grained. The rock surface exhibits striations and polished remnants formed during the Weichselian glaciation. Owing to the small size of the B3 specimen, it was studied only by petrographic microscope.

3. METHODS

3.1 Sampling

The macroscopic descriptions and sampling sites for the specimens are given in Tables 1 and 2. Specimens from the Äspö tunnel were collected at 13 sites and consisted of 0.5 to 2 kg of rock. The 19 specimens of the Stripa granite were about 0.1 to 0.3 m-long drill corepieces with a diameter of 62 mm (c. 1.2 to 3.5 kg). The samples of the weathered Bohus granite had a mass of about 1 kg and contained parts of the weathered as well as the underlying (interior) fresh protolith rock.

Parts of the fresh to gradually more altered rock samples were sawn perpendicular to the fracture plane, or rock surface, into tablets of an approximate size of 35x20x20 mm. These pieces were used for thin section preparation. Density and effective porosity determinations were made on the remaining sample material. Subsequently, the major parts of these pieces were crushed, riffle-divided down to about 100 g and thereafter milled in a W-C alloy ("vida") mortar. The geochemical and magnetic susceptibility investigations were done on this rock powder.

It should be noted that the Bohus granite samples (B1 and B2) and sample Ä11 were sawn into sub-samples containing different parts of the weathering/alteration profile (n:x in appendix A:1 and A:3). The fracture coating together with parts of the underlying altered wall-rock from samples Ä1 and Ä13 were also cut into thin slices ("+fr. surf" in appendix A:1) in order to investigate the porosity of the fracture-filling material together with outermost part of the alteration zone.

3.2 Petrography and mineralogy

The primary objective of this investigation was to identify and describe textural and mineralogical alterations responsible for the red colouring of the wall-rock along fractures (generally water-conducting) in the Äspö granite, as well as a broader zone of red colouration in the Stripa granite. The aim of the petrographic description was to determine:

1) the mineral content of rocks of varying degrees of red colouration
2) the alteration products and degree of alteration
3) the texture and grain size of fresh and altered rock
4) the degree of alteration and micro-fracturing and its effect on porosity, susceptibility and density of the rock

3.2.1 Microscopy

Polished thin sections were prepared perpendicular to the fracture surface from each sample. When appropriate, in order to obtain a larger section of the rock, additional sections were cut parallel to the fracture plane. Mineralogical alteration features were studied and microphotographs were taken of the thin sections with a polarising microscope. Opaque minerals were examined using reflected light.

The alteration products (newly formed, low-temperature hydrated minerals) are commonly fine to extremely fine-grained, making identification under polarising microscope impossible. Thus, the mineral identification was supported by the micro-chemical microprobe analyses and X-ray diffraction investigations (see below).

The mineralogical contents in volume % were determined for 12 representative samples by point counting over the thin section. Generally, 1400 to 2500 points were counted, with a denser grid on more fine-grained samples.

3.2.2 Electron microprobe

Electron-microprobe analyses were carried out on carbon-coated thin sections using a wavelength dispersive (WDS) microprobe system (Cameca SX50) at the Department of Geology at University of Uppsala. An acceleration potential of 20 kV and a beam current of 12 nA were used. The beam size was 1-2 μm, implying a size of the analysed spot of about 5 to 10 μm.

The micro-chemical investigation was carried out on primary magmatic minerals from uncoloured, "fresh" granite protolith and on secondary alteration products within the red-coloured alteration zones along fractures from the Äspö granite (Table 3.1 and appendix B). Fracture fillings from samples Ä1, Ä3 and Ä10 were also analysed with the microprobe. The objective of the micro-chemical investigation was to chemically characterise minerals of different genesis and to identify the fine-grained minerals.

The microprobe investigation was also carried out to study micro-textures in, for example, saussuritic plagioclase. Backscattered electron (BSE) images were used for the micro-textural study. The fraction of backscattered electrons is primarily a function of the mean atomic number of the sample material. This implies that the scanning image displays minerals with contrasting mean atomic numbers as well as pores and voids in the sample.

The elemental distribution of Fe, Mn and Mg in samples Ä1 and Ä8 was investigated by microprobe scanning of the thin sections. The beam was somewhat defocused during this investigation, giving a size of 20 μm for the spot analysed. Almost the entire surface (approximately 40 x 22 mm) of the thin section Ä1 was investigated by point analyses on a 640x350 grid. The step between analysed points was 62 μm. An area of 15 x 13 mm of the thin section Ä8 was investigated using a somewhat more dense grid (30 μm steps).

Table 3.1 Primary magmatic minerals from fresh (F) and secondary minerals from altered Äspö granite, investigated by electron microprobe analysis.

Sample	Pl	Bi	Mn	Ep_m	Chl	Other
Ä1	A		X	X	X	Sphene, Pr, Chl, Surface scanning. Fracture filling: Ep, Pr
Ä2 F	X	X	X	X		Sphene,
Ä3	A			X	X	Mi, Inclusions in chlorite, Sphene, Inclusions in altered Pl; Ep, clay, zircon, Fe-mineral, clay, Mi, Ab Fracture filling: clay, Ep
Ä4 F	X	X	X	X		Sphene
Ä8						Calcite, Surface scanning.
Ä10						Fracture filling: Pr, K-fsp, clay/vermiculite

Pl = plagioclase (A = altered,; albitisised, saussuritic, etc.)
Bi = biotite
Mn = magnetite
Ep_m = matrix epidote
Chl = chlorite
Ab = albite
Mi = microcline
Pr = prehnite
Clay = unspecified clay minerals
K-fsp = low-T K-feldspar

3.2.3 X-ray diffractometry

Fracture-filling minerals from three fracture planes (Ä3:f, Ä7:f and Ä1:f) and the whole rock sample Ä3 were submitted for X-ray diffractrometry (XRD) analysis at the Geological Survey of Sweden, Uppsala (Table 5.1).

The fracture fillings were scraped off the fracture surface. These samples were powdered and oriented. A second run was conducted after treatment by ethyl glycol at 400 °C to examine the occurrence of swelling clay minerals. Sample Ä3 consisted of a $<2\mu$m size fraction separated from the wall rock whole rock powder of the severely microfractured and red-coloured granite zone.

3.3 Whole rock Chemistry

Sixteen samples were analysed for whole rock major element geochemistry by atomic absorption spectrometry (Fe_{tot} Mg, Na, K and Mn), colorimetry (Si, Al and Ti) and titration (FeO and Ca) at the Department of Geology at University of Göteborg/Chalmers University. Adsorbed and crystallographic "water" contents were determined gravimetrically as weight loss at 105° C and 1100°C, respectively. The weight loss at 1100°C includes also e.g. the release of CO_2 as a result of carbonate breakdown.

The primary objective of the geochemical analyses was to determine the ferrous iron content in altered and "fresh" rock. Further, the whole rock chemistry reveals the degree of elemental mobility and support to mineralogical investigation.

3.4 Density and porosity determinations

The purpose of the density and porosity investigation was to reveal whether the amount of interconnected open pores in the altered and red-stained granite differs from that in the unaltered protolith wall rock. A further aim was to resolve wheather any pattern exists between the petrophysical parameters and the degree and type of alteration.

The following terms and symbols are used to denote masses and volumes when calculating (setting density of water to unity) density and porosity:

M_{105} = mass of 105°C owen dry specimen
M_{sat} = mass of water saturated specimen
M_{sub} = mass of water saturated submerged specimen

Bulk volume of specimen,	$V = M_{sat} - M_{sub}$
Bulk density,	$\rho = M_{sat} / V$
Dry density,	$\rho_d = M_{105} / V$
Pore volume,	$V_V = M_{sat} - M_{105}$
Porosity,	$n = 100 * V_V / V = \rho - \rho_d$

The measurements of density and porosity (porosity = effective porosity = interconnected pore volume/bulk volume) were done by the author at the Department of Geology at Chalmers University. The procedure followed basically the saturation and buoyancy method outlined by Franklin et al. (1979). However, I used a considerably higher vacuum when water-saturating these low porosity granites.

The separate samples from Äspö generally comprised *one* to *three* (most commonly two) pieces with weights in the range of 33 to 134 g (average, a=83 g, standard deviation, s=29 g). The Stripa samples consisted of drill core pieces with weights in the range of 39 to 220 g (a=85 g, s=32 g). The separate Bohus granite samples consisted of one to three pieces with masses in the range of 10 to 120 g (a=60 g, s=31 g). Thus the minimum dimension of the individual pieces was generally 10 times larger than the grain size. An analytic Mettler balance with an accuracy of 0.001 grams was used for the weighting of the rock specimens.

The specimens, generally sawn as prisms, were saturated by water immersion in a vacuum of 0.9 to 0.75 bar for about 1 hour. Their saturated-submerged mass (M_{sub}) was then determined by weighting the sample under water. The saturated-surface-dry mass (M_{sat}) was measured after drying the sample with a cloth. Specimens were then dried in an oven at a temperature of 105°C for a period of 24 hours. Finally, the samples were stored in an airtight exsiccator during cooling before determining the mass of 105°C oven-dried specimen (M_{105}).

3.4 Magnetic susceptibility

To obtain representative susceptibility values, I conducted the laboratory measurements on the homogenised rock powder. Susceptibility measurements of the small rock tablets gave inaccurate values as a result of the strong sensitivity of the position and orientation of the tablet within the sensor. Further, inhomogeneous distribution of magnetite within the rock implies that the volume of the rock tablet was too small to give statistically correct results. Consequently, in contrast to the density and porosity data, each sample and subsample from Äspö are represented by only one susceptibility value.

The measurements were condcted using a Bartington magnetic susceptibility meter, model MS2, with the standard 36 mm laboratory sensor (MS2B), which generates a low intensity magnetic field (80 A/m). 10-ml cylindrical bottles filled with sample rock powder were used. In order to avoid errors caused by different degrees of compactation of the rock powder within the bottles, I made *mass* specific measurements. Thus the corrected susceptibility values (X) were calculated as: X = measured value * 10 g reference mass/sample mass.

4. MINERALOGY AND PETROGRAPHY

This section gives a description of the mineralogy and petrography of the unaltered protolith material to the red-coloured granite. The microprobe analyses of minerals from fresh Äspö granite samples are presented in section 5.1.1, together with the mineral chemistry of the altered rocks.

4.1 Äspö granite

Macroscopically, the unaltered Äspö granite is grey to reddish-grey, medium to coarse-grained and somewhat porphyritic, with a generally massive texture. On polished rock surfaces, it can easily be seen that the central parts of many plagioclase grains are greenish owing to saussuritisation. The microcline is slightly red to pinkish-red, although the colour of the grains is somewhat inhomogeneous.

The unaltered granite contains roughly equal amounts (c. 25 to 35 vol. %) of plagioclase, quartz and microcline (cf. Table 4.1). The texture is slightly porphyritic, with small (< 1.5 cm), euhedral to subhedral microcline and, subordinately, plagioclase phenocrysts. The biotite content is 5 to 7 vol.% with the grains commonly occurring in rather large aggregates (up to about 10 mm) together with sphene, opaques, apatite and epidote (see Fig. 4.1). Locally, partly altered biotite, epidote and quartz are intergrown in a symplectitic fashion. Tiny, elongated flourite grains are occasionally found together with, or along cleavage planes within, generally slightly chloritised biotite.

The granite carries about 1 to 3 vol. %, euhedral-subhedral epidote. The sphene content ranges from 0.2 to 0.6 vol. % (cf. Table 4.1). The euhedral sphene crystals are commonly quite large, up to 1.5 mm in length. The opaque phase (c. 1 to 2 vol. %) is predominately euhedral magnetite. Apatite is the most common accessory mineral, followed by zircon, monazite and some secondary calcite.

Epidote located in the mafic aggregates displays straight, euhedral and intergrown symplectitic contacts against biotite. The borders toward the feldspars and quartz are generally highly symplectitic. These textural features indicate, as discussed by Zen and Hammarström (1984), a magmatic origin of the euhedral epidote cores (see section 5.1.1).

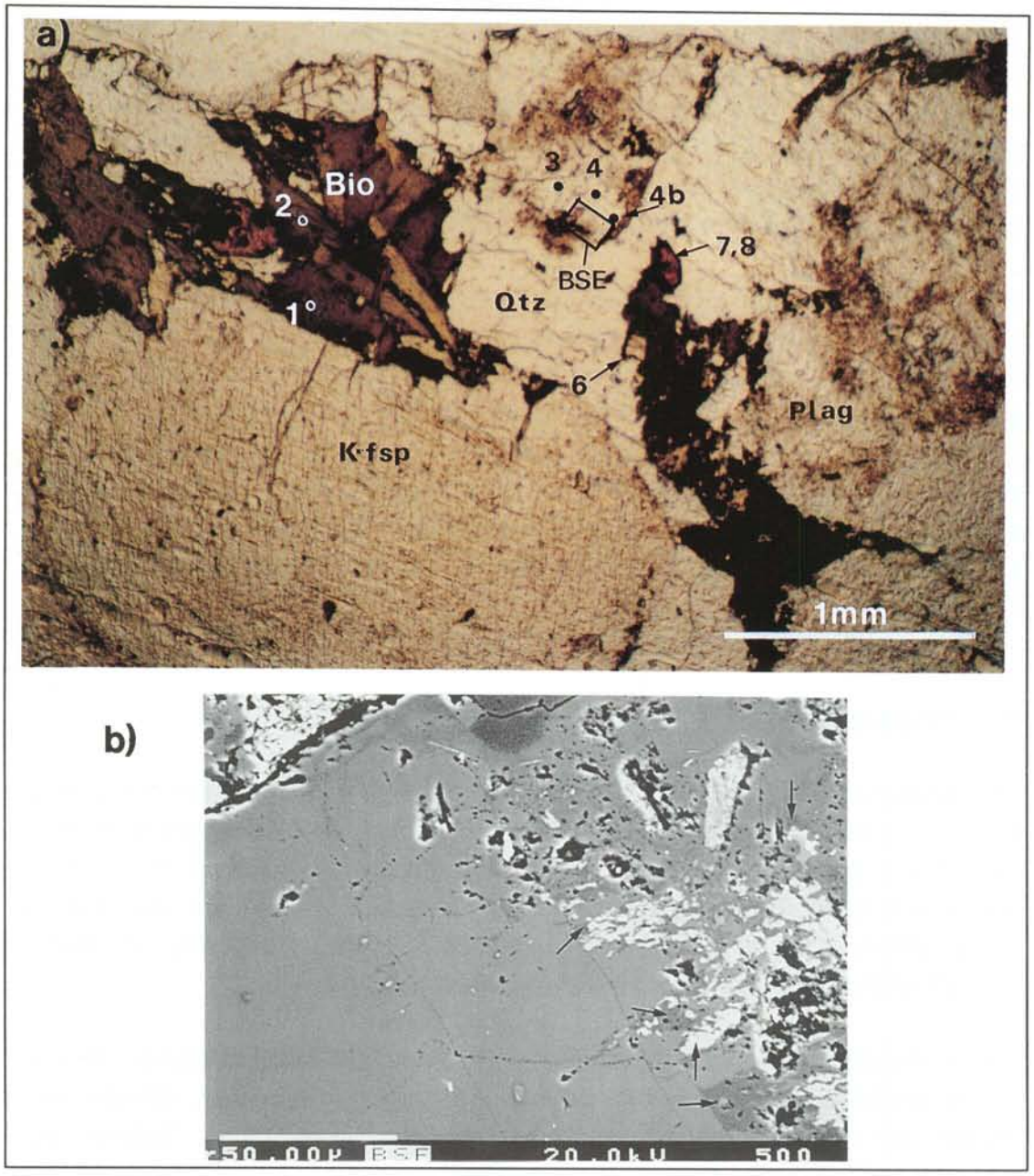

Figure 4.1 ***a)*** *Microphotograph of "fresh" Äspö monzogranite (sample Ä4). The altered equivalent (sample Ä3) to this granite is shown in Fig. 5.2. Numbers refer to spots analysed by electron microprobe (1,2=biotite; 3-4b= plagioclase; 6=epidote; 7,8=sphene; see appendix B for results).* ***b)*** *Back-scattered electron (BSE) image of saussuritic alteration of plagioclase. The BSE area is outlined in Fig. 4.1a. The light grey area in the lower left is unaltered plagioclase (An c. 25 to 26 mol. %). In the saussuritic part, the plagioclase has been replaced by albite (grey; small arrows), calcite (bright areas) and epidote (bright areas: small arrows). Note the presence of the irregular dissolution voids (black hollows).*

The granite is mainly fresh, and most mineral phases are magmatic. Although plagioclase are relatively fresh and transparent under petrographic microscope, many grains are locally saussuritic (Fig. 4.1 and Table 4.1). In addition, some late magmatic formation of chlorite ± sphene from biotite is observed. Some sphene crystals are partially altered to brown or black Ti-oxides and, subordinately, some epidote and calcite.

The mineralogical composition of the fresh granites investigated in this study show that they are true monzogranites (Fig. 4.2) and, thus, represent a fairly leucocratic facies of the TIB plutonics. The reddish-grey, medium-grained porphyritic granitoids on the Äspö island described by Kornfält & Wikman (1988) often contain less quartz and microcline, as compared with the granites investigated in this study. This is balanced by a higher plagioclase and biotite content. Petrographically, these latter biotite-rich Äspö granitoids are quartz monzodiorite, granodiorite or quartz monzonite (Kornfält & Wikman, 1988).

4.2 Stripa granite

The unaltered Stripa granite is a grey to greenish-grey, medium to coarse-grained, weakly foliated muscovite granite. It is anhedral granular with intergrown grain boundaries. Towards the altered zones at 20 to 30 m of borehole length, it grades successively over to the red to dark red, fine to coarse-grained granite (Figs. 5.12 and 8.3). The frequency of sealed microfractures also increases within the alteration zone.

The unaltered, grey Stripa granite consists of roughly equal amounts (30 vol. %) of perthitic microcline, plagioclase and quartz. Muscovite, chlorite and epidote are the principal minor constituents (cf. Table 4.1). Sphene and secondary leucoxene (brownish alteration product of sphene consisting mainly of fine-grained, crystalline rutile), calcite and prehnite are common secondary accessory phases. Monazite is a primary accessory phase. Except for the muscovite crystals and some accessories, the quartz, microcline and plagioclase crystals are anhedral and have intergrown boundaries in an anhedral equigranular texture.

The granite has a very low content of mafic minerals. The observed monzogranitic composition (cf. Fig. 4.2) of the unaltered granite samples investigated in this study agrees with the compositions given by Lundström (1983) and Wollenberg et al. (1980).

Table 4.1 Modal data (mineral content in volume %) of fresh (**F**) and altered rock from Äspö (Ä) and Stripa (S).

Sample	Qtz	K-fsp	Plag Sauss	Bio	Chl	Epi	Op	Sph	Cc	FeO	other	Acc	No.
Ä1	24.3	19.7	42.6 (36.9)	t	8.1	3.4	0.2	0.8	t	t		0.9	1826
Ä2 **F**	24.2	29.1	34 (5.5)	7.0	0.7	3.0	1.1	0.6				0.3	2499
Ä3	24.4	21.5	35.4 (30.7)		4.7	3.5	0.5	0.7	4.6*5,6*	4.0	cl	0.7	1958
Ä4 **F**	24.9	32.7	31.1 (15.3)	7.1	0.7	2.5	0.4	0.4		t		0.2	1666
Ä5	23.5	21.9	39.8 (39.8)		7.4	1.6	1.0	0.9	0.2	1.9	1.8*1*		1453
Ä6	27.2	30.1	29.1 (26.8)		5.6	2.1	0.6	0.7	0.4	0.8	2.4*1* 0.4*2*	0.6	1834
Ä11	25.2	27.6	31.2 (28.9)	t	5.7	5.0	0.8	1.0	0.7	t	0.8*1* 0.6*2*	1.4; cl	1701
Ä12 **F**	31.2	23.8	35.5 (6.3)	5.4	3.2	1.3	1.9	0.2	t	t		0.5	1362
Ä13	20.4	28.9	31.9 (28.4)		5.8	8.5	t	1.1	t	t	2.8*1*	0.6	1513
S2 **F**	30.7	31.6	28.9 (12.1)	0.5	2.9	1.6		t	t*6*		2.5*3*	1.3	1276
S6	31.5	30.9	31.0 (28.2)		0.5	0.7	t*4,7*		t*5*	t	4.0*3*	1.4; cl	1482
S7	32.5	29.9	28.7 (20.1)		0.4	0.8	t*4,7*		t*5,6*	t	5.3*3*	2.4; cl	1174

Abbreviations:
Qtz = quartz; K-fsp = K-feldspar; Plag = plagioclase; Sauss = saussurite (amount given in brackets); Bio = biotite; Chl = chlorite; Epi = epidote; Op = opaques; Sph = sphene; Cc = calcite, except saussuritic calcite; FeO = Fe-oxyhydroxides and heavily FeOOH-coloured clayish material; Acc = accessory minerals (includes minerals noted in trace amounts), dominating mineral indicated; No. = points counted over thin section; t = traces; cl = clayish material.

1) undefined altered feldspar
2) altered (vermiculitic) light brownish chlorite
3) muscovite
4) Ti-oxides/sph in chloritised biotite
5) calcite in saussuritic plagioclase
6) calcite in microfractures
7) hematite in muscovitised chlorite

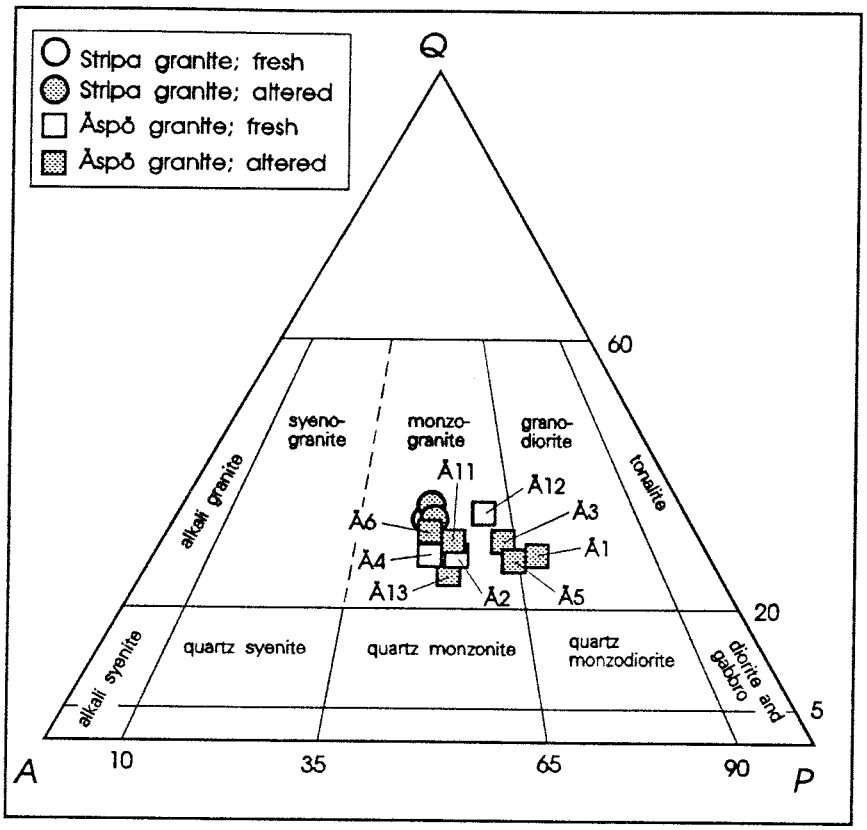

Figure 4.2 Modal distribution of quartz, alkali feldspar (microcline) and plagioclase in the Äspö and Stripa granites. Data from Table 4.1. Rock classification according to recommendations by the I.U.G.S. Subcommission on the Systematics of Igneous Rocks Classification (Streckeisen, 1976). Qz+Ksp+Pc=100%. Q = quartz, A= alkali feldspar (including e.g. perthite and albite (An 00-05), P = plagioclase (An 05-100). Note that in the altered Äspö granite sample "plagioclase" constitute saussuritic±argillaceous pseudomorphs of the pre-existing magmatic grains.

Biotite is unambiguously altered to chlorite with small elliptical exsolved sphene/Ti-oxide grains. Small relicts of biotite are, however, found in sample S2. Continued alteration, or a separate alteration phase, resulted in a muscovitisation of the chlorite, giving the last step in the following alteration sequence:

biotite → chlorite±sphene/Ti-oxides → muscovite±Fe-oxides/oxyhydroxides

These muscovite grains occur as rather large, up to 5 to 6 mm, subhedral to euhedral plates. The secondary muscovite also traverses and overgrows the granular granitic quartz and feldspar texture. Some of these muscovite plates are slightly bent and kinked. These textures show that the muscovitisation is

a *secondary*, sub-solidus, post-magmatic process. A second phase of muscovitisation (or a localised continuation of the first) is, as discussed in section 5.2, interpreted to occur coeval with, and to be partly responsible for, the red colouration of the granite.

The plagioclase is often altered, generally in a heterogeneous and patchy manner, to an extremely fine-grained sericite and/or saussurite. Microcline and quartz are commonly fresh and unaltered. However, fragmentation and incipient formations of sub-grains are observed along microfractures .

4.3 Bohus granite

The fresh sub-sample B1:3 of sample B1 is a medium-grained, subhedral to euhedral granular, biotite monzogranite with minute amounts of secondary muscovite. The main minerals are quartz, microperthitic microcline and plagioclase (oligoclase). The rock is rather rich in biotite but has a very low content of opaques (note the low magnetic susceptibility, cf. A:3). A patchy sericitic and saussuritic alteration occurs preferentially in central, anorthite-rich portions of the plagioclase grains. Some biotite grains are chloritised, with small, secondary sphene/Ti-oxide inclusions. Accessory minerals are apatite, zircon and monazite.

The unaltered rock of sample B2 and B3 is a medium-grained, reddish-grey muscovite-biotite monzogranite. Magnetite occurs as subhedral to euhedral grains dispersed in the rock (note the rather high magnetic sucseptibility). Euhedral apatite is the most abundant primary accessory mineral, followed by zircon and monazite. As in the Stripa granite, the large muscovite flakes overgrow and post-date the primary magmatic minerals. The muscovitisation is interpreted to be related to a late-magmatic hydrothermal event. This type of muscovite±biotite monzogranite occurs mostly in the northeastern part of the Bohus granite.

5. MINERALOGY AND TEXTURE OF ALTERED ROCKS

This chapter describes the alteration features observed in the red-coloured alteration zones of the investigated granites. The results of the micro-chemical investigation conducted on samples from fresh and red-coloured Äspö granite are presented in section 5.1.1.

5.1 Äspö granite

The fracture network in the Äspö area is characterised by the red coloured selvages, generally a few centimetres wide, occurring beside the fracture planes. The microscopic investigation shows that the red colouration of the granite adjacent to the fractures is caused by dispersed, fine-grained, reddish material occurring *1)* in altered and clouded plagioclase grains, *2)* along grain boundaries and *3)* along microfractures within individual grains.

The fine-grained, reddish material is interpreted to be mainly Fe-oxyhydroxides/hydroxides (see below). The colouring of plagioclase is partly also a result of the optical effect of the extremely fine-grained nature of the alteration products and the common occurrence of micropores.

In all investigated samples, the reddish colouring of the granite coincides spatially with a hydrothermal metamorphic alteration mineralogy occurring along the fracture planes. This fact, together with the observed oxidised mineral assemblage (see below) in the hydrothermally metamorphosed zones, indicates that the colouring is contemporaneous with, and a function of, the hydrothermal alteration.

Approaching the fracture planes, there is a progressive change in the mineralogy of the granite (Fig. 5.1). The alteration zones investigated exhibit a coherent course of transformations. The most diagnostic features within the altered zones are *1)* the crystallisation chlorite pseudomorphs after biotite, *2)* the alteration of plagioclase and *3)* the hematitisation of magnetite.

There is the general tendency to first decompose biotite and then plagioclase and magnetite, and finally there may be some ultimate alteration of microcline. The chloritisation of biotite is accompanied by a liberation of Ti that is incorporated into small, newly-formed sphene or Ti-oxide crystals occurring as inclusions in the chlorite (see further descriptions in section 5.1.1).

The altered rock tends to preserve the shape of the original minerals which are replaced. Textural changes occur only in highly strained (sample Ä7 and,

locally, in Ä3) and/or pervasively micro-fractured and cataclasitically deformed sections (sample Ä8), as well as in intensely hydrothermally altered sections of the granite (sample Ä13). At these locations, a high fluid/rock ratio facilitated neoformation of secondary minerals by direct precipitation from the hydrothermal fluids.

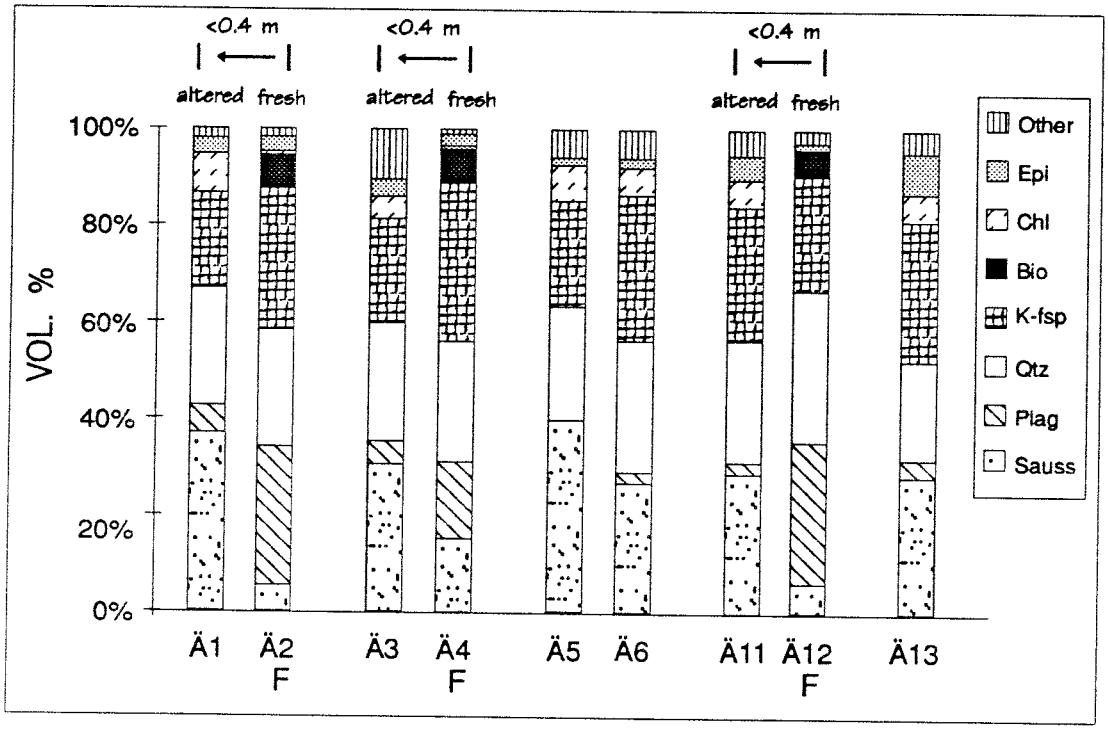

Figure 5.1 Modal composition of "unaltered" Äspö granite (F) and their hydrothermally altered equivalents occurring along fracture planes. For abbreviations, see Table 1. "Other" include minor and accessory phases (for e.g. sphene, calcite, FeOOH, clayish material etc. amounts, see Table 4.1). Sample pairs of fresh and altered granite of less than 0.4 m spacing are indicated. Note the transformation of biotite to chlorite and the increased saussuritisation of the altered samples.

It should be noted that, within the altered granite, the point-counted plagioclase grains constitute saussuritic±argillaceous pseudomorphs of the pre-existing magmatic grains. In the altered granite, the slight increase of the plagioclase content, accompanied by a decrease in K-feldspar content (Table 1 and Figs. 4-1 and 5.1) is a result of the growth of the saussuritic± argillaceous material into neighbouring microcline grains.

The very small grain size and the Fe-oxyhydroxide staining of the alteration products and fracture infillings complicated the optical mineralogical investigation. In order to facilitate identification, four samples with fine-grained alteration products and fracture fillings were investigated by XRD. The analysis confirmed the optical mineral identifications and also showed that the clay minerals belonged to the three groups illites, smectites and vermiculites (see Table 5.1 and below).

Table 5.1 Minerals identified in samples from Äspö by XRD analysis. Listed in order of decreasing amount (semiquatitative).

Sample	Identified minerals
Ä1: fracture minerals.	vermiculite, chlorite, prehnite, epidote, calcite, talc (?)
Ä3: whole rock	Quartz, K-feldspar, plagioclase, epidote, calcite, illite, swelling vermiculite, chlorite
Ä3: fracture minerals.	chlorite, vermiculite, smectite, quartz, K-feldspar, Epidote
Ä7: frac. min.	smectite-illite

The above described type of preferential Fe-oxyhydroxide impregnation of saussuritic plagioclase and along cracks and microfractures has been shown to be the principal cause of the red colouration of hydrothermally-altered granite at the Landsjärv Fault zone in northern Sweden (Eliasson et al., 1991).

The mineralogy of the altered rock is that of upper prehnite-pumpellyite to lower greenschist facies mineralogy (albite, epidote, calcite, prehnite etc.), implying that the hot fluids which permeated the fracture network generated metamorphic temperatures in the range of about 300 to 400°C in the fracture vicinity.

The Fe-oxyhydroxide and smectite formation is interpreted to be related to the final low temperature stage of the water-rock interaction. This occurred when the fracture was sealed off and the wall rock was cooled, which induced smectite and illite/smectite mixed layer precipitation within plagioclase voids and microfractures. Hydrothermal experimental results (Savage et al., 1987) indicate that smectite formation from plagioclase may occur at temperatures up to 150 to 250°C. Temperatures down to at least 150°C were suggested by AlDahan et al. (1988) during the formation of smectite-bearing assemblages in an altered granite in Siljan impact structure in central Sweden.

5.1.1 Mineralogical Features

The mineralogy and texture of the hydrothermal and locally cataclasitic alteration zones show the following characteristics:

Quartz maintains its transparent character in the red-coloured rock. In more strained samples and close to some fracture planes, it readily re-crystallises to subgrains with a polygonal texture (see Fig. 5.3). Locally, the quartz aggregates are cracked and severely micro-fractured, and a dusting of fine-grained reddish material occurs along the fractures.

The quartz crystals are fairly rich in different generations of fluid inclusions. One type, probably of primary magmatic origin, is transparent, with an irregular and relatively angular form. They are generally two-phase inclusions, with the vapour bubble making up less than 10 to 30 % of the inclusion. The later generation inclusions are located in healed, generally planar microfractures. These secondary, rounded, reddish-brown fluid inclusions which are locally also two-phase inclusions are more common in the more altered samples.

Microcline is basically unaltered and preserves its primary, slightly reddish colour. However, in pervasively altered zones and close to some fracture planes, the primary slight reddish colour of the microcline grains is somewhat deepened. For example, in samples Ä3, Ä5, Ä7 and Ä13, incipient decomposition of microcline to extremely fine-grained alteration products, interpreted to be clayish material, have been observed. The alteration occurs preferentially along microfractures and grain boundaries. It is mainly in this fine-grained material that the red staining of microcline occurs. The staining is caused by to dispersed, fine-grained, reddish material interpreted to be Fe-oxyhydroxides (see below). It is notable that samples Ä5, Ä11 and Ä13 exhibit a preferential Fe-oxyhydroxide staining of the albitic stringers of the perthitic microcline.

Plagioclase becomes dull and reddish-brow under petrographic microscope and it loses much of its transparent character (Figs. 5.2 and 5.5). This alteration and clouding increases progressively towards the fracture planes. In some grains, the alteration starts preferentially in the central, primarily more Ca-rich (anorthite rich) parts of the grains. Other grains show the most strong alteration along the grain boundaries.

The alteration involves replacement (transformation) in varying degrees of primary plagioclase by fine-grained *saussuritic* aggregates composed of albite, epidote, calcite, muscovite/sericite or K-feldspar (microcline) and clay minerals (see Figs. 5.2 and 5.3). It is notable that the shapes of the

original grains are basically preserved, as well as traces of the orginal albitic twinning. The brownish to greenish, turbid, extremely fine-grained clayish material occurs in patches and along microfracures.

Locally, the microclinisation produces rather large secondary microcline within the altered plagioclase grains (cf. Fig. 5.3). The stabilisation of K-feldspar before muscovite within the altered granite indicates a rather high activity of K^+ within the hydrothermal solution (e.g. Beane & Titley, 1981, and as shown in chapter 6).

The reddish colour of the altered plagioclase grains is the result of the presence of dispersed, extremely fine-grained to submicroscopic, colloform, probably amorphous Fe-oxyhydroxide/hydroxide ("limonite"), and subordinately some crystallised Fe-oxyhydroxide, tentatively of goethitic composition and structure. No Fe-oxides or Fe-oxyhydroxides were identified by the X-ray diffraction investigation. The very small amount of crystalline Fe-oxyhydroxides was non-detectable without any further laboratory concentration. The limonitic mineraloids (amorphous) could of course not be detected during the XRD runs. It is notable that the dispersed Fe-minerals/mineraloids cause a very strong optical red colouration of the plagioclase.

The backscattered electron (BSE) images show that the increased saussuritisation is followed by an increase in the amount of micropores within the altered grains (see Fig. 5.2). This microporosity could generally not be detected under the polarising microscope (see further descriptions in section 5.1.2).

Biotite breaks completely down to chlorite together with a small amount of exsolved, rounded to elliptical sphene/Ti-oxides grains (biotite → chlorite± Ti-minerals+ K^+). Locally, some symplectitic chlorite and epidote (addition of Ca^{2+} owing to plagioclase breakdown) formed in the biotite pseudomorphs. The liberated potassium participated in the formation of K-feldspar and/or sericite within the rock. The decomposition of biotite also implies some liberation and mobilisation of surplus silica. Vermiculite appears to be a late, low-temperature alteration product of biotite.

Magnetite/Fe-oxides/Fe-oxyhydroxides - In the unaltered samples Ä2, Ä4 and Ä12, euhedral magnetite is the predominate opaque phase. When successively approaching the fracture plane within the altered zones, magnetite is replaced to a continuously larger degree by hematite. The formation of hematite from magnetite shows evidence of a high oxygen concentration in the hydrothermal fluid (e.g. $4Fe_3O_4 + O_2 = 6Fe_2O_3$).

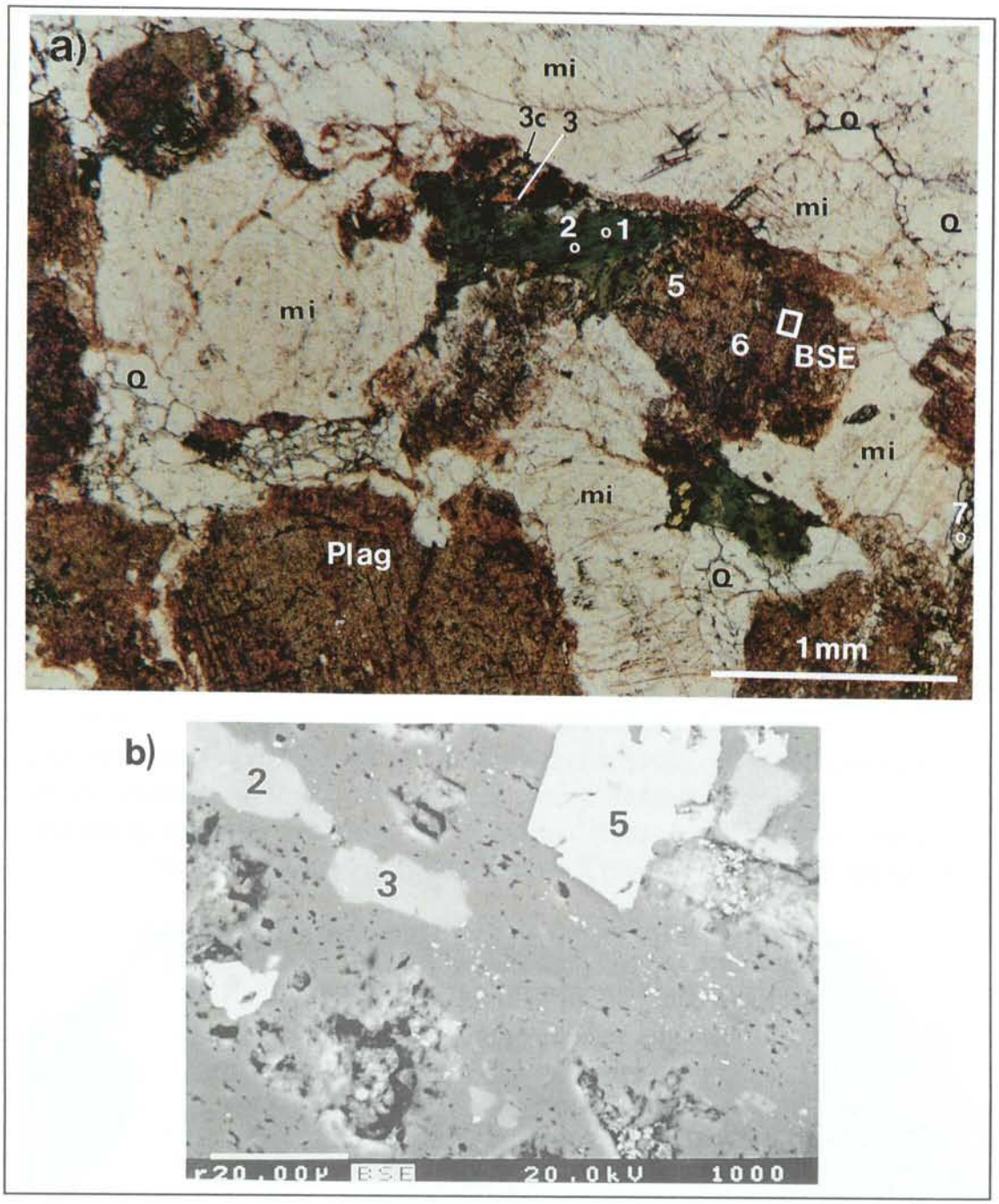

Figure 5.2 ***a)*** *Microphotograph of hydrothermally altered and red-coloured Äspö granite (sample Ä3). Note the cloudy appearance of the altered plagioclase (saussuritic pseudomorphs) and the chlorite pseudomorphs after biotite. The unaltered appearance of quartz (Q) and microcline (mi) is evident. Numbers denote spots analysed by electron microprobe (1,2=chlorite; 3=sphene; 3c,7=epidote; 5.6=altered (albitised) plagioclase, see appendix B for composition).* ***b)*** *BSE image of a severely altered plagioclase in sample Ä3. The BSE area is outlined in Fig. 4.1a. Note the abundant pits (black) and the sub- to euhedral epidote (bright; no.5). The light grey areas (nos. 2 and 3) are secondary K-feldspar, indicating a high* K^+ *activity during the alteration.*

Figure 5.3 *Microphotograph of a deformed, microclinised (Mi) and saussuritic plagioclase phenocryst (Äspö granite, sample Ä7). Note the strong alteration of the along microfractures. At the right and lower left edge of the view is polycrystalline quartz aggregates. The red coluring of the saussuritic plagioclase is partly caused to the pervasive staining of micron-sized Fe-oxyhydroxide. View of field 4.5 mm; cross-polarized light.*

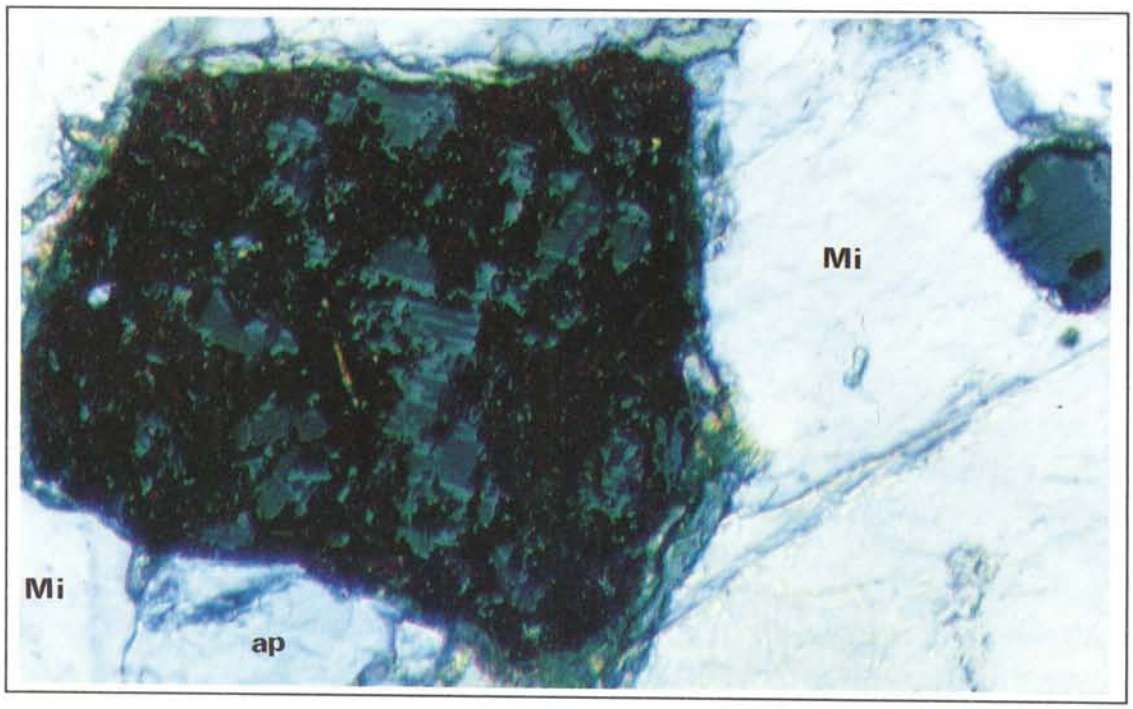

Figure 5.4. *Reflected light photomicrograph (view of field 0.8 mm, crossed polarized light) showing magnetite completely replaced by hematite (sample Ä1; ap= apatite; mi=microcline; c. 2 mm from fracture plane).*

The secondary hematite generally exhibits a patchy distribution within the parent magnetite. In e.g. sample Ä9b, the magnetite to hematiteratio is about 0.5. In the strongly altered rocks (e.g. samples Ä3 and Ä9a), only very minute remnants of magnetite can be found in the hematitised magnetite pseudomorphs. Finally, close to the fracture planes in the strongly oxidised samples (e.g. Ä1, Ä6), hematite completely pseudomorphically replaces magnetite (Fig. 5.4).

The high water activity in the alteration zones along the fracture planes caused a continued local alteration (hydration) which formed peripheral goethite and tentatively "limonite" (amorphous ferric hydroxide: $Fe(OH)_3$/ $FeOOH*nH_2O$) on hematite according to the complex dissolution and reprecipitation reaction (Fischer and Schwertmann, 1975):

$$\underset{\text{hematite}}{Fe_2O_3} + 3H_2O = \underset{\text{goethite}}{2FeOOH} + 2H_2O = \underset{\text{"limonite"}}{2Fe(OH)_3}$$

The red colouration of saussuritic plagioclase is mainly, as stated above, interpreted to be caused by dispersed goethite±limonite±hematite impregnation. Tentatively, these Fe-oxyhydroxide/oxide grains were formed during the saussuritisation by trace amounts of liberated iron *in situ* .

Sphene - There is an increase in the amount of sphene in the altered granite. In addition to the point-counted grains (0.7 to 1.1 vol. %), there are minute, exsolved sphene-Ti-oxide grains or aggregates within the chlorite pseudomorphs after biotite (see further discussion in section 5.1.1).

The increase of the sphene content is interpreted to be the result of the neoformation of relatively large and subhedral sphene crystals. These crystals generally exhibit a lamellar twinning.

Epidote - The variation of the epidote content show no coherent pattern within the altered granite. In some samples, there is a progressive increase towards the fracture plane, whereas other altered sections have less epidote than the protolith (cf. Table 4.1). As seen in section 5.1.1, epidote occurs at three textural settings: *1)* late magmatic epidote occuring together with biotite and magnetite, *2)* epidote in saussuritic plagioclase and *3)* epidote as fillings in microfracture/fractures.

Clay minerals - The clay minerals occur as fine-grained aggregates with a grain size of the individual minerals below the limit of resolution of the polarising microscope. They occur as alteration products of the main minerals (see above), principally at grain boundaries and along microfractures. Primary clayish material (hydrothermal precipitation products) also occur as fracture filling products in e.g. samples Ä3, Ä7 and

Ä10 (see Table 5.1). A slightly reddish colour of the clayish material is interpreted to be caused by staining of, and/or intergrowth with, small amounts of Fe-oxyhydroxide .

Illite and swelling vermiculite were identified whithin the wall rock sample Ä3. The illites possibly represent alteration products from feldspars, chiefly plagioclase. The fracture-filling clays identified by XRD include vermiculite (samples Ä1 and Ä3), smectite (sample Ä3) and smectite-illite (sample Ä7). The fracture-filling smectite in sample Ä7 is also swelling as was noticed when saturating the sample with fresh water.

Vermiculite was identified by X-ray diffractrometry in the whole rock sample Ä3 as well as in fracture filling in samples Ä1 and Ä3. It appears to be an important late alteration product of biotite, as shown under the microscope and indicated by the increased silica content of clayish chlorite (cf. appendix B:4).

Fracture fillings - The fractures investigated in this study comprise both monomineralic and complex mineralised, probably reactivated, fractures. A brief notation of the fracture mineralogy is given in Table 1. Macroscopically, the fracture fillings dark are green because of the greenish epidote and prehnite. The hydrothermal infillings generally show mineral assemblages of successively lower temperature, e.g. epidote±quartz, prehnite+clays, low-T K-feldspar+ flourite and calcite. The fracture-filling flourite crystallised rather late, with grains adjusting to the void created by the shape of the other minerals. Some neoformation of anhedral sphene was noticed in a fracture in sample Ä9.

Sample Ä6 is cut by microbreccia composed of small rock fragments set in matrix rich in granular epidote. This type of thin microbreccias/shear zones were commonly observed during the field investigation at Äspö.

Calcite occurs as late as well as early precipitation products. Often it occurs in the central parts of the fracture infillings. In e.g. the cataclasitic sample Ä8, a calcite vein has penetrated along, and post dates, the earlier clay and FeOOH precipitations (cf. Fig. 5.12). In sample Ä7, monomineralic calcite infillings occur in cross-cutting irregular extensional fractures. Further, in the microbreccia in sample Ä6, euhedral calcite occurs in the tensional voids formed by displacement on the fault. For more details on the fracture-filling mineralogy and the tectonic history of the Äspö granite, see e.g. Talbot & Riad (1987), Tullborg (1989) and Landström & Tullborg (1991).

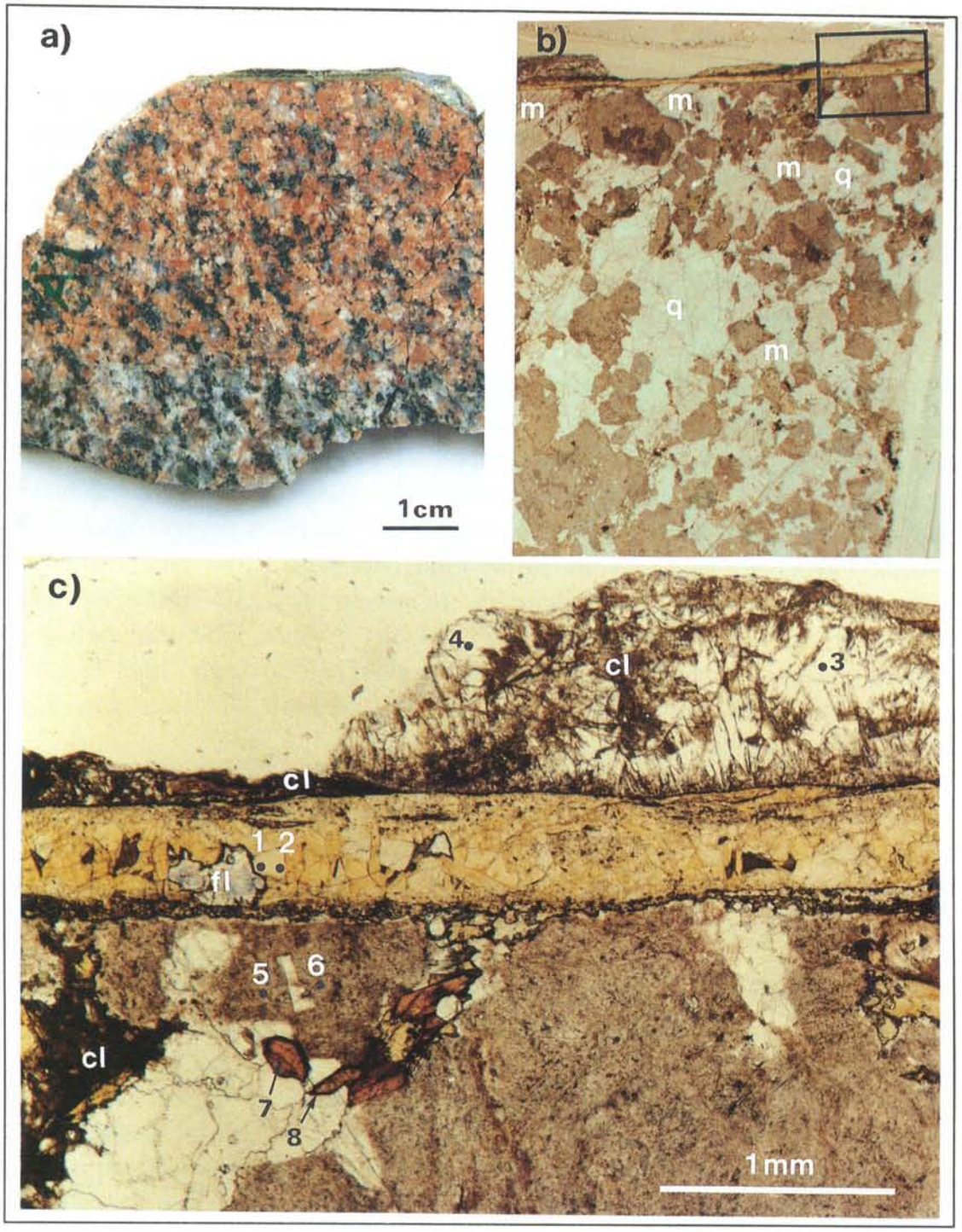

Figure 5.5 ***a)*** *Red coloured Äspö granite passing successively over to the unaltered reddish-grey granite (sample Ä1). Note the fracture plane at the upper part of the specimen with deep green prehnite and light green epidote.* ***b)*** *15 x 20 mm large part of the thin section Ä1 showing red-coloured (clouded) saussurite pseudomorphs after plagioclase and transparent quartz (q) and microcline (m; reddish in hand specimen).* ***c)*** *Photomicrograph of the area outlined in Fig. 5.4b showing the epidote+ prehnite± flourite (fl)± clay (cl; greenish-brown material corroding prehnite)-filled fracture and the altered mineralogy in the wall rock. Numbers refer to spots analysed by microprobe (1,2=epidote; 3,4=prehnite; 5,6=saussuritic plagioclase; 7,8=sphene, see appendix B).*

5.1.2 Mineral Chemistry

In this section, results, of the microprobe investigation are reported and analysed in order to examine the alteration features and processes. Primary and late-magmatic minerals were analysed from samples Ä2 and Ä4 with the purpose of chemically characterising the unaltered minerals (Table 3.1). Minerals from the altered samples Ä1 and Ä3, together with fracture fillings from samples Ä10 and Ä8, were also analysed. The most relevant results of the micro-chemical investigation are listed in appendieces B:1 to B:5.

Plagioclase - The plagioclase in the unaltered granite samples has an anorthite content in the range of about 25 to 31.5 mol. % (oligoclase ±andesine). The highest values are found in a large euhedral, early magmatic phenocryst in sample Ä2 (pos 1 and pos 2 in appendix B:1). An anhedral, late magmatic and very fresh plagioclase crystal in sample Ä2 (analyses F2 pos 3 and 4 in appendix B:1) has values at the lower limit (An 0.24.2 to 0.24.7 mol. %). The plagioclase rims are generally relatively low in anorthite with compositions comparable with the late magmatic crystals. This variation thus reflects the normal magmatic solid-solution composition from "high to low" temperature plagioclase. The K content is low (<1 mol. % Or, cf. Fig. 5.6) in the fresh magmatic crystals.

The "unaltered" plagioclase carries minute inclusions of apatite, zircon and colourless epidote. Saussuritic (albitisised) portions of plagioclase grains exhibit a microporous structure between the albite and newly formed epidote, sericite or K-feldspar and calcite micrograins (Fig. 4.1).

The magmatic plagioclase are basically completely albitised in the hydrothermally altered zones. The newly formed albite is almost of pure end-member composition (cf. Fig.5.6). The altered grains constitute extremely fine-grained, red-coloured saussurite (albite+epidote+calcite± microcline or sericite±smectite-illite mixture) pseudomorphs after the magmatic crystals. Parts of the Ca liberated from the dissolved anorthite ($Ca_2Al_2Si_2O_8$) component participated in the formation of saussuritic epidote and calcite. Most of the surplus Al and Si were mobilised from the altered plagioclase and formed the secondary clay minerals along grain boundaries and microfractures.

The BSE images (Figs. 4.1 and 5.2) show that the altered grains contain numerous small voids (micropores). These are interpreted to be dissolution voids (secondary "fluid inclusions") caused by the removal of the major part of the anorthite component from the plagioclase. The albitisation reactions have thus been accompanied by a volume reduction of plagioclase.

Albitisation of detrital plagioclase is common during burial diagenesis (e.g. Ramseyer et al., 1990). The mobilisation of the anorthite component away from the site of albitisation to adjacent pores and the formation of dissolution voids are the most common processes occurring during low temperature (<160°C), diagenetic albitisation (Morad et al., 1990; Ramseyer et al., 1992). This investigation suggests that albitisation is also an important process during hydrothermal metamorphism at greenschist facies temperatures (300 to 400°C).

It should be noted that there is no detectable difference in the iron content between fresh and altered plagioclase. In some dissolution voids, however a small increase of Fe was noticed when traversing the electron beam over the voids.

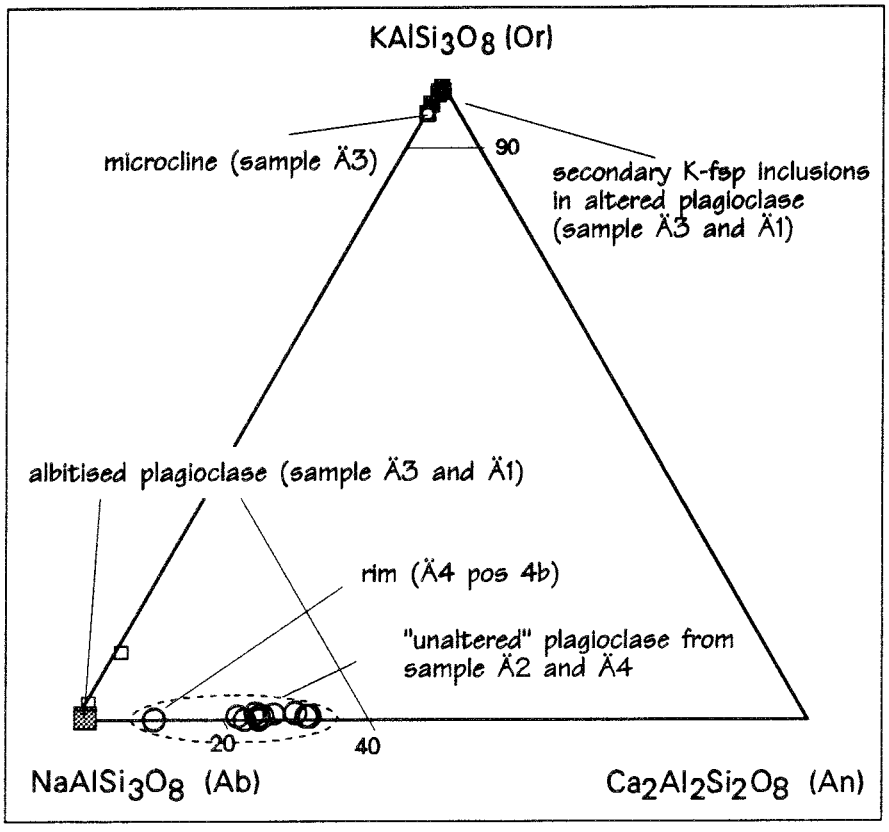

Figure 5.6 *Ternary plot of the end-member composition of unaltered plagioclase (sample Ä2 and Ä4) and hydrothermally albitised (saussuritic) plagioclase from sample Ä1 and Ä3. Also shown are the composition of the tiny hydrothermally produced K-feldspar inclusions and a primary magmatic microcline from sample Ä3. Note the almost pure end-member composition of the hydrothermal albite and K-feldspar.*

Biotite - The biotite compositions are listed in appendix B:2. The biotite has a very homogeneous composition, with an average Fe/Fe+Mg ratio (molar) of 0.42 with a standard deviation, s, of 0.01. The titanium content is rather low (a=1.58 wt. %) with a restricted variation (s=0.08).

Magnetite - The magnetite in the Äspö granite is almost pure Fe_3O_4. The minor constituents Ti, Mg, Mn and Al are generally below the detection limit of the microprobe. This is in accordance with the fact that magnetite in felsic plutonic and metamorphosed rocks commonly approaches nearly pure Fe_3O_4, which is generally attributed to extensive subsolidus/metamorphic re-equilibration on cooling (Frost, 1991 a & b). The absence of the ilmenite component implies that the observed magnetite breakdown did not contribute to the formation of secondary sphene.

Epidote - Although the epidotes analysed have different origins their composition is fairly homogeneous. The Fe_2O_3 content ranges from 12.15 to 17.63 wt. %. There is an indication (the number of analyses is rather small) that the substitution of Fe^{3+} for Al is highest in the late-stage fracture filling epidote (cf. Fig. 5.8). An anhedral rim of a second generation of epidote (Figs. 5.7 and 5.8) also has fairly high iron content. The BSE image in Fig. 5.7 illustrates the commonly occuring anhedral overgrowth rims on the late magmatic, euhedral to subhedral epidote. Saussuritic epidote located within the albitisised plagioclase contain least, but surprisingly high, Fe_2O_3.

The epidote composition presented by Tullborg et al. (1990) and Barnwart et al. (1992) from fracture fillings and wall rocks from Äspö lies within the range of the present analyses. The distinction between fracture-filling and wall rock epidote could, however, not be detected in their data.

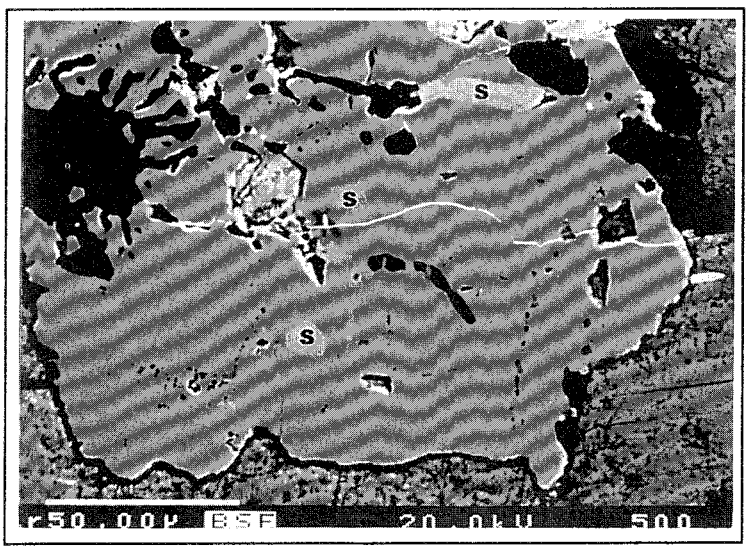

Figure 5.7 BSE image showing euhedral epidote overgrown by anhedral second generation of epidote (Sample Ä2 position 9). Light grey inclusions are sphene (s). Bright microfracture is Ce-rich monazitic epidote. Dark irregular material is plagioclase and quartz.

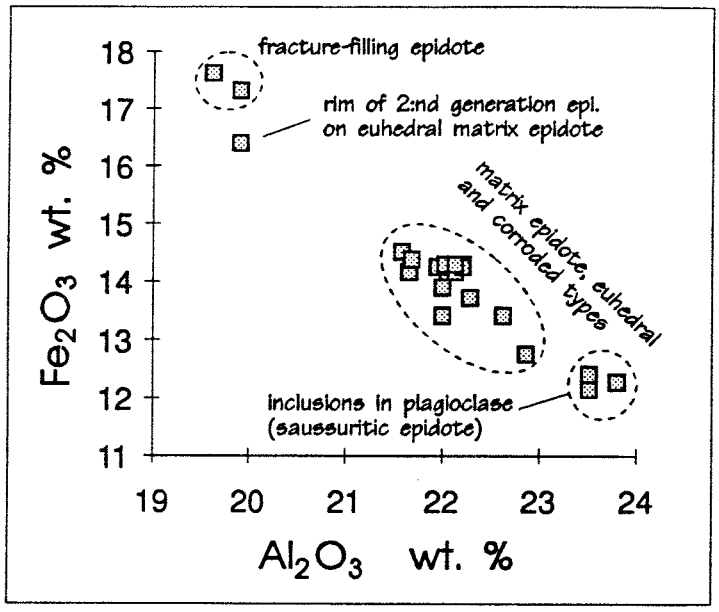

Figure 5.8 *Plot of Fe_2O_3 versus Al_2O_3 of epidotes of different generations from the Äspö granite.*

Chlorite - The chemistry of the analysed chlorites (pseudomorph after biotite) are fairly homogeneous, with an iron and magnesium content in the range of 15.9 to 17.3 wt. % and 17.1 to 18.0 wt. %, respectively (appendix B:3 and Fig. 5.9). The composition of these chlorites are similar to those from altered and red stained granite from Äspö presented by Tullborg et al. (1991) and Barnwart et al. (1992). These wall rock chlorites exhibit FeO/SiO_2 and MgO/SiO_2 trends different from fracture-filling chlorites (cf. Fig. 5.9). The less steep slopes for the wall rock chlorites indicate, according to Duplay (Tullborg et al., 1991, op. cit.), a higher formation temperature than for the fracture-filling-chlorites.

Calcite - Two microprobe analyses were conducted on late-stage fracture filling calcite from sample Ä8. The calcite has a fairly high MnO concentration, 0.70 and 1.13 wt. % ($MnCO_3$ content of 1.7 and 2.8 %). The composition of this late calcite is thus roughly similar to that is given in Barnwart et al. (1992).

Prehnite - are found as fracture-filling minerals in samples Ä1, Ä6, Ä9a, Ä10 and Ä11. In sample Ä1, it occurs as macroscopically deep green fracture coating overlying (Fig. 5.5) light yellowish-green epidote. Chemically, the analysed crystals are very pure, hydrous Ca-Al-silicate (c.f. appendix B:5) without any marked variation in composition.

Sample Ä10 contains a 2 to 3 mm-wide, dilatational fracture opening filled with predominately euhedral and tabular prehnite. These crystals are locally corroded by very fine-grained, clayish material (probably smectites). The latest interstitial mineral is K-feldspar (the crystallisation sequence: prehnite → clay→K-feldspar).

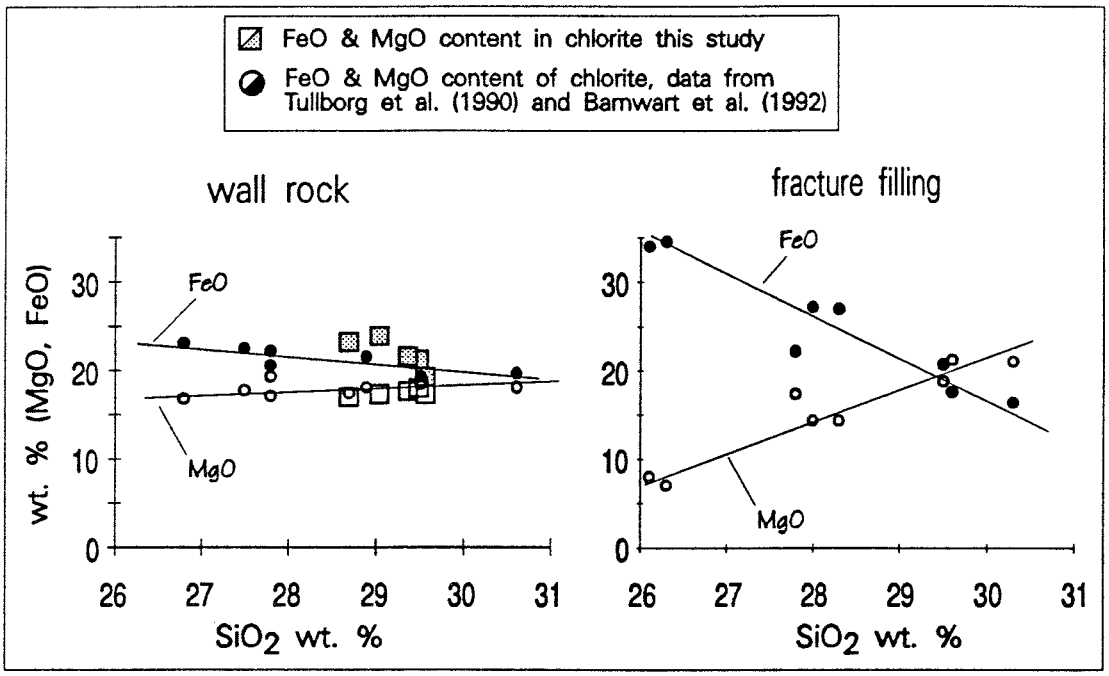

Figure 5.9 Plot of MgO and FeO versus SiO_2 for wall rock chlorites investigated in this study. Shown also are the composition of wall rock as well as fracture filling chlorites presented by Tullborg et al. (1991) and Barnwart et al. (1992).

Sphene - The microprobe investigations show that the euhedral, magmatic sphene crystals in both altered and unaltered granite have discontinuously zoned cores. The BSE image of a sphene crystal from sample Ä1 (Fig. 5.10) shows the patchy zoning texture within the euhedral core and the homogeneous composition of the euhedral to subhedral rim (the darker grey shading on the BSE image is caused by a smaller fraction of backscattered electrons owing to a lower mean atomic number). Paterson & Stephens (1992) interpret the type of zoning which occurs in the cores as being indicative of a magmatic texture.

The quantitative analyses show that the sphene cores are rich in REE and contain up to 1.8 wt% Ce_2O_3 and 2.0 wt% Nd_2O_3 (appendix B:5 and Fig. 5.11a). This would imply, assuming a relatively steep sphene REE pattern, a total content of REE_2O_3 up to 5 - 6 wt %. These cores are thus comparatively rich in REE (e.g. Exley, 1980; Gromet & Silver, 1983). The trivalent REE substitution of Ca is balanced by, for example, the entry of trivalent Fe into the Ti position (appendix B:5 and Fig. 5.11b).

There is an increase of sphene in the altered granite (cf. Table 4.1). The whole rock chemical data show that there has been no addition or long range mobility of titanium in the alteration zone (cf. Table 6.1). This implies that

most titanium necessary for the neoformation of the lamellary twinned, secondary sphene originates from the biotite decomposition.

The occurrence of REE-poor overgrowth rims on the magmatic sphene cores in both macroscopically fresh and altered granite indicate that these rims were formed during an event predating the hydrothermal metamorphism occurring along the fracture planes. Tentatively, the overgrowth rims could have formed from a hypothetical ilmenite component expelled from early magmatic magnetite during the granite solidification.

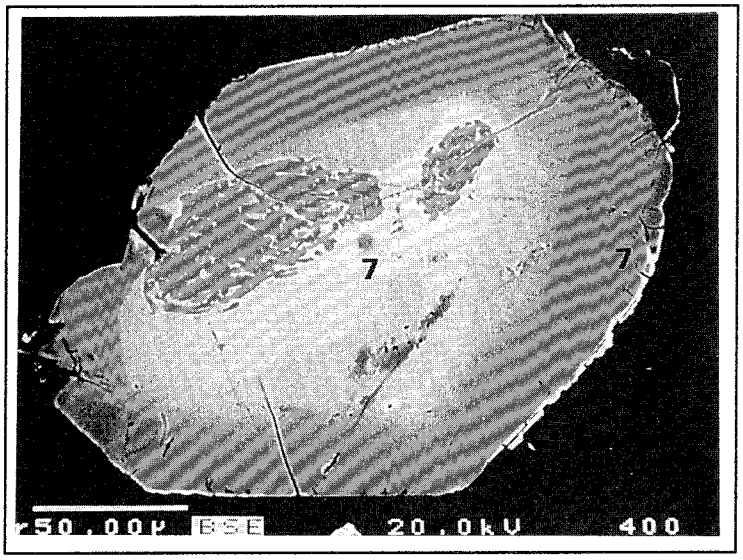

Figure 5.10 *BSE image illustrating the patchy discontinuous zoning in a sphene crystal from sample Ä1 (P7). The bright core (highest average atomic number) is enriched in the REE as compared with the dark grey rim. Numbers (7) refer to spots analysed with microprobe (see appendix B:5).*

A microprobe analysis of a small secondary inclusion within a chlorite pseudomorph after biotite showed that it contained c. 7 wt% Al_2O_3 and only about 26.5 wt % TiO_2 (analysis Ä3 P1 in appendix B:5). This secondary mineral phase is interpreted to be a highly aluminous grothite (a variety of sphene high in Al and Fe^{3+}). The pronounced Al ($\pm$Mg) substitution for Ti is not found in the matrix sphene (Fig. 5.11b). It is notable that the inclusion had a very low REE content (Fig. 5.11a). This type of small, secondary grothitic inclusions are, as stated above, very common in the secondary chlorite. They are formed because the Ti hosted within the biotite is expelled from the chlorite crystal lattice.

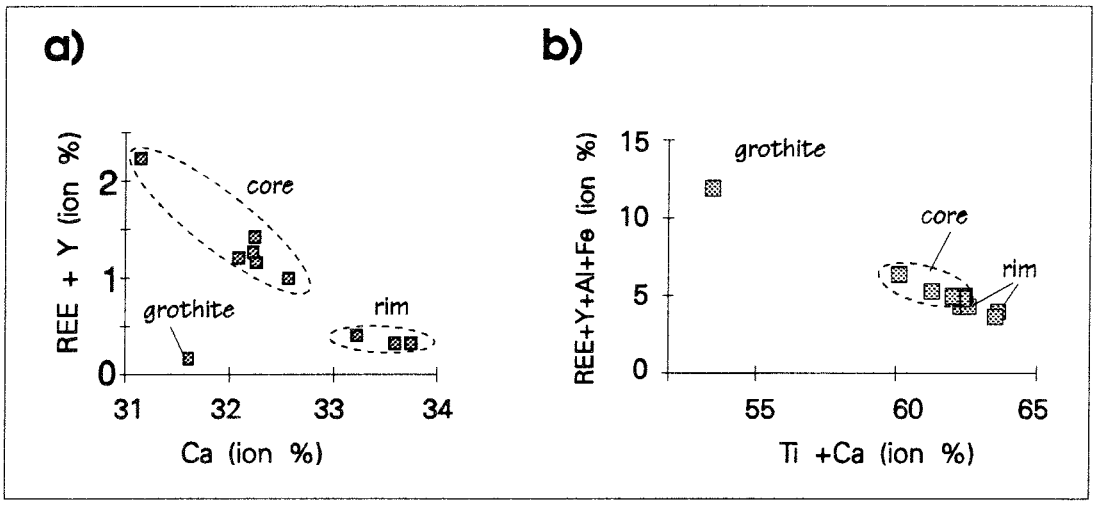

Figure 5.11 *The chemical variation of sphene from fresh (Ä4) and altered (Ä1 and Ä3) Äspö granite.* ***a)*** *shows the substitution of Ca by trivalent REE and Y.* ***b)*** *illustrates the substitution of Ti by Al in the grothite and the substitution of Ti by* Fe^{3+} *magmatic sphene.*

Elemental distribution - The investigation of elemental distribution of Fe and Mn by microprobe scanning over the thin section from sample Ä1 shows that there are no detectable differences in content of these redox sensitive elements between red-stained saussuritic plagioclase and the other relatively fresh salic phases or the uncoloured fresh plagioclase. In the altered granite, Fe and Mn are mainly hosted in the chlorite (±epidote) pseudomorphs after biotite. Some Fe (cf. Fig 5.12) and Mn are redistributed into chlorite-filled microfractures. Otherwise basically *in situ* transformations and neofomations of the mafic Fe-Mn-(and Mg) phases occurred during the hydrothermal alteration.

In the cataclasitic sample Ä8, there is some redistribution of iron from the salic rock fragments into the chlorite+epidote+clay±Fe-oxyhydroxide-rich matrix, and microfractures (cf. Fig. 5.12b). However, as indicated by the whole rock chemistry, there is some gain of iron in the bulk sample. This is caused by the precipitation of Fe-oxyhydroxides from the external fluids along the main conduits. In this sample, the calcite-filled fracture postdates the Fe-oxyhydroxide precipitation (cf. Fig. 5.12b). In the most severely altered parts of the cataclasite, there is an extensive chloritisation and argillitisation of the rock fragments (CR in. Fig. 5.12b).

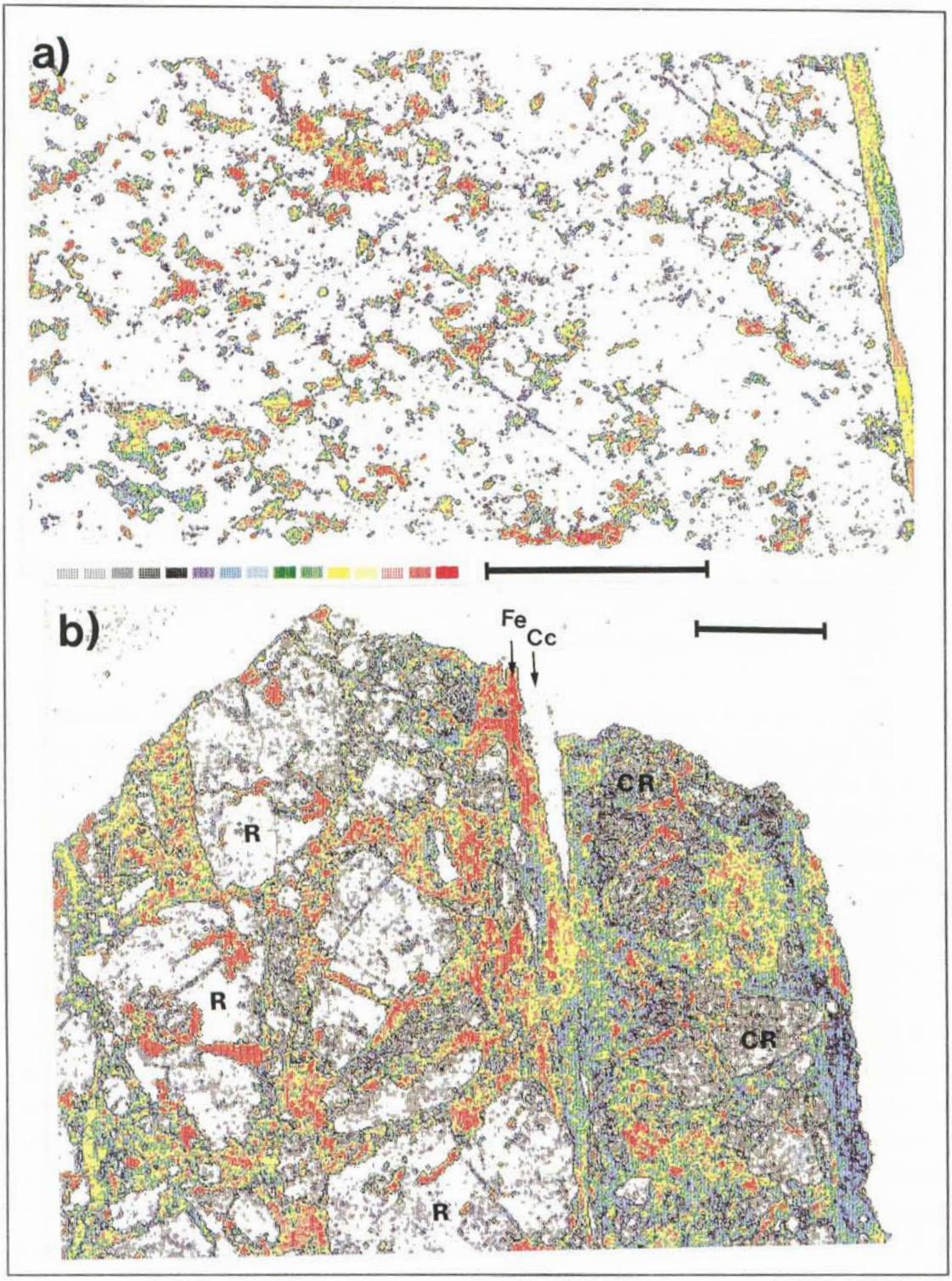

Figure 5.12 *Distribution of Fe in altered and crushed Äspö granite (electron microprobe scanning over the thin sections). The colour scale (X-ray intensity) is proportional to the Fe concentration, with the red colour representing >20-25 wt. % (e.g. chlorite and hematite/Fe-oxyhydroxides).* ***a)*** *shows the uniform distribution of iron in sample Ä1. Scale bar 10 mm. A photograph of the lower left part of a) is shown in Fig. 5.5.* ***b)*** *shows the iron redistribution in the cataclasitic sample Ä8. R= rock fragments; C-R= chloritic and clayish rock fragments: Cc= late, calcite filled fracture; Fe= Fe-oxyhydroxide. Scale bar 2.5 mm.*

5.2 Stripa granite

The mineralogy of the red-coloured Stripa granite is characteristic, although only slightly modified compared with the protolith. The amount of quartz and feldspar is unchanged when going from the fresh into the altered granite (cf. Table 4.1 and Fig. 5.13). However, the degree of saussuritisation of plagioclase increases somewhat in the red-coloured granite. An increase in the abundance of muscovite and a significant decrease of chlorite was observed in the altered granite (Fig. 5.13). There is also a slight decrease in the amount of epidote within the red-coloured granite. A small amount of prehnite is found in the matrix of the altered granite. Thin calcite and muscovite infillings are also found in grain boundaries and as very small patches in the main minerals.

The red colouration of the granite is caused by impregnation of extremely small (generally < 5-10 μm) hematite and, subordinately, Fe-oxyhydroxide grains along *1)* cracks and microfractures, *2)* grain boundaries (Fig. 5.15) and *3)* subordinately within the main salic minerals.

The microscopic investigation of the altered granites shows that secondary chlorite (pseudomorphing biotite at a late magmatic stage) is to a very large degree altered/oxidised to muscovite, hematite and, subordinately, Fe-oxy-hydroxides (chlorite → muscovite+hematite±Fe-oxyhydroxides). In e.g. the red-coloured sample S6, hematite generally forms along the cleavage plane within the muscovitised chlorite grains (Fig. 5.15). Oxidised and re-precipitated iron liberated during the muscovitisation is interpreted to be the cause of the red colouration of the granite.

The small size of the Fe-oxyhydroxides makes optical identification difficult. Generally they are red to orange-yellow and appear colloidal, anhedral with probably an amorphous structure. However, some grains are crystalline with a platy, very thin euhedral to subhedral habit. They lack the characteristic lepidocrocitic pleochroism and are interpreted to be goethite. In contrast, the large hematite grains formed within chlorite were easily identified in reflected light. Furthermore, the observed mineralogy may well be a result of goethite dehydration giving hematite (Deer et al., 1974).

In general, the grain size is somewhat reduced, the texture is more granular, and the fracture frequency is increased in the altered granite (Fig. 5.14). Furthermore, the individual minerals are also more fractured. There is thus a positive correlation between the degree of alteration and deformation.

The deformation observed among the samples investigated is inhomogeneous and concentrated to thin zones (microshears/microfractures). In these shear

zones, often with a somewhat irregular orientation, the granite is fine-grained granular, chloritised and muscovitised. Furthermore, quartz is highly strained and exhibits a pronounced undulatory extinction and sub-grain formation. Along and within these microshears are feldspars altered to fine-grained aggregates, interpreted to be partly clayish material.

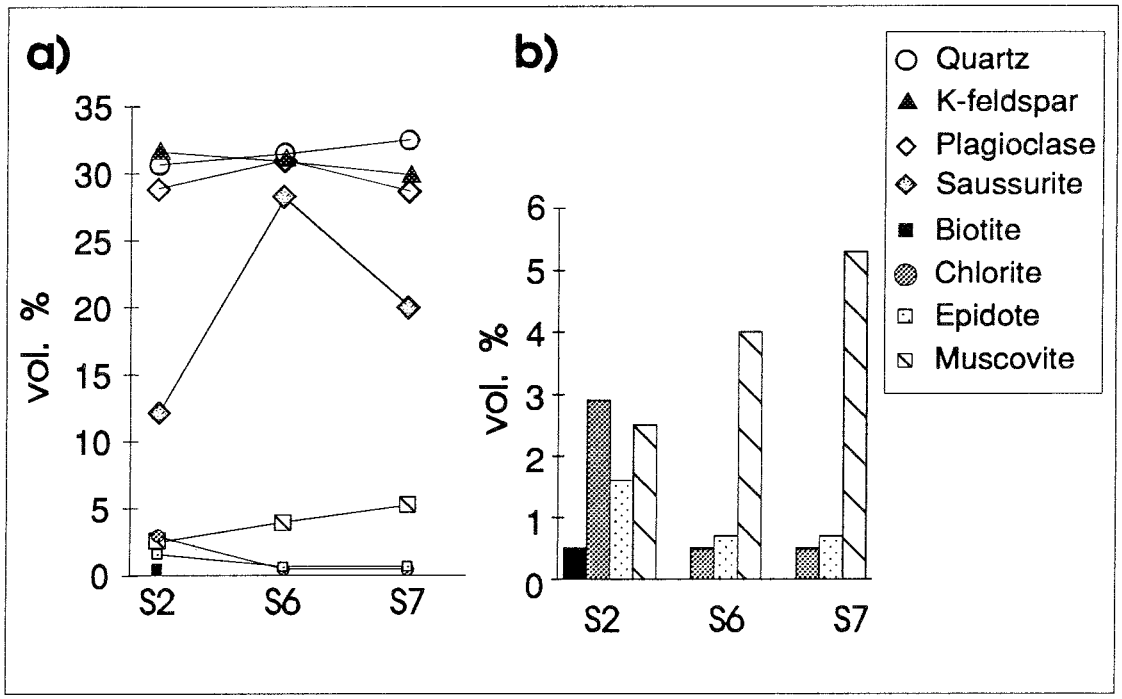

Figure 5.13 ***a)*** *Modal composition of grey unaltered (S2), slightly reddish (S6) and deep red (S7) Stripa granite.* ***b)*** *Histogram showing the abundance of the minor phase shown in a). Note the decomposition of chlorite and increase of muscovite in the red-coloured samples.*

Fractures were generally avoided during the sampling and sample preparation, as the aim of the work was to describe the mineralogy and measure the petrophysical properties of intact rock. However, a few thin quartz, epidote and prehnite sealed fractures were found in the thin sections. According to Gale et al. (1990) chlorite is the most abundant "primary" fracture mineral, followed by epidote and calcite, while epidote is the most abundant "secondary" fracture filling. In addition, quartz, hematite, prehnite and fluorite have been identified as subordinately occurring primary fracture minerals (Carlsten, 1985; Gale et al. 1990).

The mineralogy of the grey, porous granite from borehole D5 is not a subject of the present investigation. However, the general conclusion by Carlsten (1985) that quartz dissolution is the major cause of the porosity is also valid for the porous granite from core D5. The mobility of SiO_2 is e.g.

indicated in sample S18, where large, up to 3-4 mm, mono-crystalline, strain-free, euhedral quartz crystals occur at the walls of a void.

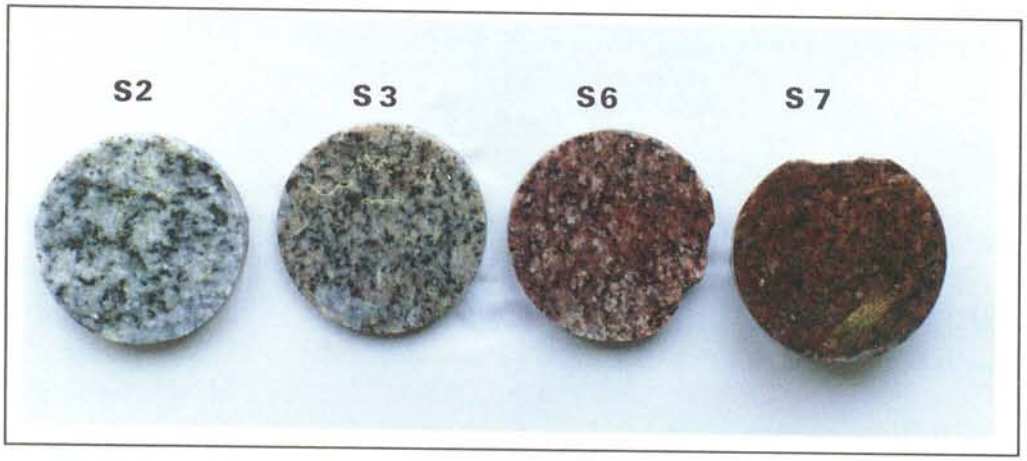

Figure 5.14 *Four samples of Stripa granite illustrating the gradual red coloration in drill-hole D3 (core diameter 60 mm).*

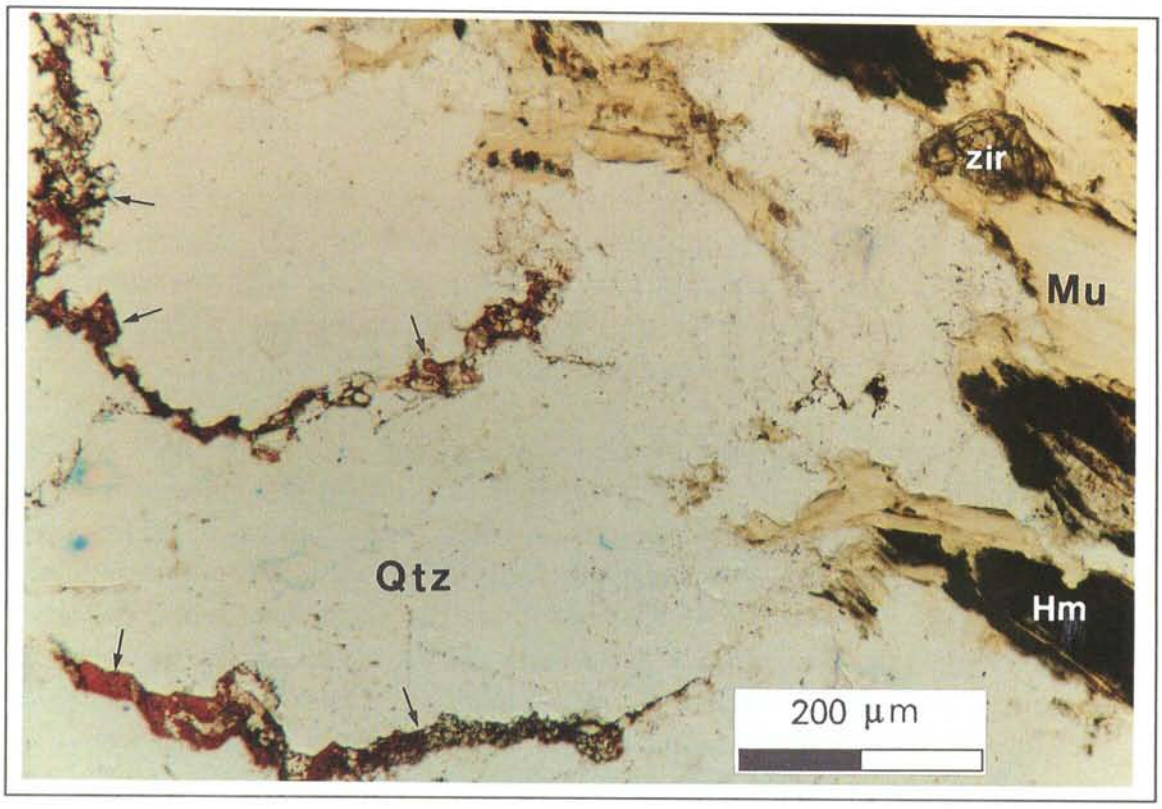

Figure 5.15 *Microphotograph of altered and red-coloured Stripa granite (sample S6) showing hematite and Fe-oxyhydroxide (reddish-brown; small arrows) precipitation along grain boundaries and microfractures in a quartz aggregate (clear areas, Qtz) close to a muscovitised (Mu) chlorite. Note the formation of secondary hematite (Hm) and Fe-oxyhydroxide in the chlorite pseudomorph. zir=zircon, Plane polarised and converging light.*

5.3 Bohus granite

The alteration profile/weathering rind of samples B1 to B3 have a 1 to 5 mm thick, greyish-white, "bleached" outer (exterior) zone. The bleached appearance of this zone is caused by the white colour of the altered plagioclase. The other minerals remain basically unchanged. Further into the rock, and partly superimposed on the bleached (plagioclase weathered) zone, a reddish-brown, 10 to 50 mm wide, Fe-oxyhydroxide stained zone occurs (Fig. 5.16).

Under the petrographic microscope, the white colouring is seen as a replacement (transformation) of the fine-grained saussuritic/sericitic patches of the hydrothermally (high-temperature) altered plagioclase grains to extremely fine-grained, low-birefringence (probably partly amorphous), argillaceous material (microaggregates). The formation of clay minerals also occurred along microfractures in the plagioclase grains (Fig. 5.16).

No major alteration related to the low-temperature weathering could be observed under the petrographic microscope of the main minerals quartz, microcline, biotite and muscovite. However, some biotite loses its olive-green to brown colour and becomes lighter and less pleochroic.

It is notable that parts of plagioclase grains unaltered by previous high temperature processes (saussuritisation) are often unaffected by the weathering-induced argillitisation. This shows that the argillitic transformation processes principally affected the small-sized minerals, presumably principally the albite grains, in the micro-porous, saussuritic portions of the plagioclase grains, which further suggests that the increased intracrystalline porosity in the altered plagioclase grains facilitated the diffusion processes (e.g. Na^+ outward H^+ and H_2O inward) as well as increased the relative surface area of the minerals (higher water/mineral ratio).

The weathering of albite before the other silicates agrees, with the general alterability sequences obtained from field, experimental and theoretical studies (Nahon, 1991). In the plagioclase series, the calic plagioclase is the most alterable during weathering (e.g. Nahon, 1991). However, as discussed above, the alteration of albite before the more calic plagioclase was probably facilitated by the microporous texture.

The slight lowering of the magnetic susceptibility in the bleached zones (see section 8.3) indicates that there is some decomposition of magnetite. Despite the very small area of the bleached part of the thin section, the microscopic study showed that most magnetite persists all the way to the external surface

of the weathered granite. However, it should be noted that some magnetite grains exhibit an incipient peripheral alteration within the bleached zone. The extremely low content of opaque phases in sample B1 made it impossible to reveal whether the lowering of the susceptibility was a result of the breakdown of magnetite.

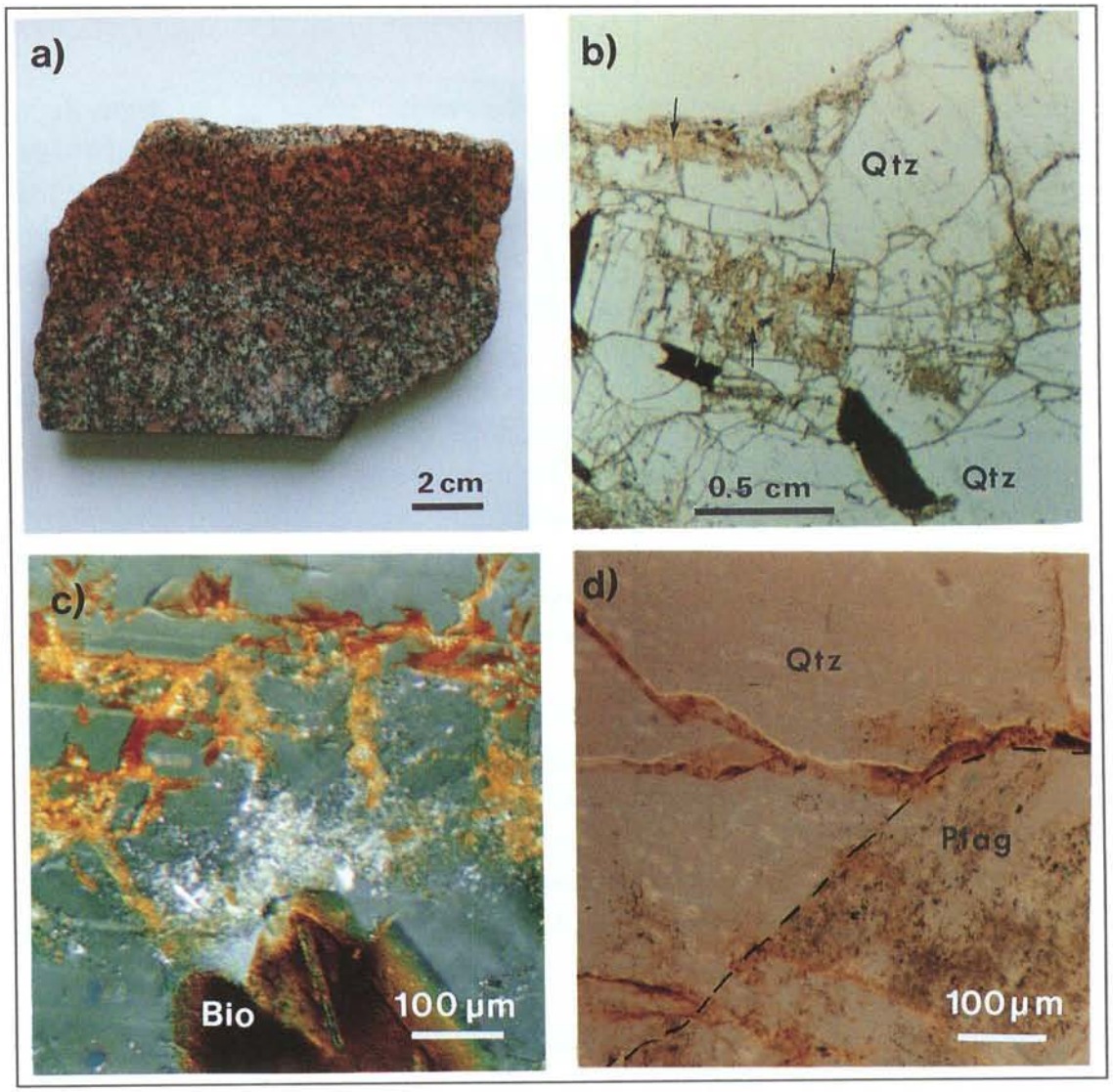

Figure 5.16 *a) Zonal alteration/weathering profile in the Bohus granite sample B1. Microphotographs b) of bleached exterior part of sample B1. Note the pervasive microfracturing of the granite and argillitic alteration of plagioclase (black arrows). External surface at top of view. Plane-polarised light. c) Fe-oxyhydroxide staining within slightly altered plagioclase in the reddish-brown zone. Cross-polarised and converging light. d) Fe-oxyhydroxide staining within microfractures. Plane-polarised light.*

In the *reddish-brown zone,* the colouration is caused by a fine powdering of orange to reddish-brown, translucent to semi-translucent minerals at: ***1)*** grain boundaries, ***2)*** microfractures and ***3)*** sericitic/saussuritic and argillitic patches of altered plagioclase grains (Fig. 5.16). The orange to reddish-brown, submicroscopic material is interpreted to be partly amorphous Fe-hydroxide minerals (limonite) and perhaps some goethite. These types of Fe-oxyhydroxides typically form under conditions of low temperature and low pressure during weathering processes (Deer et al., 1974).

The texture is unchanged over the weathering profile. However, samples B1 to B3 all exhibit a clear increase in the amount of "grain boundary" microfractures in the bleached zone and red-coloured zones.

It should be noted that, under the petrographic microscope, the salic minerals, except some plagioclase grains, maintain their transparent character within the brownish-red coloured rock. However, the above described dusting along microfractures and grain boundaries cause the macroscopic colouring of the rock. It is notable that there are no signs of any hydrothermal metamorphism/alteration (no high-temperature hydrated *metamorphic* minerals such as epidote, chlorite etc.) predating the low-temperature weathering profile along the fracture plane at sample B1 or in the surface weathering rind.

In conclusion, the weathering of plagioclase in the bleached zone and the precipitation of Fe-oxyhydroxides in the brownish-red zone, within the weathering rind of the glacial polished rock surface (samples B2 and B3), were developed by water-rock reactions during the last 12,000 years at atmospheric conditions. The alteration zone along the hydraulically open fracture (sample B1) exhibits the same alteration features as the granite in the weathering rind. The somewhat wider alteration zone along the fracture is caused by a longer period of water-rock interaction and/or larger water/rock ratio.

6. WHOLE-ROCK GEOCHEMISTRY

The aim of this section is to evaluate the chemical changes that accompany the mineralogical modifications. The geochemical study must be considered as preliminary because there are relatively few whole-rock analyses and most of the observed chemical modifications are minor (Table 6.1). This implies, although the investigated rocks are rather homogeneous, that a greater number of analyses would help to reveal (statistically more reliably) the natural chemical variability within the fresh protolith and altered rock. In addition, analyses of e.g. feldspar-hosted, "mobile" trace elements such as Ba, Rb and Sr, as well as "immobile" trace elements such as Hf, Zr, Ta, REE etc., would be very useful when evaluting the alteration processes.

During hydrothermal metamorphism, in contrast to the normal situation during regional or contact metamorphism, fluids pass through/penetrate the rock. These fluids can remove and/or add components to the rock, giving rise to metasomatic processes. Thus water-rock reactions adjacent to the fractures could have resulted in open system rock transformations.

A comparison of chemical analyses of the granitic rocks and their hydrothermal alteration products can demonstrate apparent variation in elemental concentrations. During the alteration, the abundance of a chemical component may change by: ***1)*** real gain or loss, ***2)*** dilution with addition of other components, ***3)*** concentration with leaching of soluble components, or ***4)*** change in rock volume (e.g. Gresens, 1967; Studemeister & Kilias, 1987). In this study, the mass balance equation of Gresens (1967) was used to compare element concentration in fresh and altered granites. The compared sample pairs and sequences are listed in Table 6.2. Samples Ä8 and B2:0 are not included in the calculation because of a lack of density data.

The mass balance equation of Gresens (1967) takes into account changes in rock volume and specific gravity. The gain or loss in the abundance of component *i* is, according to Gresens (1967):

$$\Delta X_i = 100((F y_i \beta/\sigma)-x_i), \quad (1)$$

where ΔX_i is changes in abundance in g/100 g of parent rock; x_i and y_i are the weight fractions of component i in fresh granite and alteration product, respectively; σ and β are the specific gravities of altered and fresh granite, respectively; and F is the volume factor (for more details, see Gresens 1967).

The volume factor is determined by first establishing the immobile behaviour of two or more components, and then solving equation (1) for F by

substituting $\Delta X=0$ for the immobile components. As seen in Table 6.1, the Al_2O_3 to TiO_2 ratios are rather uniform in each granite studied, suggesting minor mobility during the hydrothermal alteration. Thus, the volume factor for each comparison was estimated by solving equation (1) for F, substituting $\Delta X(Al_2O_3)=0$, repeating the calculation for TiO_2, and then taking the average of the two solutions. The mass balance calculations were thereafter conducted by comparing fresh and altered granite. The results of mass balance calculations are listed as gain or loss in g/100 g of each element in relation to unaltered protolith (Table 6.2).

The composition of all samples analysed is plotted on the igneous spectrum diagram of Hughes (1973) in Fig. 6.1 and on a conventional A'KF diagram (Fig. 6.2). The diagram by Hughes was developed to separate altered from unaltered samples, based on their Na and K content. Unaltered igneous rocks are believed to plot inside the broad zone outlined in the diagram. The A'KF diagram is useful for illustrating hydrothermal chemical modifications of igneous rocks.

6.1 Äspö granite

Although the mineralogical modifications of the altered Äspö granite samples are important the chemical modification of the red-coloured granites are rather small when compared with the unaltered protolith.

In the igneous spectrum diagram (Fig. 6.1), the samples from the Äspö tunnel plot in a restricted area in the granite (rhyolite) field within the "igneous spectrum", indicating no major Na or K mobilisation. An exception is the position of the strongly fractured and altered sample Ä8, which indicates some degree of potassic alteration. However, the position of the altered samples on the A'KF diagram (Fig. 6.2) show some degree of K enrichment. This K gain is not directly evident on the igneous spectrum diagram, as Na is also enriched in the altered granite (c.f. Tables 6.1 and 6.2 and the slightly higher Na_2O+K_2O value of the altered samples in Fig. 6.1). It is notable that the iron content ($\approx$F in Fig. 6.2) is basically unchanged when going from fresh into reddish altered granite.

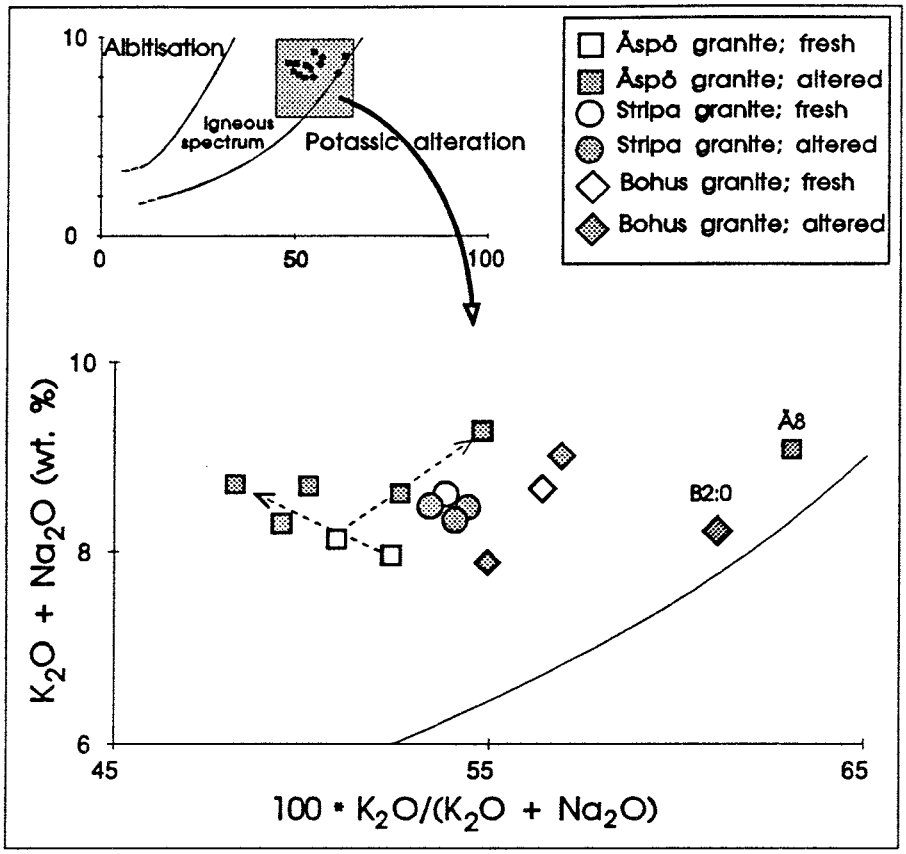

Figure 6.1 The igneous spectrum diagram of Hughes (1973) with plots of fresh and altered rock samples from Äspö, Stripa and the Bohus granite. Thin dashed arrows connect sample pairs of less than 0.4 m spacing (Ä3-Ä4 and Ä11-Ä12).

The results of the mass balance calculations (Table 6.2) mirror the observed mineralogical alterations (transformation, dissolution and neoformation). The elements Na and K hosted in the secondary phases' albite, sericite and microcline have been added, although in highly varying amounts, to the altered granite. The gain of potassium and sodium are up to 26 and 22 %, respectively.

Calcium displaced during the breakdown of oligoclase is mainly found in the secondary phases epidote, calcite and prehnite disseminated in the matrix and microfractures *within* the altered granite. However, as seen from the mass balance calculations, up to 20% of the calcium have been *lost* from the altered granite. Tentatively, parts of the leached calcium may has been re-precipitated as the Ca-rich fracture fillings calcite, epidote and prehnite within the brittle fracture network.

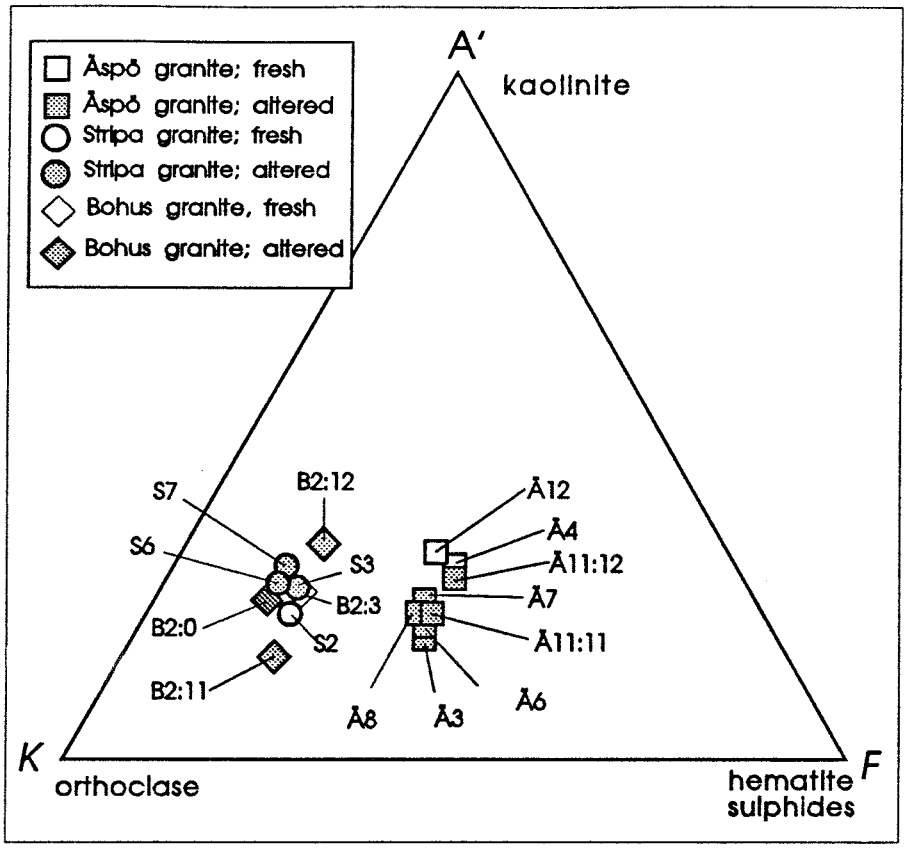

Figure 6.2 A'KF diagram (molecular proportions $A'=Al_2O_3-(Na_2O+K_2O)$; $K=K_2O$; $F=FeO_{tot}+MgO+MnO$) for fresh and altered equivalents of granite samples analysed. The diagram illustrates the roughly similar chemical composition of altered and fresh granites.

The chemical data clearly show that the alteration of the Äspö granites involved net gains of the volatile component H_2O and possibly CO_2 (H_2O+ in Tables 6.1 and 6.2). There is evidence for the introduction of CO_2 in the formation of calcite in altered plagioclase, as well as the common occurrences of calcite in microfractures.

In samples Ä3, Ä6 and Ä7, there is an increase of the trivalent iron accompanied by a decrease in ferrous iron compared with the granite protolith. In contrast, the chemical data for sample Ä11:1 and Ä11:2, from the red-coloured zone adjacent to a fracture in the fresh granite Ä12, show no indication of oxidation. However, the microscopic investigation shows a rather pervasive oxidation of magnetite to hematite within the red-coloured zone. This observation is also strengthened by the susceptibility investigation (see section 8), which shows a notable lowering of the magnetic susceptibility (decomposition of magnetite) of the altered granite. This indicates that the Fe^{2+}/Fe^{3+} determination may be somewhat unreliable.

Table 6.1 Chemical analyses (wt. %) of fresh (F) and altered samples from Äspö (Ä3-Ä12), Stripa (S3-S7) and the Bohus granite (B2:0- B2:3).

Sample	Ä3	Ä4 F	Ä6	Ä7	Ä8	Ä11:1	Ä11:2	Ä12 F	S2 F	S3	S6	S7	B2:0	B2:11	B2:12	B2:3 F
SiO_2	66.40	68.18	68.77	68.62	67.04	69.48	69.20	69.26	74.38	74.24	73.59	73.86	75.36	73.90	73.25	73.63
TiO_2	0.30	0.31	0.28	0.29	0.34	0.26	0.28	0.27	0.07	0.07	0.07	0.07	0.11	0.13	0.11	0.12
Al_2O_3	14.41	14.62	13.79	14.46	14.69	14.23	14.55	14.41	13.27	13.51	13.31	13.77	12.73	13.18	13.53	13.70
Fe_2O_3	1.37	0.97	0.93	1.35	1.30	0.52	0.59	0.67	--	0.01	0.57	0.07	--	0.26	0.20	0.12
FeO	1.17	1.33	1.11	1.11	1.45	1.43	1.61	1.45	1.00	0.94	0.45	0.78	0.83	0.89	0.89	1.00
MnO	0.07	0.06	0.05	0.05	0.05	0.05	0.06	0.05	0.03	0.03	0.03	0.03	0.04	0.06	0.06	0.06
MgO	0.78	0.79	0.73	0.58	0.77	0.59	0.72	0.61	0.05	0.05	0.04	0.06	0.05	0.07	0.07	0.09
CaO	2.94	3.78	2.66	3.08	3.64	2.52	3.08	3.22	0.70	0.70	0.70	0.84	0.84	0.98	0.84	1.12
Na_2O	4.19	3.99	4.08	4.33	3.35	4.51	4.19	3.79	3.97	3.95	3.83	3.86	3.20	3.88	3.62	3.78
K_2O	5.08	4.14	4.53	4.36	5.72	4.20	4.10	4.17	4.63	4.53	4.51	4.61	5.02	5.13	4.38	4.89
H_2O-	0.08	0.03	0.03	0.07	0.07	0.03	0.09	0.05	0.08	0.00	0.03	0.05	0.10	0.04	0.02	0.04
H_2O +	2.13	0.77	1.25	1.26	1.42	1.03	1.20	0.58	0.61	0.69	0.65	0.92	0.77	0.42	0.59	0.54
Total	98.92	98.97	98.21	99.56	99.84	98.85	99.67	98.53	98.79	98.72	97.78	98.92	99.05	98.94	97.56	99.09
Fe/Fe_{tot} (1)	0.54	0.42	0.46	0.55	0.47	0.27	0.27	0.32	0.00	0.01	0.56	0.08	0.00	0.23	0.18	0.11

(1) $Fe_2O_3/(Fe_2O_3 + FeO)$;

Table 6.2 Results of mass balance calculations (Gresens, 1967of sample pairs and sequences from the Äspö, Stripa and Bohus granites. Gain and loss in g/100 g in relation to unaltered reference sample (*F*) .

Sample pair	Ä3 →Ä4*F*	Ä6 →Ä12F	Ä7 →Ä12F	Ä11:1 →Ä12*F*	Ä11:2 →Ä12*F*	S3 →S2*F*	S6 →S2*F*	S7 →S2*F*	B2:1 →B2:3*F*	B2:2 →B2:3*F*
SiO_2	0.22	-0.17	-3.17	2.03	-1.65	-0.81	-0.91	-1.88	-1.12	3.44
TiO_2	0.00	0.01	0.01	0.00	0.00	0.00	0.00	0.00	0.01	0.00
Al_2O_3	0.23	-0.56	-0.48	0.19	-0.19	0.12	0.02	0.25	-0.77	0.53
Fe_2O_3	0.45	0.27	0.64	-0.14	-0.09	0.01	0.58	0.07	0.14	0.09
FeO	-0.13	-0.34	-0.39	0.02	0.13	-0.07	-0.56	-0.24	-0.13	-0.06
MnO	0.01	0.00	0.00	0.00	0.01	0.00	0.00	0.00	0.00	0.00
MgO	0.01	0.13	-0.05	0.00	0.10	0.00	-0.01	0.01	-0.02	-0.02
CaO	-0.76	-0.56	-0.26	-0.65	-0.21	-0.01	0.00	0.13	-0.16	-0.24
Na_2O	0.33	0.31	0.39	0.85	0.31	-0.06	-0.15	-0.18	0.03	0.03
K_2O	1.10	0.39	0.03	0.14	-0.17	-0.14	-0.13	-0.10	0.15	-0.29
H_2O+	1.44	0.69	0.64	0.48	0.60	0.07	0.04	0.30	-0.13	0.08
F [1]	1.05	1.02	0.97	1.03	0.99	0.99	0.99	0.99	0.99	1.04

[1] F = volume factor; the average of the volume factors estimated for Al_2O_3 and TiO_2.

6.2 Stripa granite

Four samples of different degrees and types of red colouration from drill-core D3 were analysed for their major element composition (see Fig. 5.14). The unaltered (sample S2) as well as altered granite samples (S3 to S7) from Stripa have very high and restricted silica contents, and corresponding limited range in the other major elements (Tables 6.1 and 6.2). The highly felsic character of the granite is also shown by the very low content of the compatible elements Mg and Ti. The Stripa samples, as well as the Äspö and Bohus granite, plot in the field of unaltered granite on the igneous spectrum diagram (Fig. 6.1).

As indicated on the igneous spectrum diagram and on the A'KF diagram (Fig. 6.2), there is no major mobilisation (depletion or enrichment) of the alkali elements K and Na within the altered granites. The degree of oxidation of the red-coloured sample S6 contrasts with the values for its unaltered equivalent (S2) in having a significantly higher $Fe_2O_3/FeO+Fe_2O_3$ ratio (cf. Table 6.1). The total Fe content is basically similar in all samples (cf. Figs. 6.2 and 6.3).

The microscopic investigation of the altered granites showed (see section 5.2 and Fig. 5.12) that *in situ* formation of Fe-oxyhydroxides and hematite

occurred during the muscovitisation of chlorite. This transformation can thus be a retrograde process of the somewhat similar prograde reaction suggested by Morton & Nebel (1984):

$$\text{muscovite} + (Fe+Mg)^{2+} + \text{quartz} + H_2O = \text{chlorite} + K^+ + H^+ + H_4SiO_4$$

However, in the present case, oxidised conditions prevailed and the ferrous iron liberated was oxidised incorporated mainly in ferric oxides/hydroxides and in oxidised muscovite. Furthermore, the water activity was also low while, as shown by the calcite impregnations in the altered Stripa granite, the CO_2 activity was relatively high.

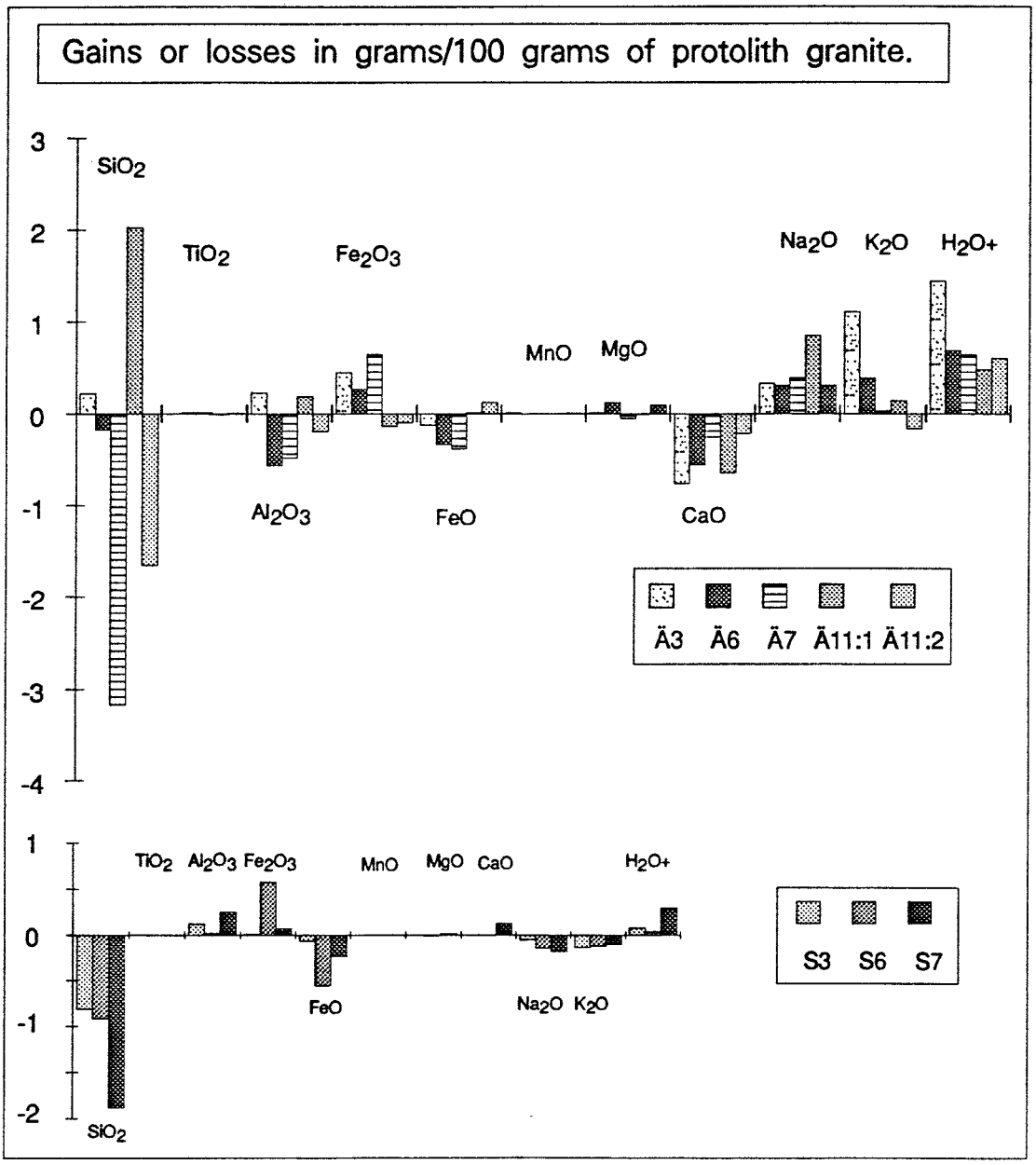

Figure 6.3. *Histogram showing the chemical alterations of the Äspö (Ä) and Stripa (S) granites. Mass balance calculations according to Gresens (1967).*

The mass balance calculations show that the alteration of the granite involved a slight net loss of SiO_2, Na and K and an oxidation of iron. Compared with the hydrothermal alteration along the fracture planes at Äspö, the red-coloured Stripa granite is much less hydrated (cf. Fig. 6.3). The slightly increased CaO and H_2O (CO_2) contents in sample S7 are caused by calcite impregnation along grain boundaries and in microfractures.

6.3 Bohus granite

The basically constant mineralogy from the interior fresh granite to the bleached exterior zone explains the unchanged chemistry of the sub-samples from the traverse over the weathering rind.

The indication of a slight "potassic" alteration within the exterior bleached part (B2:0) of the weathering rind is a reflection of the incipient argillitic alteration (loss of Na) of the altered plagioclase grains (breakdown of the albite in the saussuritic patches?). The chemical index of alteration [$(Al_2O_3 / (Al_2O_3+CaO+Na_2O+K_2O))*100$], CIA, of Nesbitt & Young (1982) shows rather small variations (49 to 52) between the fresh and altered rocks. This value ranges from about 50 for unweathered silicic crustal rocks to about 100 for severely weathered residual clays, showing that the weathering profile is fairly immature without any major removal of alkali or alkaline earth elements.

As seen in Table 6.1, the granite is somewhat more oxidised in the red-coloured zone (B2:11 and B2:12). The bleached exterior zone (B2:0) is somewhat lower in total iron. This could perhaps be the result of mobilisation of some iron from the exterior zone by oxidised acid water (dissolved organic acids) and re-precipitation of iron as ferric compounds in the red-coloured zone. However, because of the scarce amount of data, it cannot conclusively be shown that mobilisation of iron occurred.

7. DENSITY AND POROSITY

The density of an igneous rock depends primarily on the type and proportion of individual minerals and the porosity of the rock. Consequently, hydrothermal alteration and weathering change the density of the rock if the new mineral assemblage has a density different from the protolith. Microfracturing and formation microporosity in minerals and along grain boundaries also loosen up the rock and decrease its density and strength. Thus, an increase in porosity and decrease in bulk density is an indication of lower strength and increased deformability (weakness) of the rock.

The porosity and density data of all samples and sub-samples investigated in this study are listed in appendieces A1 to A3 and displayed in Figs. 7.1 to 7.3. In the cases in which the individual Äspö and the Bohus granite samples consisted of more than one single rock lump, the measured density and porosity data are presented for each piece. This is done in order to visualise the heterogeneity within different parts of the rock. In contrast, as the susceptibility measurements were conducted on the homogenised rock-powder, only this single value is given for each sample (see chapter 8).

A presentation and a general interpretation of the petrophysical data for each rock studied is given below. Furthermore, a brief comparison with previously published petrophysical data on the granites investigated is also presented.

7.1 Äspö granite

Specimens of the fresh, unaltered monzogranitic protolith (samples Ä2, Ä4 and Ä12) show very homogeneous *density* values in the range of 2672 - 2691 kgm^{-3} (average, a=2681 kgm^{-3}). Densities of the altered granite facies are lower (a=2651 kgm^{-3}) and somewhat more heterogeneous (standard deviation, s=17.5), as compared with the unaltered granitic protolith (Fig. 7.1 and appendix A:1).

The *porosity* values of the unaltered wall rock granite at Äspö fall in a rather narrow range of 0.13 to 0.20 % (a=0.17). The altered rocks have values in the range of 0.15 to 0.83 % (a=0.35 and s=0.18). It is notable that the different rock pieces of the individual samples of the *altered* rocks exhibit large variations in porosity (Fig. 7.1). This is interpreted to be a result of the heterogeneous distribution of open microfractures.

The highest possible density difference between the rock and poor-void material (intact granite and low density gas, respectively) is about 2.68. As

shown in Fig. 7.1, the altered granite displays density drops two to three times larger than would be the result of air-filled pores in an amount equal to the observed effective porosity.

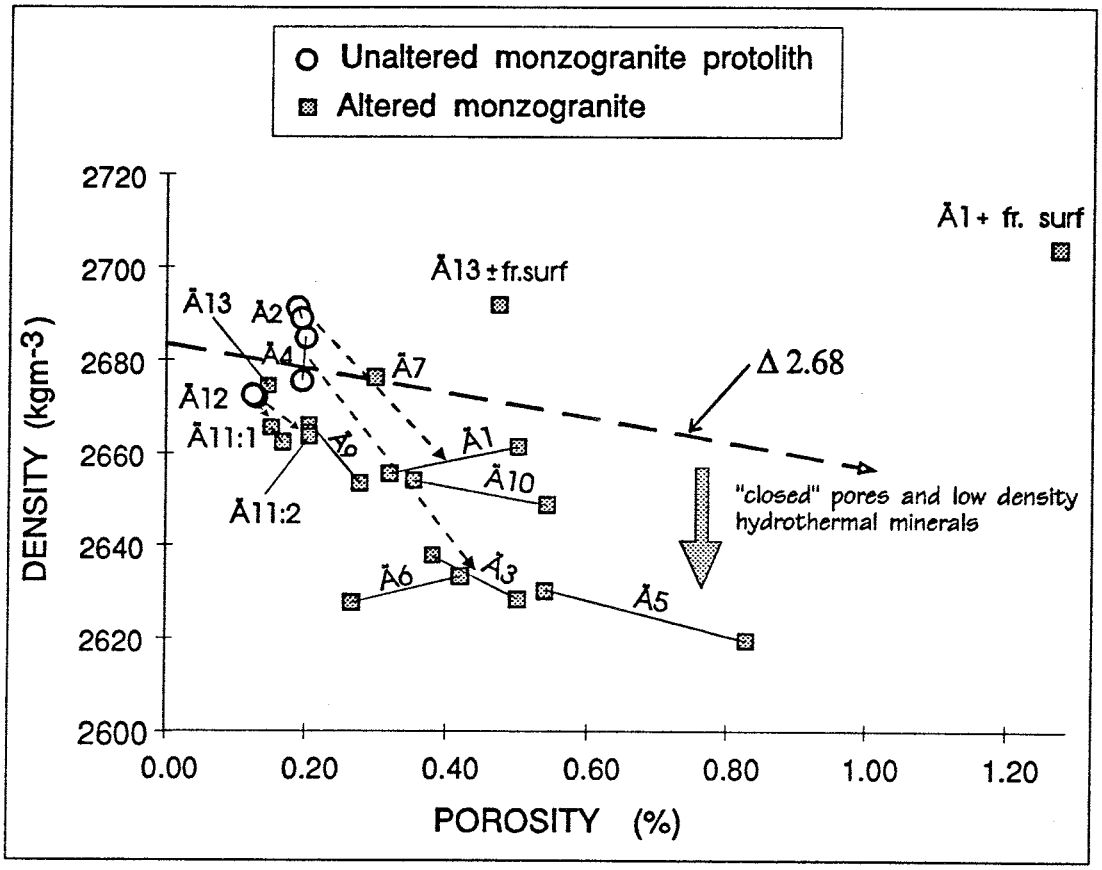

Figure 7.1 Plot of dry density versus porosity of specimens from Äspö. The solid lines that connect pieces of individual samples illustrates the large spread of porosity of the altered samples. Dashed arrows connect sample pairs of less than 0.4 m spacing and display the trend in the change of density and effective porosity during hydrothermal alteration (cf. appendix A:1). Bold dashed arrow displays, assuming a maximum density contrast (Δ2.68) between rock and poor void material (gaseous), the relationship between density and effective porosity.

In the undisturbed rock, sealed pores, microfractures, fluid inclusions etc. are most likely filled with water or denser saline fluids. Thus the maximum density difference between rock and sealed voids is less than 1.68. This implies that, even if the granite has a sealed porosity as high as the effective porosity, the total amount of pores will not be sufficient to cause the observed density drop. Consequently, the lowering of the density of the altered granite is to a great extent caused by the formation of the observed

"low density," hydrous and/or low-temperature hydrothermal assemblage in the altered granite. When, for example, replacing 30 vol.% plagioclase (An 25) and 10 vol.% biotite with 30 vol.% albite, 8 vol.% chlorite and 2 vol. % vermiculite, the density of the rock is reduced by 25 kgm^{-3}.

The increase in effective porosity of the altered granite is chiefly a result of *1)* cracking and microfracturing of primarily the quartz aggregates, *2)* microfracturing along grain boundaries *3)* and some grain expansion during the chloritisation of biotite, resulting in radial fractures. The high porosity of the rock pieces where one surface is made up of a fracture plane and its coating, sample Ä13 ±fr.surf and Ä1+fr.surf (see Fig. 7.1), is caused by the porous texture of the fracture filling-material. In contrast, their rather high densities are a result of the high specific gravity of 3.35 to 3.45 and 2.8 to 2.95 of the principal fracture-filling minerals epidote and prehnite, respectively.

Results similar to those presented here were reported by Lindberg et al. (1992). They showed that an altered granite had a porosity three to five times higher than the porosity of the unaltered equivalent. The increased porosity was due to widening of microfractures and formation of microporosity within altered minerals, mainly biotite, plagioclase and K-feldspar.

The mean density, 2681 kgm^{-3}, of the unaltered Äspö granite samples investigated in this study agrees well with the mean density of 2680 kgm^{-3} presented by Nisca (1988) 23 unaltered, grey to grey-red granite samples from core KAS 02 from Äspö. The mean porosity of these samples was 0.28 (Nisca 1988), which is somewhat higher than the average of 0.17% for the three samples investigated in this study.

In conclusion, it is observed that the altered and red-coloured granite adjacent to the fractures and have an average porosity two to three times higher than the porosity of the unaltered granite protolith. Furthermore, it is observed that the porosity of the altered granite is very heterogeneous. The increase in effective porosity is responsible for about 30 to 40 % of the density reduction displayed by the altered granite. Closed pores, the observed micro-porous structure of the altered plagioclase grains and fluid inclusions in the other minerals, also contribute to the density reduction. However, the lowering of the density is in great part caused by the formation of the "low density," hydrous hydrothermal assemblage in the altered granite.

7.2 Stripa granite

The *density* of all samples from drill core D3 is restricted to the range 2623 to 2640 kgm^{-3}. Exceptionally low, 2482 and 2523 kgm^{-3}, values were measured for the leached, miarolitic drill core D5 samples S18 and S19, respectively (cf. Fig. 7.2 and A:2). Sample S17 also shows a pronounced drop in density owing to the occurrence of the dissolution voids discussed above.

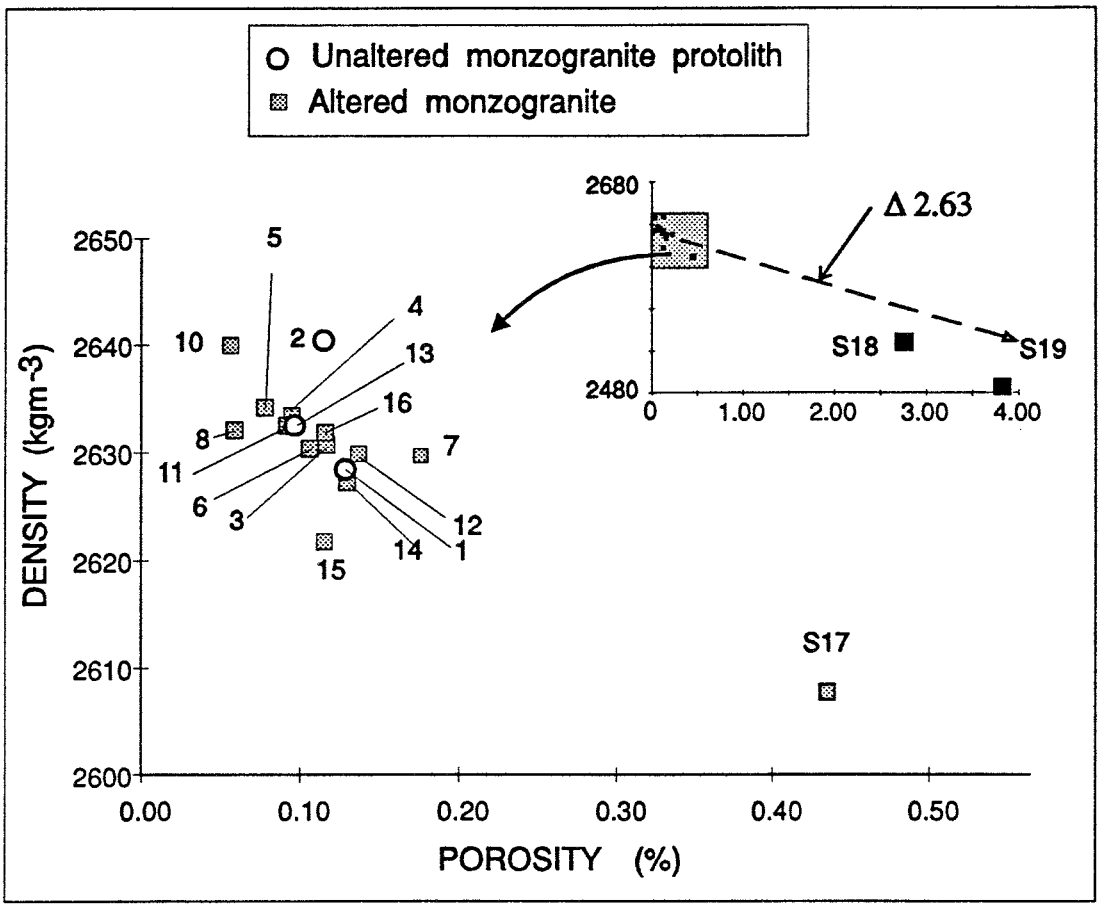

Figure 7.2 Plot of density versus porosity of samples from the Stripa mine. Inset diagram displays the porosities and densities of the miarolitic granite from drill core D5. Bold dashed arrow displays the relationship between density and porosity, assuming a maximum density contrast (Δ2.63) between intact rock and poor void material (gaseous).

The *porosity* values of the unaltered grey and the red-coloured Stripa granite from drill core D3 show remarkably constant values, lying, in the range of 0.05 to 0.14 % with a mean of 0.11 % (samples S1 to S15 in A:2). This contrasts greatly with the very porous (porosity in the range of 2.72 to 3.79 %) nature of the grey, leached granite at 81 to 85 m core length in drill hole D5 (cf. Fig. 7.2). A similar highly porous granite (porosity of up to 9%) has

also been observed in cores from boreholes F1 and F2 at the 360 m level in the Stripa mine (Carlsten, 1985).

The density values of the unaltered Stripa granite presented in this study are basically the same as those, 2630-2640 kgm^{-3} given by Olsson & Jämtlid (1984). The porosity values are, however, considerable lower than the average of 0.47% presented by Olsson & Jämtlid (1984). This discrepancy is probably a result of the differences in laboratory procedures when conducting the density determinations, as higher porosity would give lower density values as seen by the negative correlation between porosity and density (cf. Fig 7.2).

The rather homogeneous density and porosity values of the grey and of the red-coloured, altered granites from drill-core D3 reflect the rather minor change in the mineralogy when going from fresh into altered granite.

The lowering of the density of the leached samples S18 and S19 are about 1.5 times larger than would be the result of the measured effective porosity, assuming a density contrast between poor voids and intact rock of 2.63. Sample S17 exhibits a density drop 2.3 times larger than what would be caused by 0.43 % of air-filled pores (Δ 2.63). The mineralogy of samples S17 to S19 are basically similar to the unaltered granite protolith (the dissolution of quartz, density$\approx$2.65$kgdm^{-3}$, would not affect the density). Furthermore, only clay minerals have densities as low as 2400 kgm^{-3}. This shows that the granites have a high closed porosity.

7.3 Bohus granite

The *density* of the two unaltered Bohus granite sub-samples B1:3 and B2:3 are 2632 and 2631 kgm^{-3}, respectively (see A:3 and Fig. 7.3). These values agree with the average of 2632 kgm^{-3} for 92 basically unaltered Bohus granite samples (Eliasson, in prep.). The *porosity* of 0.57 % and 0.39 % of the unaltered granite seems somewhat high. This is possibly the result of increased micro-fracturing close to the fracture plane or rock surface, respectively, of these "unaltered" rock pieces.

Sample B2 displays a progressive lowering of the density, accompanied by an increase in porosity (Fig. 7.3), from the interior, unweathered protolith (B2:3), via the slightly weathered granite B2:2 towards the brownish-red-coloured granite (B2:1) immediate to the exterior, leached zone (B2:0). Unfortunately, it was not possible to obtain any rock pieces large enough to conduct density and porosity measurements on the outermost, leached zone of the weathering profile of this sample.

The relationship between porosity and density for the samples from the weathering profile B2 strongly suggests that new pores and microfractures (formed during the post-glacial weathering) are air-filled and connected with one another (effective porosity = total porosity). This is probably caused by mechanical micro-fracturing owing to e.g. freezing and thawing, which would cause pores and microfractures to coalesce and increase the permeability of the external weathering rind of the granite.

The sample at the fracture plane (B1) and its sub-samples have, except for the bleached outer zone B1:0 (closest to the fracture plane), rather constant density and porosity values (Fig. 7.3). The low density of sub-sample B1:0 is only slightly lower than what would be the result of only air-filled pores in an amount equal to the measured effective porosity (Δ 2.63 in Fig. 7.3). This is a reflection of the unchanged mineralogy when going from the interior fresh granite to the bleached granite.

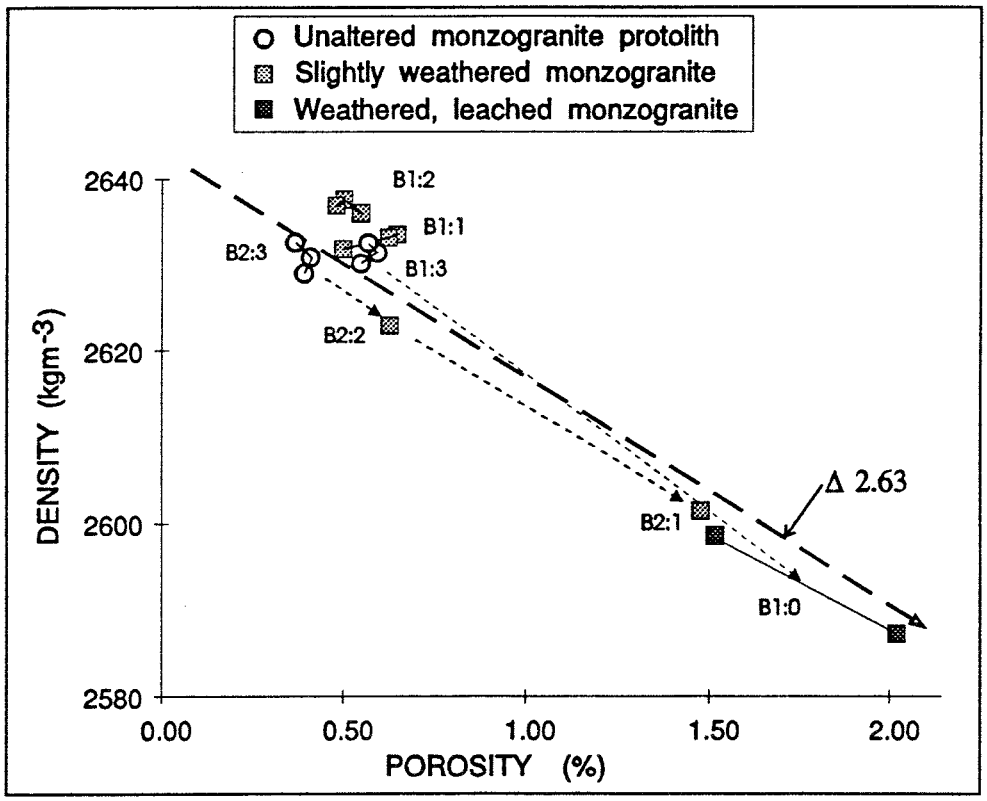

Figure 7.3 Plot of dry density versus porosity of weathered and fresh samples from the Bohus monzogranite showing that most pores and microfractures in the weathered granite are connected with one another. Solid lines connect pieces of the individual samples. Thin dashed arrows display the trend of change of density and porosity during weathering/alteration (cf. Table 1). Bold dashed arrow displays the relationship between density and effective porosity assuming gaseous voids (Δ 2.63).

The unchanged density and porosity of the brownish-red-coloured sub-sample (B1:1 and B1:2) of sample B1 indicate that different weathering processes were in operation at this part in the rock mass as compared with the surface sample B2. Tentatively, the low-temperature weathering of the rock adjacent to the water conduction fracture was only of a chemical (dissolution) nature at this locality 2 m below the rock surface (in the "recent" blasted road cut). In contrast, at the surface (sample B2), climatically induced, mechanical weathering processes (freezing and thawing cycles) were also in operation. This may have opened up and created microfractures within the weathering profile.

In conclusion, the weathering rind in the granite sample B2 displays a progressive lowering of the density, accompanied by an increase in porosity towards the exterior bleached zone of the weathering profile. The good correlation between density and effective porosity is a reflection of the minor change in mineralogy when going from the unaltered granite to the bleached outer part of the alteration/weathering zone. The sample at the fracture plane (B1) exhibits no density or porosity change in the brownish-red-coloured zone. This shows that, as compared with the surface sample B2, different weathering processes were in operation at this site.

8. MAGNETIC SUSCEPTIBILITY

The magnetisation of rocks is partly caused by induction by the magnetisation force associated with the earth's field and partly of their remanent (permanent) magnetisation. The induced magnetic intensity depends primarily upon the magnetic susceptibility of the rock, which is almost entirely controlled by the amount of ferrimagnetic minerals, the most important of which is *magnetite* (e.g. Frost, 1991b).

Hydrothermal alteration and low-temperature weathering cause the oxidation of magnetite to hematite, Fe-oxyhydroxide, (e.g. goethite) or more or less water-bearing hydroxides (e.g. limonite). This results in a lowering of the susceptibility of the rock. Thus, a lowering of the rock susceptibility is indicative of hydrothermal and low-temperature alterations of igneous rocks.

8.1 Äspö granite

The magnetic susceptibility measurements reveal a significant lowering of the magnetic susceptibility with increased alteration (appendix A:1 and Fig. 8.1). This reflects the observed oxidation of magnetite with the formation of hematite and, subordinately, Fe-oxyhydroxides.

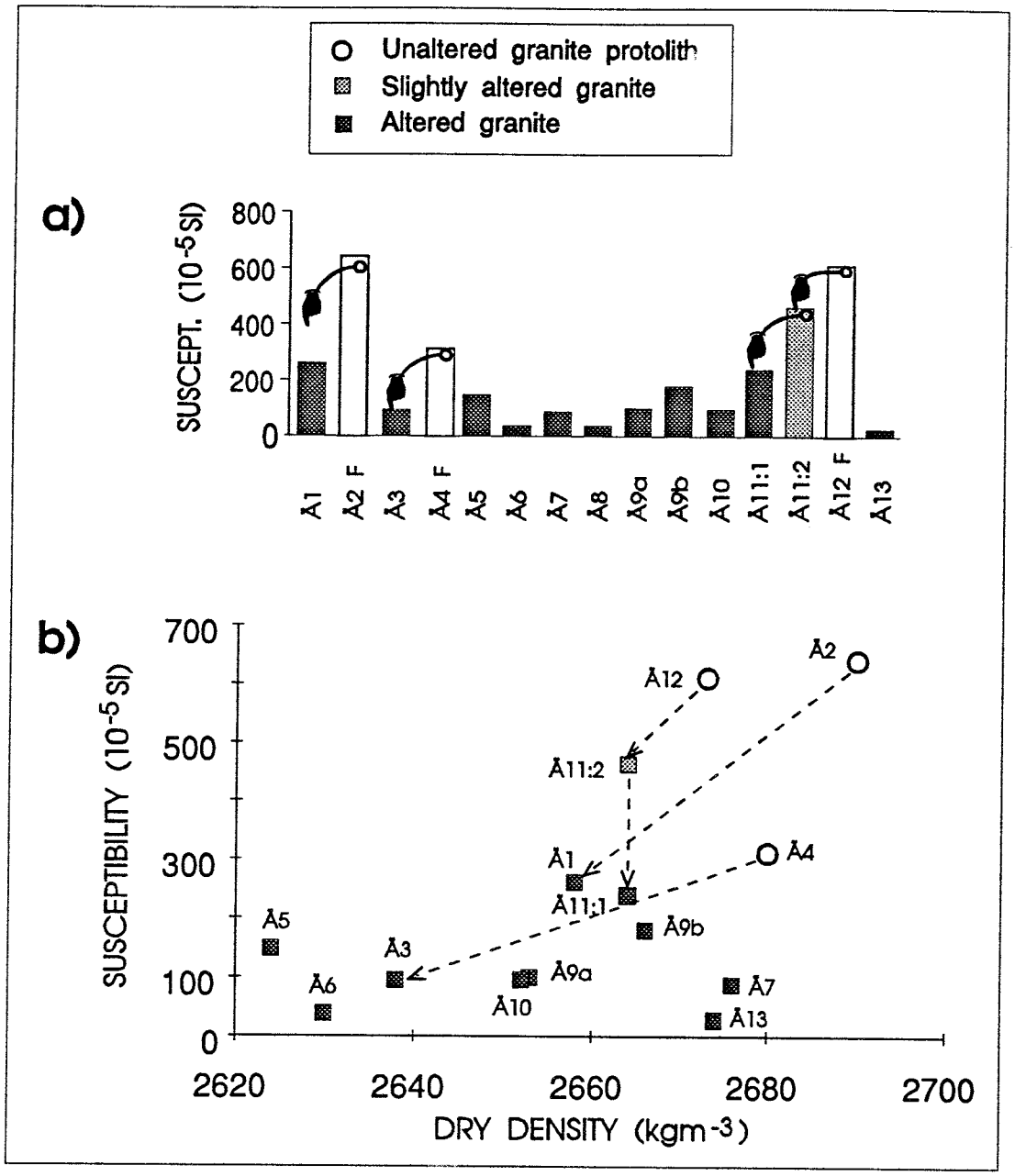

Figure 8.1 a) Magnetic susceptibility for fresh (F) and altered granite samples from Äspö. Note the lowering of susceptibility when going from fresh to adjacent (0.2 to 0.4 m) altered granite for the sample pairs Ä2-Ä1, Ä4-Ä3 and Ä12-Ä11. b) Plot of magnetic susceptibility versus density for Äspö granite samples. Dashed arrows connect pairs of altered and adjacent fresh granite.

The highest mass-specific magnetic susceptibility values of the unaltered granites are about 650x10-5 SI. This is thus somewhat lower than the volume-specific mean value of 1.89x10-5 SI given by Nisca (1988).

The ratio between the remanent and induced magnetisation (Q value) for leucogranitic to mafic rocks in the Äspö region are in the range of 0.13 to 0.25 (Nisca, 1988). This implies that the magnetite content principally control the magnetic characteristic of the granite.

Nisca (1988) concluded that alterations and alteration (magnetite oxidation) zones in granitic rock material from Äspö area can be identified by using the two-variable diagram, magnetic susceptibility versus density. Plotting the samples investigated in this study on this type of diagram discriminates clearly between altered and unaltered granite (cf. Fig. 8.1).

8.2 Stripa granite

The very low magnetic susceptibility of both fresh and altered Stripe granite (Fig. 8.2) is a reflection of the very low content of magnetic oxides in the granite. The oxidation of the red-coloured samples (S6 and S7 in Table 6.1) could thus not be detected by the susceptibility data. The increased susceptibility values for samples S5g and S8 indicate some formation of weakly magnetic oxides (e.g. maghemite).

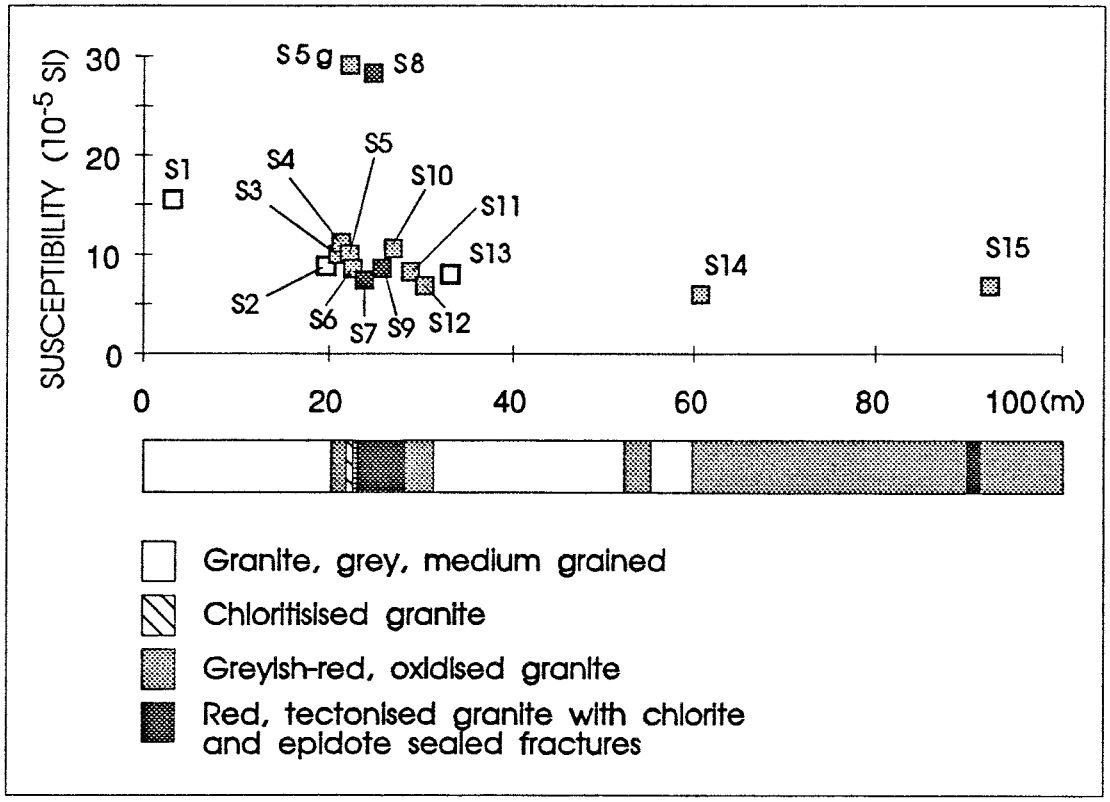

Figure 8.2 Magnetic susceptibility of rock samples from borehole D3 from the SCV block in the Stripa mine. Shown also is a simplified rock log (after Gale et al., 1990).

8.3 Bohus granite

The results of the laboratory susceptibility measurements of the samples from the Bohus granite are presented in appendix A:3 and in Fig. 8.3. The susceptibility of the sample B2 granite lies within the lower part of the range, 100 to 700 SI units (a=335), found for Bohus granites with preserved magmatic mineralogy (Eliasson, in prep). The susceptibility of the brownish-red coloured zones within the weathering profile from this sample remains nearly unchanged (Fig 8.3). However, the outermost bleached zone (B2:0) exhibits a slight drop in its susceptibility.

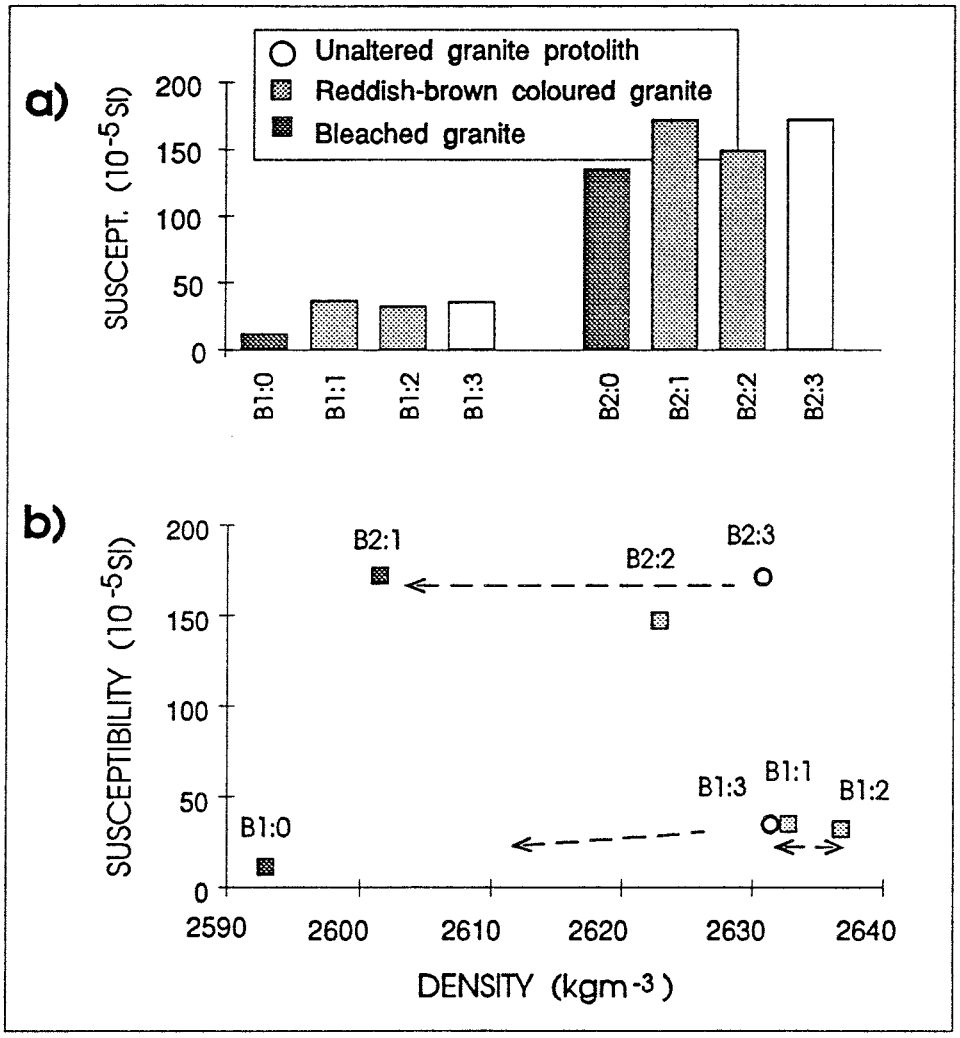

Figure 8.3 a) Magnetic susceptibility of fresh and weathered Bohus granite. b) Plot of magnetic susceptibility versus dry density of samples from the weathering rind in the granite.

The low content of magnetite in sample B1 is expressed as the low susceptibility of this rock. The reddish-brown coloured granite (B1:1 and

B1:2) have susceptibility values similar to those found in the protolith. However, in the outermost bleached zone B1:0 (Fig. 8.3), there is a clear drop in susceptibility.

The tendency toward a lowering of the susceptibility in the upper part of the weathering profile can tentatively be explained by incipient magnetite dissolution and iron mobilisation owing to interaction with acid surface water. (The acidity is caused by humic acids and, perhaps, present day anthropogenic air pollutants. On the Swedish west coast, the rain water has a pH in the range of 4 to 4.5). Reprecipitation of the iron as oxyhydroxides/hydroxides may thus responsible for the observed reddish-brown colouration in the weathering rind.

9. SUMMARY AND CONCLUSION

Narrow zones of red-coloured rock adjacent to fractures are commonly observed in granitic crystalline rocks. The aim of the present study was to investigate the cause of the redness of the colouration in the Äspö granite. An investigation was also made of a weak to rather strong red-coloured granite from the Stripa mine, as well as a weak brownish-red colouration, definitely not hydrothermal in origin, of weathered rinds at and near a glacial polished rock surface in the Bohus granite.

The mineralogy and geochemistry of the altered and red-coloured granites are compared with their unaltered equivalents. The petrophysical properties of effective porosity, density and magnetic susceptibility of the red-coloured rock, as well as of the "uncoloured" wall-rock (protolith), were also investigated.

Äspö granite

The fracture network in the Äspö area is characterised by the red-coloured selvages, generally a few centimetres wide, occurring beside the fracture planes. The microscopic investigation shows that the red colouration of the granite adjacent to the fractures is mainly caused by the presence of dispersed, very fine-grained, reddish Fe-oxyhydroxides/hydroxides *1)* in saussuritic and clouded plagioclase grains, *2)* along grain boundaries and *3)* subordinately along microfractures within individual grains. The clouding of plagioclase is also partly a result of the optical effect of the extremely fine-grained nature of the alteration products and the common occurrence of micropores.

The reddish colouring of the granite spatially coincides with the hydrothermal metamorphic alteration mineralogy occurring along the fracture planes. This fact, together with the observed oxidised mineral assemblage in the hydrothermally metamorphosed zones, indicates that the formation of the ferric compounds (colouring) is contemporaneous with, and a function of, the hydrothermal alteration.

Besides the Fe-oxyhydroxide staining, the most diagnostic *mineralogical features* within the altered zones are (see also Fig. 9.1):

1) the crystallisation of chlorite pseudomorphs after biotite
2) the decomposition and formation of clouded, microporous, extremely fine-grained, saussuritic (albitised) pseudomorphs after the magmatic oligoclase±andesine
3) the hematisation of magnetite.

The quartz+ microcline+ albite (saussurite)+ chlorite+ epidote mineralogy of the altered granite is that of upper prehnite-pumpellyite to lower greenschist facies mineralogy, implying alteration temperatures in the range of about 300 to 400 °C in the fracture vicinity.

The Fe-oxyhydroxide formation is interpreted to be related to the final low temperature stage (tentatively in the range of 150 to 250 °C) of the water-rock interaction. This occurred when the fracture was sealed off and the wall rock was cooled. At this stage, the low temperature fluids were able to react with and locally alter the high temperature minerals occurring within the fracture itself, as well as in the altered wall rock. This is e.g. seen as a corrosion of fracture-filling prehnite by clay and Fe-oxyhydroxide minerals and as the vermiculitisation of the wall-rock chlorite and formation smectite and illite within altered plagioclase and microfractures.

The fracture-filling mineralogy and crystallisation sequences reflects the successive lowering of the temperature of the alteration fluids. Commonly, the fractures have an outer border of epidote± chlorite, followed by prehnite bands. In the centre of the fracture, calcite has percipitated. Finally,clays and Fe-oxyhydroxides have formed.

The altered rocks generally preserve the *texture* of the protolith, in which the original minerals are pseudomorphically replaced. However, the albitised plagioclase grains are made up of extremely fine-grained saussuritic albite, epidote, calcite and sericite/K-feldspar. The saussurite grains contain numerous small *micropores* (dissolution voids) caused by the removal of the major part of the anorthite component from the plagioclase. At heavily fractured, sites high fluid/rock ratios facilitated the neoformation of fine-grained chlorite + epidote ± clay ± calcite.

The most striking *chemical features* of the altered Äspö granite are:

1) The high H_2O+ content (loss of ignition) of the altered granite. This is mainly caused by the high content of hydrated minerals, mostly phyllosilicates (e.g. chlorite, muscovite, prehnite and clay minerals) and disseminated calcite.
2) The gain of up to 26 and 22 % of K and Na, respectively. This indicate to high activities of potassium and sodium in the hydrothermal fluid. These elements participated in the formation of the secondary phases sericite, K-feldspar and albite.
3) The loss of up to 20 % of Ca. This suggests that it partly has been re-precipitated as the Ca-rich fracture fillings calcite, epidote and prehnite.
4) The decrease in FeO. This reflects the observed oxidation of magnetite with the formation of hematite and, subordinately, Fe-oxyhydroxides.

The *petrophysical properties* of porosity, density and magnetic susceptibility exhibit a good correlation with the intensity of alteration. This illustrates the importance of these parameters for identifying fractures/fracture zones in the Äspö area.

In general, the petrophysical properties show the following characteristics:

1) There is a two to three-fold increase in the effective *porosity* of the hydrothermally altered and red-coloured rims adjacent to the fractures.
2) The *density* of the altered granite is reduced by 0.7 to 1.5 %.
3) The *magnetic susceptibility* is reduced generally two to five times in the altered granite.

The increased effective porosity is responsible for less than approximately 40 % of the *density* reduction displayed by the altered granite. Closed pores and the "low-density" hydrothermal assemblage are responsible for the remainder of the density reduction displayed by the altered granite.

It should be stressed that the increased effective porosity, together with the formation of chlorite and complex clay minerals such as smectite, vermiculite and illite, considerably increase the *cation-exchange capacity* within the red-coloured wall-rock zones along the fracture planes. The "closed" microporosity and small grain size of the saussuritic plagioclase also have a significant bearing on the diffusivity and sorptive area of the altered granite.

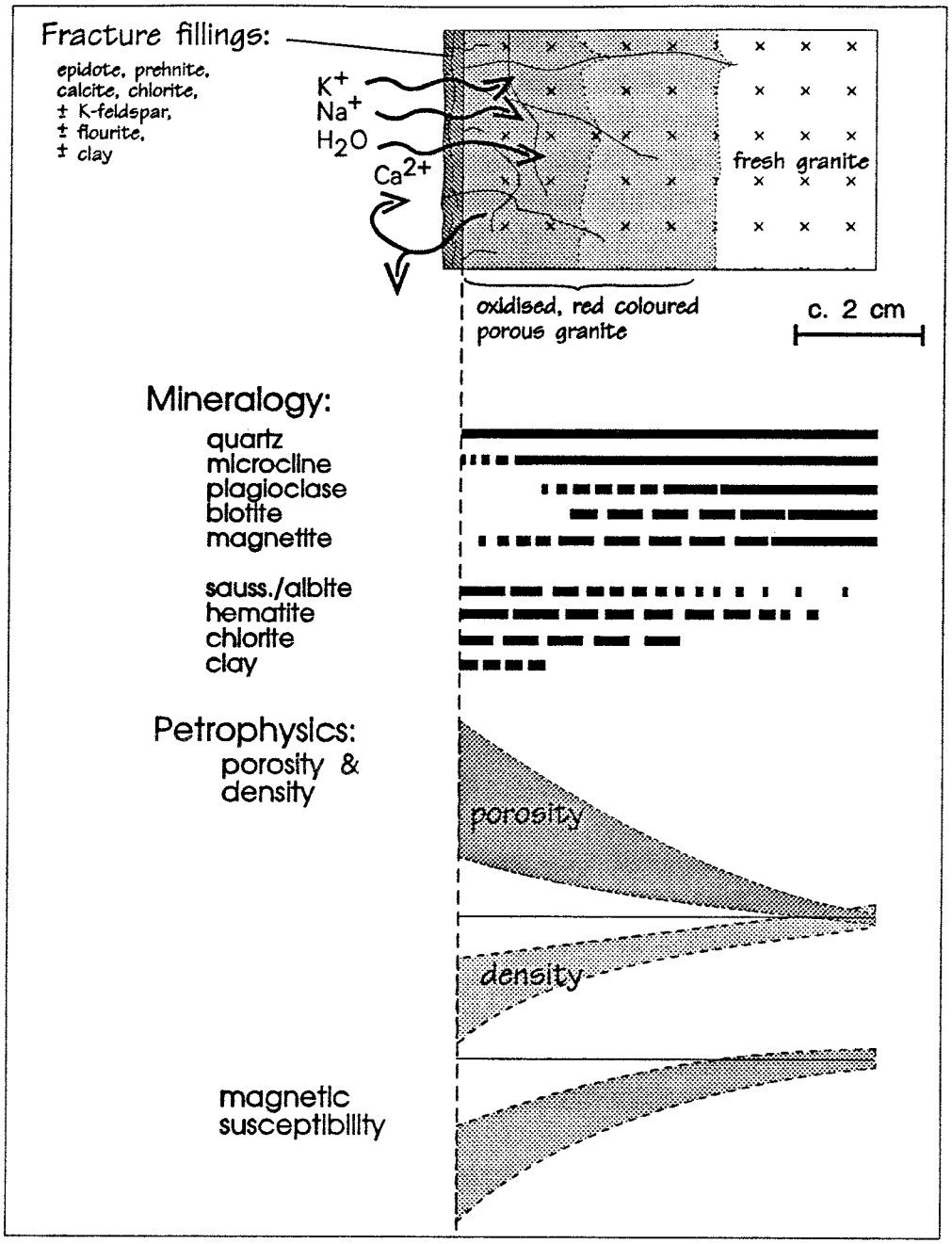

Figure 9.1 Schematic illustration of the most important alteration features in the red-coloured wall rock along fracture in the Äspö granite.

Stripa Granite

The mineralogy of the red-coloured Stripa granite is characteristic, although only slightly modified compared with the protolith. The amount of quartz and feldspar is unchanged when going from the fresh into the altered granite. In the red-coloured granite the secondary chlorite (pseudomorphing biotite at a late magmatic stage) is to a very large degree altered/oxidised to muscovite hematite and, subordinately, Fe-oxyhydroxides.

The red colouration of the granite is caused by impregnation of extremely small (generally < 5 - 10 μm) hematite and, subordinately, Fe-oxyhydroxide grains along *1)* cracks and microfractures, *2)* grain boundaries and *3)* subordinately within the main salic minerals. Oxidisation and re-precipitation of iron liberated during a retrograde muscovitisation is interpreted to be the cause of the formation of the ferric oxides.

The grain size is somewhat reduced, the texture is more granular and the fracture frequency is increased in the altered granite. Furthermore, the individual minerals are also more fractured. There is thus a positive correlation between the degree of alteration and deformation.

The alteration occurred at slightly oxidising conditions in a basically isochemical system. The rather homogeneous *density* and *porosity* values of the grey and of the red-coloured, altered granites from drill core D3 reflect the rather minor change in the mineralogy when going from fresh into altered granite. The very low *magnetic susceptibility* of both fresh and altered Stripe granite is a reflection of the very low content of magnetic oxides in the granite.

Bohus granite

The weathering rind below a rock surface of Bohus granite, polished during the Weichselian glaciation (i.e. <12.000 years), is composed of an upper 1 to 3-mm thick, bleached, greyish-white zone. It is followed by a 2 to 5 cm wide, reddish-brown zone with a slight yellowish tint. Weathering (incipient argillitisation) and whitening of plagioclase in the bleached zone and precipitation of small quantities of Fe-oxyhydroxides/hydroxides in the brownish-red zone is responsible for the colouration of the rock.

There is a marked increase (3 to 4 times) in porosity from the interior fresh (c. 0.4-0.5%) towards exterior bleached zone (c. 1.5-2%) of the subaerialy weathered Bohus granite surface. The constant *grain* density (dry density-porosity) reflects the unchanged mineralogy within the weathering profile. The incipient decomposition of magnetite is shown as a slight lowering of the magnetic susceptibility of the weathered granite.

Acknowledgements. I would like to thank Hans Harryson at Uppsala University, who supervised the microprobe investigation. Christian Annertz receives thanks for guidance and assistance during the sampling in the Äspö tunnel. I also thank Rob Hellingwerf for stimulating discussions on alteration processes and opaque mineralogy, and I would like to express my appreciation to Sven Åke Larson for critically reading the manuscipt and making valuable suggestions.

10. REFERENCES

AlDahan, A.A., Ramseyer, K., Morad, S., and Collini, B., 1988: Low temperature alterations in granitic rocks from the Siljan ring structure, central Sweden. *In* Boden, A., and Eriksson, K.G. (eds.): *Deep Drilling in Crystalline Bedrock*: Vol. 1, 209-216. Springer Verlag, Berlin.

Barnwart, S., Laaksoharju, M., Nilsson, A-C., Tullborg, E-L. and Wallin, B., 1991: The large scale redox experiment; Initial characterization of the fracture zone. *SKB Progress Report*: 25-92-04, Stockholm.

Beane, R.E. and Titley, S.R., 1981: Porphyry copper deposits; Part II. Hydrothermal Alteration and Mineralization. *Economic Geology 75th Anniversary Volume*: 235-269.

Carlsten, S., 1985: Hydrogeological and Hydrogeochemical Investigation in Boreholes - Compilation of geological data. *Stripa project. Internal report*: 85-04. SKB, Stockholm, Sweden.

Deer, W.A., Howie, R.A. & Zussman, J., 1992: An introduction to the Rock-forming Minerals. Longman, London, 696 pp.

Eliasson, T., & Schöberg, H., 1991. U-Pb dating of the post-kinematic Sveconorwegian (Grenvillian) Bohus granite, SW Sweden: evidence of restitic zircon. *Precambrian Research 51*: 337-350.

Eliasson, T., Tullborg, E-L. & Smellie, J., 1991: Mineralogical Studies of the Post-Glacial Fault Exposed at Molberget, Lansjärv Area, Northern Sweden. *SKB Arbetsrapport*: 91-14. pp 22.

Exley. R.A., 1980: Microprobe studies of REE-rich accessory minerals: Implications for Skye granite petrogenesis and REE mobility in hydrothermal systems. *Earth and Planetary Science Letters 48*: 97-110.

Fischer, W.R. & Schwertmann, U., 1974: The formation of hematite from amorphous iron (III) oxide. *Clays and Clay Minerals 23*: 33-37.

Franklin, J.A.M, Vogler, U.W., Szlavin, J., Edmond, J.M. and Bieniawski, Z.T., 1979: Suggested Methods for Determining Water Content, Porosity, Density, Absorption and Realated Properties and Swelling and Slake-Durability Index Properties. *In* Brown, E.T. (ed.): *Rock Characterization Testing and Monitoring, ISRM Suggested Methods*: 81-94. Pergamon Press, Oxford.

Frost, B.R., 1991a: Stability of oxide minerals in metamorphic rocks. *In* Lindsley, D.H. (ed.): Oxide Minerals: Petrology and Magnetic significance. *Mineralogical Society of America. Reviews in Mineralogy*: Vol. 25: 469-487.

Frost, B.R., 1991b: Magnetic Petrology: Factors that control the occurrence of magnetite in crustal rocks. *In* Lindsley, D.H. (ed.): Oxide Minerals: Petrology and Magnetic significance. *Mineralogical Society of America. Reviews in Mineralogy*: Vol. 25: 489-509.

Gale, J., MacLeod, R., Stråhle, A. and Carlsten, S., 1990: Site Characterization and Validation - Drift and Borehole Fracture Data, Stage 3. *Stripa project. Internal report*: 90-02. SKB, Stockholm.

Gorbatschev, R:; 1980: The Precambrian development of southern Sweden. *Geologiska Föreningens i Stockholm Förhandlingar 102*: 129-136.

Gromet, L.P. and Silver, LT., 1983: Rare earth element distributions among minerals in a granodiorite and their petrogenetic implications. *Geochimica et Cosmochimica Acta 47*: 925-939.

Gresens, R.L:; 1967: Composition-volume relationships of metasomatism. *Chemical Geology 2*: 47-65.

Hemley, J.J. and Hunt, J.P., 1992: Hydrothermal Ore-Forming Processes in the Light of Studies in Rock-Buffered System: II. Some General Geologic Applications. *Economic Geology 87*: 23-43.

Hughes, C.J., 1973: Spilites, keratophyres, and the igneous spectrum. *Geological Magazine 109*: 513-527.

Johansson, B.T., 1982: Deglaciationen av norra Bohuslän och södra Dalsland. Geologiska Institutionen. Chalmers Tekniska Högskola och Göteborgs Universitet, Publ. A 38. Göteborg.

Kornfält, K-A. and Wikman, H., 1988: The rocks of the Äspö island. *SKB Progress Report*: 25-88-12. Stockholm.

Lindberg, A., Hellmuth, K-H., Siitari-Kauppi, M. and Suksi, J., 1992: Effects of water-rock interactions on the porosity and composition of rock studied by impreganation with carbon-14-polymethylmethacrylate. *In* Kharaka, Y.K. and Maest, A.S. (eds.): *Water Rock interaction,* 573-576. Balkema, Rotterdam.

Lundström, I., 1980: Beskrivning till berggrundskartan Lindesberg SV. *Sveriges Geologiska Undersökning*: Af 126. Uppsala.

Morad, S., Bergan, M., Knarud, R. and Nystuen, J.P., 1990: Albitization of detrital plagioclase in Triassic reservoir sandstone from the Snorre Field, Norwegian North Sea. *Journal of Sedimentary Petrology 60*: 411-425.

Morton, R.L. and Nebel, M.L., 1984: Hydrothermal alteration of felsic volcanic rocks at the Helen siderite deposite, Wawa, Ontario, *Economic Geology 79*: 1319-1333.

Nahon, D.B., 1991: *Introduction to the petrology of soils and chemical weathering*. 313pp. John Wiley & Sons, New York.

Nisca, D.H., 1988: Geophysical laboratory measurements on core samples from KLX01, Laxemar and KAS02, Äspö. *SKB Progress Report*: 25-88-06, Stockholm.

Olsson, O. and Jämtlid, A., 1984: Hydrogeological and hydrogeochemical investigations-geophysical borehole measurements. *Stripa project. Internal report*: 84-03. KBS, Stockholm.

Paterson, B.A. & Stephens, W.E., 1992: Kinetically induced compositional zoning in titanite: implications for accessory-phase/melt partitioning of trace elements. *Contributions to Mineralogy and Petrology 109*: 373-385.

Ramseyer, K., Boles, J.R. and Lichtner, P.C., 1992: Mechanism of Plagioclase albitization. *Sedimentary Petrology 62*: 349-356.

Savage, D., Cave, M.R., Milodowski, A.E., & George, I., 1987: Hydrothermal alteration of granite by meteoric fluid: an example from the Carnmenellis Granite, United Kingdom. *Contributions to Mineralogy and Petrology 96*: 391-405.

SKB Annual Report 1991: *SKB TR*: 91-64, Stockholm.

Stanfors, R., Erlström, M. and Markström, I., 1991: Äspö Hard Rock Laboratory. Overview of the investigations 1986-1990. *SKB TR*: 91-20. Stockholm.

Studemeister, P.A. and Kilias, S., 1987: Alteration pattern and fluid inclusions of Gold-Bearing Quartz Veins in Archean Trondhjemite near Wawa, Ontario, Canada. *Economic Geology 82*: 429-439.

Talbot, C. and Riad, L., 1987: Natural fractures in the Simpevarp area. *SKB Progress Report*: 25-87-03, Stockholm.

Tullborg, E-L., 1989: Fracture fillings in the drillcores KAS05-KAS08 from Äspö, Southeastern Sweden. *SKB Progress Report*: 25-89-16, Stockholm.

Tullborg, E-L., Wallin, B. and Landström, O., 1991: Hydrochemical studies of fracture minerals from water conducting fractures and deep groundwaters at Äspö. *SKB Progress Report*: 25-90-01, Stockholm.

Wollenberg, H., Flexser, S., Andersson, L., 1980: Petrology and radiogeology of the Stripa pluton. *Lawrence Berkeley Laboratory report* LBL 11654, SAC-36. Berkeley, California.

Zen, E-an, & Hammarström, J.H., 1984: Magmatic epidote and its petrological significance. *Geology 12*: 515-518.

Appendix A:1

Brief rock description, bulk density (ρ), dry density (ρd), porosity (n) and magnetic susceptibility (susc.) data of samples from the **Äspö tunnel.**

Sample, 1)	tunnel lenght (m)	Rock description	ρ kgm^{-3}	ρd kgm^{-3}	n %	Susc. (10^{-5}SI)
Ä1,	546	Red coloured granite.	2659	2655	0.32	261.1
			2666	2661	0.50	
+fr.surf			2716	2703	1.27	
Ä2,	546	**Fresh** granite protolith,	2691	2689	0.19	643.1
		20 cm east of Ä1.	2693	2691	0.19	
Ä3,	538	Red coloured granite.	2642	2638	0.38	94.9
± fr.surf			2633	2628	0.50	
Ä4,	538	**Fresh** granite protolith,	2687	2685	0.20	313.3
		40 cm east of Ä3.	2678	2676	0.19	
Ä5,	525	Red, altered granite.	2636	2630	0.54	147.4
			2628	2619	0.83	
Ä6,	525	Red to pinkish-	2637	2633	0.42	38.5
		red,altered granite.	2630	2628	0.27	
Ä7,	516.6	Heavily altered granite.	2679	2676	0.30	88.1
Ä8,	516	Red blastocataclasite				38.5
Ä9a,	516	Red altered granite	2656	2653	0.28	100.3
Ä9b,	516	Gray bleached variety of	2668	2666	0.20	179.9
		the granite Ä9a				
Ä10,	516	Light reddish granite.	2654	2649	0.54	96.4
			2657	2654	0.35	
Ä11:1,	526	Red coloured granite.	6672	2665	0.15	239.4
		0.5-2 cm from fracture.	2664	2662	0.17	
Ä11:2		Weakly red coloured	2666	2664	0.20	464.0
		granite. 2-4 cm from fr.	2666	2664	0.20	
Ä12,	526	**Fresh,**granite protolith,	2674	2673	0.13	612.5
		20 cm W of Ä11.	2674	2672	0.13	
Ä13,	781.1	Red pervasively altered	2676	2674	0.15	27.9
± fr. surf		granite.	2697	2691	0.47	

1) ± fr. surf. = sample where one surface is made up of the fracture plane and its coating.

Appendix A:2

Brief rock description, bulk density (ρ), dry density (ρd), porosity (n) and magnetic susceptibility data of samples from the **Stripa mine.**

Sample	Rock description	ρ kgm^{-3}	ρd kgm^{-3}	n %	Susc. 10^{-5} SI
DRILL CORE D3					
S1	Grey, slightly greenish, fresh granite	2630	2628	0.13	15.4
S2	Grey, fresh granite.	2642	2640	0.12	8.8
S3	Incipiently red-coloured, grey granite.	2632	2631	0.12	10.0
S4	Reddish-grey granite.	2634	2633	0.09	11.1
S5	Reddish-grey granite as above with a zone of green colouration.	2635	2634	0.08	10.0 Red 29.2 Green
S6	Weakly-red, altered granite .	2632	2630	0.11	8.5
S7	Dark-red, altered granite.	2631	2630	0.18	7.3
S8	Dark greenish-red, pervasively altered granite.	2633	2632	0.06	28.1
S9	Light-red, silicified, salic granite.	2630 1)		--	8.5
S10	Red-grey,slightly greenish granite.	2640	2640	0.05	10.6
S11	Weakly reddish coloured granite.	2633	2633	0.09	8.2
S12	Incipiently red-coloured, grey granite.	2631	2630	0.14	6.9
S13	Grey, fresh granite. .	2633	2633	0.10	7.9
S14	Incipiently red-coloured, grey granite.	2629	2627	0.13	5.9
S15	Incipiently red-coloured, grey granite.	2623	2622	0.12	6.7
DRILL CORE D5					
S16	Incipiently red coloured granite.	2633	2632	0.12	8.8
S17	Weakly red coloured granite.	2612	2608	0.43	16.6
S18	Grey, bleached porous granite.	2520	2483	3.79	7.8
S19	Grey, bleached, porous granite.	2551	2524	2.72	7.4

1) measured with "low precision" balance: $\pm .1$ g

Appendix A:3

Brief rock description, bulk density (ρ), dry density (ρd), porosity (n) and magnetic susceptibility (sucs.) data on specimens from the **Bohus monzogranite**. a= average of the different pieces making up the separate samples.

Sample1)	ROCK DESCRIPTION	ρ kgm^{-3}	ρ a	ρd kgm^{-3}	ρd a	n (%)	n a	Susc. (10^{-5}SI)
B1 :O	Bleached, exterior part (c. 5mm thick) of	2614		2599		1.52		
	alteration zone at vertical fracture.	2608	*2611*	2587	*2593*	2.02	*1.77*	11.6
B1 :1	Altered, brownish-red part of alteration	2640		2634		0.65		
	zone. 1 to 2 cm from fracture plane.	2639		2633		0.62		
		2637	*2637*	2632	*2633*	0.50	*0.59*	36.3
B1 :2	Slightly altered, brownish-red part of	2641		2636		0.55		
	alteration zone. 2 to 4 cm from fracture	2643		2638		0.50		
	plane.	2642	*2642*	2637	*2637*	0.48	*0.51*	31.9
B1 :3	Medium-grained, reddish-grey, **fresh,**	2636		2630		0.55		
	interior, protolith muscovite granite.	2638		2633		0.57		
	About 6 cm from fracture plane.	2637	*2637*	2631	*2631*	0.59	*0.57*	35.2
B2 :0	Greyish-white, bleached zone at outer part							
	of weathering rind.	- 2)		- 2)		- 2)		135.1
B2 :1	Altered, brownish-red granite.	2616		2601		1.5		171.9
B2 :2	Weakly altered, brownish-red granite.	2629		2623		0.6		148.7
B2 :3	Medium-grained, reddish-grey, **fresh,**	2633		2629		0.39		
	interior protolith granite.	2635		2631		0.41		
		2636	*2635*	2633	*2631*	0.37	*0.39*	171.7
B3	Weathering rind of Bohus granite, c. 5 cm deep.	2570 3)-		--		--		--

1) n:0 = ≤ 1cm from fracture plane/exterior rock surface; n:1 = 1.0 to 2 cm from fracture plane/exterior rock surface; n:2 = 2-4 cm from fracture plane/exterior rock surface; n:3 = unaltered monzogranitic protolith.

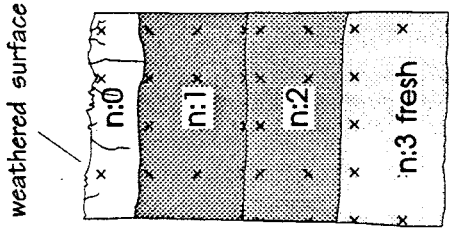

2) specimen too small for accurate measurements
3) measured with "low" precision balance

Appendix B:1

Microprobe analyses of unaltered (sample Ä2 and Ä4) and albitisised/saussuritic (sample Ä3 and Ä1) **plagioclase** and **K-feldspar** from the Äspö granite. Analyses Ä3, f20 Pos3 is a primary microcline.

Sample	Ä2 f2						Ä4 f1			Ä4 f2		Ä3 f3
	Pos 1	same	Pos 2	2b rim	Pos 3	Pos 4	Pos3	Pos4	Pos4brim	Pos5	Pos6	Pos6 P1
SiO_2	60.55	60.93	60.86	63.04	62.00	62.63	63.06	62.02	67.20	63.12	63.54	69.25
TiO_2	0.00	0.00	0.00	0.00	0.00	0.02	0.03	0.00	0.00	0.00	0.02	0.00
Al_2O_3	23.78	24.58	24.32	23.26	23.96	23.71	23.41	23.64	21.38	23.38	23.33	19.80
FeO	0.14	0.07	0.14	0.05	0.08	0.07	0.07	0.09	0.07	0.03	0.01	0.12
MnO	0.03	0.00	0.00	0.00	0.00	0.00	0.00	0.00	0.00	0.00	0.00	0.00
MgO	0.00	0.00	0.00	0.00	0.00	0.00	0.00	0.00	0.00	0.01	0.00	0.01
CaO	6.38	6.44	6.12	5.01	5.32	4.97	5.21	5.60	2.24	4.78	4.82	0.09
Na_2O	7.69	7.66	7.90	8.36	8.87	8.51	8.49	8.52	10.29	9.29	9.05	11.03
K_2O	0.14	0.10	0.16	0.05	0.15	0.16	0.10	0.18	0.06	0.07	0.05	0.42
Total	98.71	99.77	99.50	99.77	100.37	100.06	100.37	100.04	101.23	100.67	100.83	100.72
Molecular composition												
An	31.2	31.5	29.7	24.8	24.7	24.7	25.2	26.4	10.7	22.1	22.7	0.4
Ab	68.0	67.9	69.4	74.9	74.5	74.9	74.3	72.6	89.0	77.6	77.1	97.2
Or	0.8	0.6	0.9	0.3	0.8	0.9	0.6	1.0	0.3	0.4	0.3	2.4
									±altered	slightly altered		albitised alt. plag

appendix B:1 continued...

					f4		f20					Ä1 f1		Ä10
Pos6 P2	Pos5 P1	incl2	incl3	Pos15	Pos16	Pos1	Pos3	Pos4	Pos 5	Pos 6	Pos 5	Pos 6	Pos2
66.22	68.90	64.35	63.68	66.60	67.76	65.94	65.19	64.02	69.21	65.12	69.64	68.99	64.70
0.00	0.00	0.00	0.00	0.00	0.00	0.00	0.00	0.00	0.00	0.00	0.03	0.00	0.01
21.07	19.13	18.05	17.75	18.44	18.75	18.08	18.44	17.78	19.71	18.22	19.82	19.79	18.20
0.32	0.07	0.01	0.00	0.00	0.00	0.00	0.02	0.90	0.02	0.08	0.17	0.01	0.02
0.00	0.00	0.00	0.00	0.00	0.00	0.00	0.00	0.00	0.00	0.00	0.00	0.03	0.00
0.26	0.00	0.00	0.01	0.00	0.00	0.00	0.00	0.00	0.00	0.00	0.00	0.01	0.00
0.14	0.19	0.00	0.00	0.21	0.20	0.00	0.00	0.00	0.15	0.00	0.24	0.23	0.00
10.46	10.79	0.48	0.31	11.00	10.98	0.04	0.48	0.11	11.56	0.09	11.46	11.34	0.16
1.92	0.07	15.71	15.65	0.10	0.03	15.87	15.89	15.75	0.12	16.38	0.10	0.05	16.29
100.38	99.14	98.59	97.39	96.34	97.71	99.92	100.01	98.56	100.77	99.88	101.45	100.44	99.38
0.65	0.97	0.00	0.00	1.01	0.98	0.00	0.00	0.00	0.69	0.00	1.12	1.11	0.00
88.66	98.64	4.42	2.92	98.39	98.81	0.33	4.41	1.09	98.64	0.82	98.29	98.61	1.49
10.69	0.39	95.58	97.08	0.59	0.20	99.67	95.59	98.91	0.67	99.18	0.59	0.28	98.51
inhomo-geneous alt. plag	albitised alt. plag.	K-fsp inclusion		albitised alt. plag.		K-fsp in micro-fracture	Microcline	K-fsp inclusion	albitised alt. plag.	K-fsp inclusion	albitised alt. plag.		K-fsp. in fracture

Appendix B:2

Microprobe analyses of **biotite** from unaltered Äspö granite (sample Ä4 and Ä2).

Sample	Ä4 f1			Ä4 f2	Ä2 f1			
	Pos1 P1	Pos 2a	Pos 2b	P2	P1	same	P2	same
SiO_2	38.22	37.52	38.21	38.72	38.28	38.01	38.19	38.65
TiO_2	1.72	1.61	1.61	1.43	1.56	1.55	1.62	1.52
Al_2O_3	15.01	15.12	14.93	15.71	14.89	15.06	14.82	14.94
FeO	16.54	16.27	16.49	16.19	16.26	16.04	16.51	16.21
MnO	0.51	0.48	0.62	0.55	0.59	0.61	0.58	0.53
MgO	12.83	12.53	12.68	12.88	12.74	12.83	13.17	13.35
CaO	0.00	0.00	0.00	0.00	0.00	0.03	0.00	0.00
Na_2O	0.16	0.04	0.06	0.07	0.12	0.14	0.04	0.13
K_2O	9.63	9.90	9.67	9.84	9.71	9.90	9.65	9.68
Total	94.62	93.46	94.27	95.38	94.15	94.15	94.58	94.99

appendix B:2 continued...

Sample	Ä2 f2				
	Pos 5	Pos 5b	same	Pos 6	Pos 6b
SiO_2	38.01	38.11	37.59	37.78	37.47
TiO_2	1.50	1.51	1.65	1.57	1.66
Al_2O_3	14.80	15.36	14.83	14.84	14.93
FeO	17.41	16.97	17.53	16.40	16.71
MnO	0.65	0.65	0.63	0.58	0.71
MgO	12.09	11.82	11.73	12.76	12.37
CaO	0.00	0.00	0.00	0.00	0.00
Na_2O	0.03	0.11	0.04	0.13	0.05
K_2O	9.54	9.88	9.53	9.57	9.92
Total	94.02	94.41	93.52	93.64	93.82

Appendix B:3

Microprobe analyses of **epidote** in fresh (F) and altered Äspö granite.

Sample	Ä2F						Ä4F				Ä3
	P3	P3	P4	P4	P9core	P2rim	P10	P6	P4d	P3	P3c
SiO_2	37.76	37.74	38.85	37.54	37.03	36.93	38.32	37.44	38.13	37.68	37.09
TiO_2	0.07	0.04	0.04	0.02	0.00	0.17	0.03	0.00	0.00	0.04	0.03
Al_2O_3	22.06	22.13	21.95	22.62	21.99	19.91	23.80	22.86	23.50	22.28	21.59
Fe_2O_3	14.18	14.17	14.25	13.44	13.92	16.40	12.27	12.76	12.41	13.71	14.51
MnO	0.34	0.50	0.34	0.31	0.45	0.51	0.17	0.36	0.51	0.40	0.31
MgO	0.00	0.00	0.00	0.00	0.00	0.00	0.00	0.00	0.00	0.00	0.00
CaO	22.99	22.96	23.35	23.17	23.12	22.83	23.17	22.88	23.20	23.13	23.08
Na_2O	0.00	0.00	0.00	0.00	0.00	0.00	0.00	0.06	0.00	0.00	0.07
K_2O	0.00	0.03	0.00	0.00	0.00	0.00	0.00	0.02	0.02	0.00	0.00
Total	97.41	97.56	98.78	97.09	96.51	96.75	97.75	96.37	97.77	97.23	96.68
			euhedral matrix epidote		anhedral crystal with euhedral core		incl. in plag.	matrix epidote	incl. in plag.	matrix epidote	subhed. matrix epidote

appendix B-3 continued...

Sample							Ä1			
	P7	P5	P1	P2	P9	P10	P1	P2	P3	P3
SiO_2	37.08	37.65	37.19	37.33	36.93	36.71	37.03	37.39	37.72	37.67
TiO_2	0.00	0.00	0.01	0.02	0.05	0.00	0.02	0.09	0.03	0.24
Al_2O_3	22.00	23.52	22.03	22.22	21.65	21.68	19.91	19.63	22.21	22.14
Fe_2O_3	13.42	12.15	14.27	14.27	14.15	14.40	17.32	17.63	14.25	14.30
MnO	0.37	0.42	0.32	0.33	0.33	0.41	0.44	0.05	0.39	0.37
MgO	0.00	0.00	0.00	0.00	0.00	0.00	0.00	0.00	0.00	0.00
CaO	22.94	23.41	23.30	23.73	22.97	23.22	22.40	23.12	22.86	23.14
Na_2O	0.00	0.00	0.00	0.00	0.06	0.01	0.00	0.00	0.00	0.03
K_2O	0.00	0.03	0.00	0.00	0.00	0.04	0.00	0.00	0.00	0.00
Total	95.80	97.16	97.12	97.89	96.15	96.47	97.11	97.90	97.45	97.87
	subhed. matrix epidote	incl. in plag.	subhed. matrix epidote		disrupted matrix epidote in fracture		euhedral fracture filling epidote		subhedral matrix epidote	

Appendix B:4

Microprobe analyses of **chlorite** and **argillitic** material from altered Äspö granite.

Sample	Ä1 f2				Ä3 f3		f4
	Pos 6	Pos 7	Pos 5	Pos 6	Pos 1	Pos 2	Pos 5
SiO_2	29.04	28.70	37.87	42.17	29.47	29.36	29.57
TiO_2	0.03	0.00	0.00	0.01	0.00	0.01	0.00
Al_2O_3	17.30	17.10	16.05	17.98	15.92	16.48	17.28
FeO_{tot}	23.75	23.34	14.85	13.49	21.23	21.50	19.16
MnO	0.60	0.68	0.54	0.46	0.64	0.71	0.67
MgO	17.25	17.12	14.40	13.67	17.98	17.69	17.43
CaO	0.05	0.08	0.70	0.59	0.08	0.13	0.20
Na_2O	0.00	0.00	0.00	0.00	0.00	0.00	0.10
K_2O	0.00	0.02	2.04	2.72	0.00	0.04	0.05
Total	88.00	87.05	86.46	91.09	85.30	85.91	84.46
	chlorite		fine-grained clayish mix.		chlorite		slightly alt. chl.

appendix B:4 continued...

Ä3 f4		10x10μ[1]			10x10μ[1]	Ä10	
Pos8	Pos7	Pos 8b	Pos11	Pos12	Pos 11b	Pos 3	Pos 4
46.82	47.81	47.20	39.85	39.49	41.03	41.97	41.72
0.02	0.03	0.02	0.01	0.01	0.00	0.00	0.00
21.20	20.25	21.00	18.77	18.69	19.87	20.55	16.39
9.49	9.94	9.08	15.82	15.73	14.33	4.74	5.62
0.19	0.24	0.22	0.37	0.38	0.31	0.32	0.46
8.31	12.77	8.31	12.00	11.52	10.54	18.42	21.96
0.68	0.72	0.61	0.71	0.72	0.61	0.77	0.52
0.02	0.02	0.03	0.00	0.00	0.00	0.04	0.04
4.76	3.52	4.53	1.85	1.78	2.50	0.84	1.265
91.50	95.30	90.99	89.38	88.31	89.18	87.67	87.97
argillitic matrix material			argillitic fracture filling material			spherulitic argillitic frac. filling material	

1) Defocused electron beam.

Appendix B:5

Microprobe analyses of **sphene** from altered and unaltered Äspö granite samples.

Sample	Ä4f1		Ä1f1						Ä3 f3	
	P7 core	rim	P7 core	P7 core	P7 rim	P8 core	p8 core	P8 rim	P3 core	P1 incl.
SiO_2	29.50	30.04	28.76	28.97	29.16	28.96	29.50	29.77	28.96	30.39
TiO_2	34.94	34.72	35.40	35.42	35.74	34.71	34.05	36.55	33.36	26.55
Al_2O_3	1.26	1.84	1.28	1.39	1.52	1.41	1.59	1.41	1.52	7.00
FeO	1.64	1.74	1.84	1.73	1.70	1.89	2.11	1.47	2.17	2.92
MgO	0.00	0.00	0.00	0.00	0.00	0.00	0.00	0.00	0.00	1.00
CaO	26.82	28.56	26.50	26.36	28.11	26.36	26.56	28.10	25.16	27.04
Y_2O_3	0.14	0.00	0.18	0.00	0.00	0.23	0.06	0.21	1.20	0.11
Ce_2O_3	1.27	0.30	1.85	1.70	0.56	1.39	1.44	0.43	1.47	0.06
Nd_2O_3	0.96	0.47	1.33	1.25	0.22	1.24	1.18	0.28	2.04	0.18
Yb_2O_3	0.00	0.00	0.05	0.00	0.00	0.06	0.10	0.00	0.10	0.00
ThO_2	0.00	0.00	0.22	0.00	0.07	0.00	0.00	0.03	0.08	0.00
Total	96.54	97.67	97.42	96.82	97.08	96.25	96.58	98.26	96.05	95.27
	euhedral sphene		euhedral sphene			euhedral sphene			euhedral sphene	grothite in alt. chl

Microprobe analyses of fracture filling **prehnite** from altered Äspö granite samples.

Sample	Ä1		Ä10	
	Pos 4	Pos 3	Pos 1	Pos 5
SiO_2	44.41	43.94	44.38	42.81
TiO_2	0.01	0.00	0.00	
Al_2O_3	23.99	24.51	24.14	23.89
FeO	0.34	0.06	0.13	0.12
MnO	0.04	0.00	0.00	0.00
MgO	0.00	0.00	0.00	0.00
CaO	27.64	27.59	27.35	27.24
Na_2O	0.11	0.00	0.00	0.02
K_2O	0.00	0.01	0.00	0.00
Total	96.54	96.10	96.00	94.08

List of SKB reports

Annual Reports

1977-78
TR 121
KBS Technical Reports 1 – 120
Summaries
Stockholm, May 1979

1979
TR 79-28
The KBS Annual Report 1979
KBS Technical Reports 79-01 – 79-27
Summaries
Stockholm, March 1980

1980
TR 80-26
The KBS Annual Report 1980
KBS Technical Reports 80-01 – 80-25
Summaries
Stockholm, March 1981

1981
TR 81-17
The KBS Annual Report 1981
KBS Technical Reports 81-01 – 81-16
Summaries
Stockholm, April 1982

1982
TR 82-28
The KBS Annual Report 1982
KBS Technical Reports 82-01 – 82-27
Summaries
Stockholm, July 1983

1983
TR 83-77
The KBS Annual Report 1983
KBS Technical Reports 83-01 – 83-76
Summaries
Stockholm, June 1984

1984
TR 85-01
Annual Research and Development Report 1984
Including Summaries of Technical Reports Issued during 1984. (Technical Reports 84-01 – 84-19)
Stockholm, June 1985

1985
TR 85-20
Annual Research and Development Report 1985
Including Summaries of Technical Reports Issued during 1985. (Technical Reports 85-01 – 85-19)
Stockholm, May 1986

1986
TR 86-31
SKB Annual Report 1986
Including Summaries of Technical Reports Issued during 1986
Stockholm, May 1987

1987
TR 87-33
SKB Annual Report 1987
Including Summaries of Technical Reports Issued during 1987
Stockholm, May 1988

1988
TR 88-32
SKB Annual Report 1988
Including Summaries of Technical Reports Issued during 1988
Stockholm, May 1989

1989
TR 89-40
SKB Annual Report 1989
Including Summaries of Technical Reports Issued during 1989
Stockholm, May 1990

1990
TR 90-46
SKB Annual Report 1990
Including Summaries of Technical Reports Issued during 1990
Stockholm, May 1991

1991
TR 91-64
SKB Annual Report 1991
Including Summaries of Technical Reports Issued during 1991
Stockholm, April 1992

1992
TR 92-46
SKB Annual Report 1992
Including Summaries of Technical Reports Issued during 1992
Stockholm, May 1993

Technical Reports
List of SKB Technical Reports 1993

TR 93-01
Stress redistribution and void growth in buttwelded canisters for spent nuclear fuel
B L Josefson[1], L Karlsson[2], H-Å Häggblad[2]
[1] Division of Solid Mechanics, Chalmers University of Technology, Göteborg, Sweden
[2] Division of Computer Aided Design, Luleå University of Technology, Luleå, Sweden
February 1993

TR 93-02
Hydrothermal field test with French candidate clay embedding steel heater in the Stripa mine
R Pusch[1], O Karnland[1], A Lajudie[2], J Lechelle[2], A Bouchet[3]
[1] Clay Technology AB, Sweden
[2] CEA, France
[3] Etude Recherche Materiaux (ERM), France
December 1992

TR 93-03
MX 80 clay exposed to high temperatures and gamma radiation
R Pusch[1], O Karnland[1], A Lajudie[2], A Decarreau[3],
[1] Clay Technology AB, Sweden
[2] CEA, France
[3] Univ. de Poitiers, France
December 1992

TR 93-04
Project on Alternative Systems Study (PASS)
Final report
October 1992

TR 93-05
Studies of natural analogues and geological systems. Their importance to performance assessment
Fredrik Brandberg[1], Bertil Grundfelt[1], Lars Olof Höglund[1], Fred Karlsson[2],
Kristina Skagius[1], John Smellie[3]
[1] KEMAKTA Konsult AB
[2] SKB
[3] Conterra AB
April 1993